Parks Victoria Technical Series

Number 111

Hydroacoustic Mapping of Wilsons Promontory Marine National Park

March 2017

Parks VICTORIA

Healthy Parks Healthy People®

State Government Victoria

Published by Parks Victoria

Level 10, 535 Bourke St, Melbourne Vic 3000

Author(s)

Alexandre C. G. Schimel & Daniel Ierodiaconou.

Deakin University, Faculty of Science, Engineering & Built Environment, School of Life and Environmental Sciences, Centre for Integrative Ecology.

National Library of Australia

Cataloguing-in-publication data

Includes bibliography.

ISSN 1448-4935

Citation:

Schimel, A. and Ierodiaconou, D. (2017) Hydroacoustic Mapping of Wilsons Promontory Marine National Park.

Parks Victoria Technical Series No. 111. Parks Victoria, Melbourne.

Front cover: Port Phillip Heads Marine National Park

Photo: Museum Victoria

Executive Summary

Deakin University was commissioned by Parks Victoria to undertake a hydroacoustic survey of the Wilsons Promontory Marine National Park (WPMNP) using a Multibeam echosounder (MBES), process the data into a number of geoacoustic datasets to be used for future habitat mapping efforts and use this dataset to aid in prioritizing the future biological sampling survey of the MNP.

The survey resulted in 100% coverage of the WPMNP being achieved combining the extensive MBES survey in this study and existing bathymetric LiDAR data collected as part of the Future Coasts Program. The survey required 31 days between the 8th of April 2013 and the 12th of June 2013, with MBES data acquired over 24 separate days using a Kongsberg Maritime EM2040C MBES fitted on Deakin University's research vessel *Yolla*.

The data were processed into two bathymetry grids and two backscatter mosaics at 1 m and 5 m resolution. A suite of derivative products was then obtained from these original datasets to assist in future predictive modelling applications. A total of nine derivative layers were produced from the bathymetry including Northness, Eastness, Rugosity, Maximum Curvature, Slope, Complexity and three Bathymetric Position Indices (BPI) computed at three different scales. Three derivatives layers were produced from the coarse backscatter mosaic: Red, Green and Blue bands of a "Hue, Saturation and Intensity" (HSI) transformation of the backscatter mosaic.

A procedure for the automated objective prioritisation for subsequent ground-truthing data collection was designed to ensure that adequate sampling across the variability of habitats within the WPMNP will be achieved. In the absence of ground-truth biological data, the variability in the physical data products can be assumed to be the best available proxy to characterize the variability in habitat types. Under that assumption, we designed a methodology based on object-based segmentation and a clustering algorithm, which was applied to the original bathymetry grid, the original backscatter mosaic and a subset of the derivatives, to result in establishing 100 locations characterising the full range of the variability in the original geoacoustic data, to be used for the ground-truth survey.

This report is accompanied by a library of spatial data obtained from the Multibeam sonar (including the original layers, derivatives layers, segmentation and clustering outputs), and in appendices, the list of the 100 proposed ground-truth locations as well as the research outputs resulting from this project.

Contents

Index of figures

Index of tables

1. Introduction

Parks Victoria manages a system of Marine National Parks (MNPs) and Sanctuaries that make up approximately 5.3% of the state waters. The Wilsons Promontory Marine National Park (WPMNP) is the largest of these MNPs and the only one in the Flinders bioregion (Figure 1). The WPMNP supports a variety of habitats including shallow subtidal reefs, deep subtidal reefs, intertidal rocky shores, sandy beaches, seagrass, subtidal soft substrates and expansive pelagic areas. These habitats support a number of unique and important species and communities. The WPMNP marks the mixing zone of warmer waters of the eastern Australian coast and the colder waters of western Bass Strait, which is likely driving the high species richness and diversity observed in monitoring programs. These important natural values are subject to threats such as marine pests, nutrients from sewage, propeller scour, major oils spills, climate change and visitor impacts.

Good park management requires a thorough understanding of the natural values that occur within parks and reserves and ecological knowledge of important processes. Parks Victoria has been involved in several projects to map marine habitats in the various MNPs across the state. The WPMNP has only had a small proportion (<20%) of its 150km2 area mapped prior to this project (Figure 1). This has resulted in a limited understanding of the distribution and extent of marine habitats within this ecologically important MNP.

Parks Victoria has made a priority to fill this knowledge gap. It therefore established a research project to obtain a complete coverage of the seafloor of the WPMNP using high-resolution Multibeam echosounder (MBES). This project is to provide a complete coverage of the bathymetry and seafloor backscatter of the WPMNP, which can be used for future benthic habitat characterisation and species distribution modelling. Deakin University was commissioned to undertake this project.

The project objectives were to:

(1) Develop a detailed sonar survey plan to ensure 100% overlap in survey operations and efficiency in survey design,

(2) Collection of high-resolution Multibeam sonar data for the Wilson's Promontory MNP to provide of full-coverage of bathymetry and backscatter information to be used in predictive modelling applications,

(3) Trial the collection of water column data for regions of interest and test the applicability of this data to inform the habitat characterisation process,

(4) Develop a suite of derivative products from the Multibeam data that characterise the variability in acoustic terrain and acoustic facies (i.e. softness/hardness, bathymetry maps, etc.), and

(5) Develop a prioritised biological sampling plan to ensure variability in terrain characteristics are sampled in future ground-truthing operations.

This report presents the result of this research project, addressing each of the above objectives. As per the research permit application, it is accompanied by:

- A library of spatial data from the Multibeam sonar data (raw in folder 'acquisition', processed in folder 'processing' and exported as GIS layers in folder 'deliverables'),
- Derivative products (in folder 'deliverables'),
- Segmentation products (in folder 'deliverables'), and
- Proposed ground-truth locations (Appendix B to this report).

Other appendices to this report present the results of research related to this project, including:

- A research article titled "*Granitic coastal geomorphology: applying integrated terrestrial and bathymetric LiDAR with multibeam sonar to examine coastal landscape evolution*", published in *Earth Surface Processes and Landforms* by Kennedy et al., (2014), using the MBES bathymetry data acquired for this project, reproduced in Appendix C.

- A thesis report titled "*Integration of object-based image analysis, multibeam data and video data for benthic habitat mapping in Wilsons Promontory National Park, Australia*", submitted in partial fulfilment of the degree of Bachelor of Environmental Science Honours of Deakin University (unpublished to date), by Grace Gaylard, using MBES bathymetry and backscatter data acquired in nearby Refuge Cove during weather conditions preventing the acquisition of data in the WPMNP, reproduced in Appendix D.

- A presentation titled "Multibeam water column data: show me those plants!", presented at the GeoHab conference held in Lorne, VIC, Australia in May 2014, by Alexandre Schimel and Daniel Ierodiaconou, using MBES water column data from the same MBES used for this research project, to attempt at imaging and detecting Giant Kelp in the water column, reproduced in Appendix E.

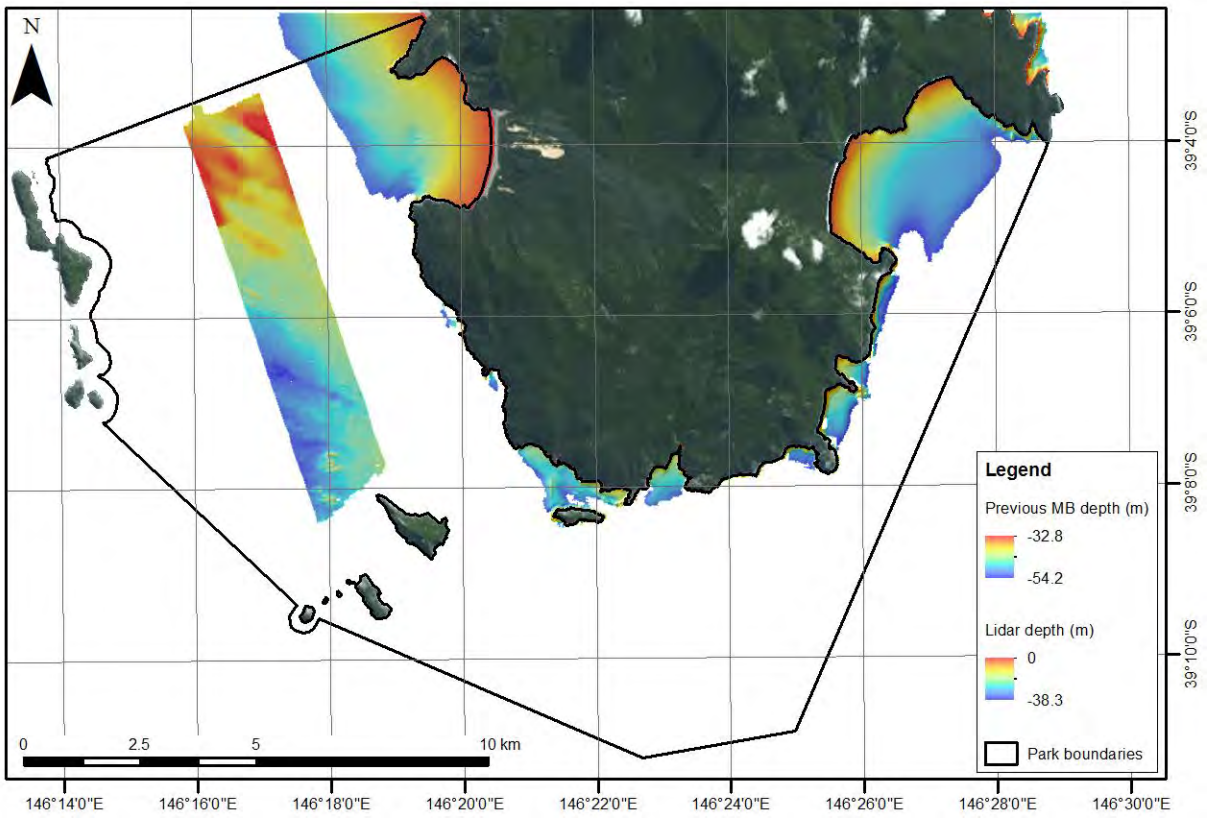

Figure 1 The Wilsons Promontory Marine National Park (boundaries shown as a black polygon), overlaid with existing bathymetry data prior to this project, including Lidar data (shallow waters near the coast) and a MBES dataset previously acquired by Fugro (offshore in the western part of the study site).

2. Methods

2.1 MBES survey planning

MBES are sonar systems recording depth and seafloor backscatter intensity for a large number of soundings across the vessel track, resulting in a swath of data being recorded as the vessel steams along. The swath width is dependent on the sonar transmit sector aperture and the depth. For example, a system with a constant ±65° transmit aperture would ensonify a total across-track length of only 42.8 m of a flat seafloor 10 m in depth, but 428.9 m of a flat seafloor 100 m in depth. This operational constraint implies that the total time required to ensure complete "100% coverage" of any given site is dependent on the site's depth. In the case of the WPMNP, the absence of prior good knowledge of the site's bathymetry prevented an accurate estimation of the required survey time. The survey was estimated to require a total of 20-30 complete survey days.

In addition to the uncertainty about the required survey time, it was recognized that the WPMNP is subject to extreme weather and oceanographic conditions including large waves and strong currents, which must be taken into account when deciding the best survey location on a daily basis.

Given the uncertainty in required survey time, it was decided to target, by order of priority:

1. The deep-water parts of the site (over shallow-water parts), in order to maximize coverage achieved;
2. The waters near the islands and reefs (over areas of flat soft-sediment), in order to ensure that the sites of known biological significance would be surveyed;
3. The areas not already covered by the previous LiDAR and MBES surveys, in order to obtain complete coverage in the event of unforeseen circumstances such as unsuitable weather or gear malfunction preventing the completion of the survey.

Given the uncertainty in marine weather conditions, it was decided to target, by order of priority:

1. Open-waters areas (over enclosed areas such as bays and lee of islands), in order to make the most of small-waves conditions when available;
2. Areas around islands, in order to make the most of low tidal-induced currents when they occur.

These priorities guided the choice of the location to survey on a daily basis, depending on weather forecasts.

2.2 MBES data acquisition

MBES data were acquired over a total 24 days of actual survey between the 8th of April 2013 and the 12th of June 2013 (Table 1). The data were obtained with a Kongsberg Maritime EM2040C MBES fitted on Deakin University's 9.2 m research vessel *Yolla* (Figure 2). The sonar was operated with Kongsberg Maritime software SIS, using a constant frequency of 300 kHz, a varying ping rate and pulse length (resp. up to 50 Hz and down to 0.025 ms) automatically adjusting to water depth, in high-density equidistant mode (400 soundings per ping) and with a constant sector coverage of ±65° athwartships.

An Applanix POS MV WaveMaster mounted on the vessel measured the precise position of the sonar head in Differential GNSS mode using GPS/GLONASS corrections received by radio from the Fugro MarineStar satellite positioning service. The POS MV WaveMaster also measured precise vessel motion data (roll, pitch, yaw, true heave). The sonar position and motion thus measured were fed into SIS in real-time to aid in data acquisition, but were also recorded separately for later post-processing.

One profile of sound speed in the water column was captured at the start of each day of survey with a Valeport Monitor Sound Velocity Profiler (Figure 3) and imported in SIS to correct soundings for the effects of sound velocity variation with depth. SIS integrated this profile with a real-time measurement of sound velocity at the depth of the sonar head measured by a Valeport Mini-SVS mounted next to the sonar head (Figure 4).

The data acquisition resulted in a total of over 120 GB of data, including approximately 100 GB of MBES raw data files.

Table 1 MBES survey final schedule.

Day #	Date	Data day #	Notes
1	April 8th, 2013		Mobilization. Transport boat to Port Welshpool (PW). Fuelling & supplies. Systems tests. Survey planning.
2	April 9th, 2013	**1**	Launch from PW. Transit to Refuge Cove (RC). Survey S end of site. Moored at RC overnight.
3	April 10th, 2013	**2**	Continue survey S end of site. Moored at RC overnight.
4	April 11th, 2013	**3**	Vessel engine issues. Abort survey. Transit to PW. Refuel & resupply. Transit to RC. Moored at RC overnight.
5	April 12th, 2013	**4**	Continue survey S end and islands. Moored at RC overnight.
6	April 13th, 2013	**5**	Survey S coast of Prom. Moored at RC overnight.
7	April 14th, 2013	**6**	Survey SW corner of site, around islands, SW boundary. Moored at RC overnight.
8	April 15th, 2013	**7**	Survey S coast of Prom. Transit to PW. Refuel & resupply. Stay in PW overnight.
9	April 16th, 2013	**8**	Launch from PW. Transit to RC. Continue survey S coast and W end of Prom. Moored at RC overnight.
10	April 17th, 2013	**9**	Continue survey W and SW end of site. Moored at RC overnight.
11	April 18th, 2013	**10**	Survey E end of site. Bad weather. Abort survey. Transit to PW. Engine service. Refuel & resupply.
12	April 21st, 2013		Launch from PW. Transit to RC. Bad weather. Abort survey. Moored at RC overnight.
13	April 22nd, 2013		Site inspection. Bad weather and forecast. Abort survey. Transit to PW and demobilize. End of leg #1.
14	May 26th, 2013		Remobilization for leg #2. Transport to PW. Fuelling & supplies. Systems tests. Transit to RC, moored overnight.
15	May 27th, 2013	**12**	Continue survey E end of site. Tour of vessel and survey for Parks Victoria staff. Moored at RC overnight.
16	May 28th, 2013	**13**	Continue survey W end of site. Moored at RC overnight.
17	May 29th, 2013	**14**	Continue survey W end of site. Moored at RC overnight.
18	May 30th, 2013		Technical issues with Hydrographic PC. Abort survey. Transit to PW to repair, refuel & resupply. Transit to RC.
19	May 31st, 2013	**15**	Equipment issues in morning. Continue survey W end of site. Moored at RC overnight.
20	June 1st, 2013	**16**	Continue survey W end of site. Moored at RC overnight.
21	June 2nd, 2013	**17**	Weather too rough for W end of site. Continue survey E end of site. Moored at RC overnight.
22	June 3rd, 2013		Bad weather. Abort survey. Transit to PW to refuel & resupply. Transit to RC. Moored at RC overnight.
23	June 4th, 2013	**18**	Continue survey W end of site. Technical issues, return to RC. Moored at RC overnight.
24	June 5th, 2013	**19**	Continue survey W end of site. Moored at RC overnight.
25	June 6th, 2013	**20**	Survey SE corner, E side and Little Waterloo Bay. Moored at RC overnight.
26	June 7th, 2013		Weather too rough. Abort survey. Transit to PW to refuel & resupply and back to RC. Survey of RC.
27	June 8th, 2013	**21**	Continue survey Little Waterloo Bay. Continue RC survey. Moored at RC overnight.
28	June 9th, 2013	**22**	Continue survey SW end of site. Weather deteriorating. Abort survey. Transit to PW to refuel & resupply.
29	June 10th, 2013	**23**	Launch from PW. Continue survey W end of site (Oberon Bay). Moored at RC overnight.
30	June 11th, 2013	**24**	Patch test. Complete RC survey. Transit to PW. End of leg #2. End of survey.
31	June 12th, 2013		Demobilize. Transport boat back to Warrnambool.

Figure 2 Yolla RV with sonar head mounted on a pole over the portside.

Figure 3 Valeport Monitor Sound Velocity Profiler.

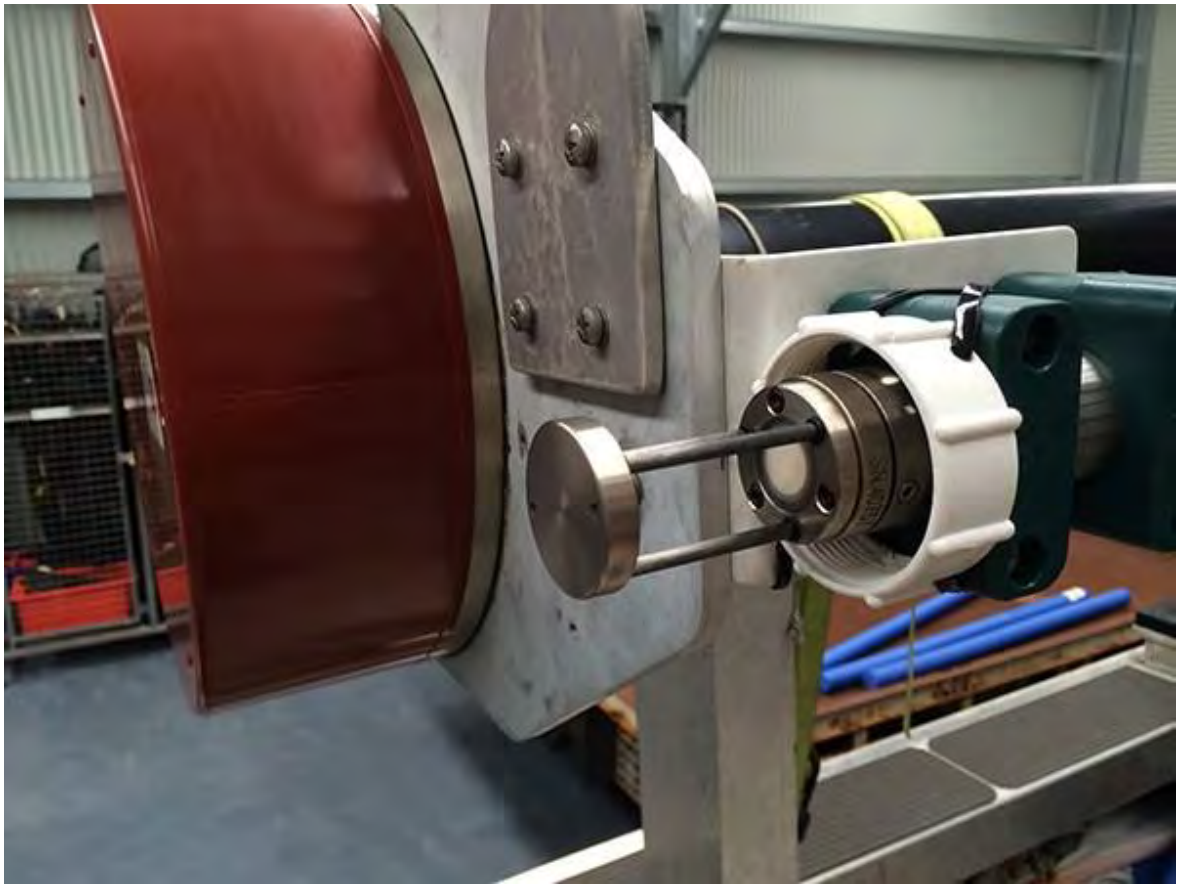

Figure 4 EM2040c sonar head (in red on the left) and Valeport mini-SVS sound velocity sensor (on the right), mounted at the end of the pole, in transit/transport position (out of water).

2.3 Navigation, bathymetry and backscatter processing

The bathymetry data were processed with CARIS software HIPS & SIPS 8.1.6. The navigation data and the soundings data were first cleaned manually to remove outliers. A second automatic cleaning of soundings was applied to thin the data further from the most uncertain soundings. The soundings were then gridded at a resolution of 1 m (fine) and 5 m (coarse) using the CUBE algorithm using the "1a" IHO standard settings (Calder and Mayer, 2003).

Backscatter data were processed in QPS FMGT 7.4.1. Processing settings included using EM2040 sonar settings, the built-in angular dependence compensation "AGV Trend" with a window size of 300 pings, and blending of overlapping lines with a setting of 50%. The backscatter mosaic was gridded at 1 m and 5 m.

Bathymetry grids and backscatter mosaics were exported in various formats of deliverables for data exploration and further data processing. Appendix A reproduces the metadata file accompanying these deliverables, which presents a technical summary of the processing and deliverables generated.

2.4 Derivatives

Using ARCGIS 10.2.2 and ENVI 4.7, a number of derivative layers were obtained from the coarse bathymetry grid and backscatter mosaic (Table 2). A total of nine derivative layers were produced from the bathymetry: Northness, Eastness, Rugosity, Maximum Curvature, Slope, Complexity and three Bathymetric Position Indices (BPI) computed at three different scales (Weiss, 2001; Wilsons et al., 2007; Lundblad et al., 2006; Schmidt et al., 2003). Three derivatives layers were produced from the coarse backscatter mosaic: Red, Green and Blue bands of a "Hue, Saturation and Intensity" (HSI) transformation of the backscatter mosaic (Daily, 1983). All

layers were selected based on their successful application in thematic benthic habitat map construction of previous studies (Rattray et al., 2009; Ierodiaconou et al., 2007; 2011; Che Hasan et al., 2014).

Table 2 Derivatives obtained from the coarse bathymetry grid and the coarse backscatter mosaic.

Derivative (original layer)	Description	Analysis neighbourhood size (in pixels)	Software
Northness (bathymetry)	Sinus component of the azimuthal direction of the steepest slope through the points in the analysis window (Wilson et al., 2007).	3x3	Spatial Analyst (ArcGIS 10.2.2)
Eastness (Bathymetry)	Cosinus component of the azimuthal direction described above.	As above	As above
Rugosity (Bathymetry)	Ratio of surface area to planar area (Lundblad et al., 2006). A measure of topographic roughness.	3x3	Benthic Terrain Modeller Tool for ArcGIS
Maximum curvature (Bathymetry)	Steepest curve of either plan or profile convexity through a defined cell neighbourhood (Schmidt et al., 2003)	3x3	ENVI 4.7
Very fine Bathymetric Position Index (BPI) (Bathymetry)	Difference between each cell elevation and the mean elevation of the surrounding cells within an annulus of user-defined inner and outer radius (Weiss, 2001; Lundblad et al., 2006). A measure of a location elevation relative to the overall landscape.	Inner radius=10 Outer radius=30	Benthic Terrain Modeller Tool for ArcGIS
Fine BPI (Bathymetry)	As above, different parameters	Inner radius=25 Outer radius=50	As above
Coarse BPI (Bathymetry)	As above, different parameters	Inner radius=100 Outer radius=200	As above
Slope (Bathymetry)	Maximum change in elevation between each cell and cells in its analysis neighbourhood. Calculated in degrees from the horizontal (Wilson et al., 2007).	3x3	Spatial Analyst (ArcGIS 10.2.2)
Complexity (Bathymetry)	Second derivative of slope (or rate of change of slope) (Wilson et al., 2007). A measure of the terrain's local variability.	3x3	ENVI 4.7
Red band of Hue, Saturation and Intensity (Backscatter)	The red band of a synthetic Red, Green, Blue (RGB) colour image obtained from the transformation of a Hue, Saturation and Intensity (HSI) image, which was formed by mapping the high and low frequency information of the original backscatter image to the Hue and Intensity layers, respectively, while maintain the saturation value fixed (Daily, 1983).	High-pass filter: 3x3 Low-pass filter: 11x11	ENVI 4.7
Green band (Backscatter)	Green band of the image described above.	As above	As above
Blue band (Backscatter)	Blue band of the image described above	As above	As above

2.5 Automatic ground-truthing sites selection

Ground-truthing is a significant effort in both time and resources, drastically limiting the number of locations targetable in any given survey. This is a major issue considering that for a survey to be successful, all habitats must be targeted a number of times each, taking into account the fact that the dataset need to be later split between algorithm training and map accuracy assessment. To mitigate this, a ground-truthing survey is often planned so as to target the spatial variability in the environmental datasets. Although the link between the spatial variability in the environmental dataset and the site's habitat distribution cannot be formally established until the environmental and ground-truth datasets are integrated, such approach contributes to increasing the chance that the site's representative habitat types will be targeted in the absence of existing ecological data.

This "supervised" planning is usually performed manually: from the environmental datasets, an operator visually identifies a number of broad "categories" that are visually different from each other and selects a number of locations for each category. In this project, we aimed at automating this decision process to allow for a more objective, repeatable procedure. We designed a methodology consisting of three steps: object-based segmentation, clustering, and random point selection.

2.5.1 Object-based segmentation

Object-based segmentation consists in partitioning a site into small, contiguous, non-overlapping regions (or "objects") for which data characteristics (obtained from a set of environmental layers) are internally consistent but different from that of neighbouring objects (Blaschke, 2010). Although object-based segmentation is a tool for mapping habitats in itself (e.g. Lucieer, 2008; Lucieer and Lamarche, 2011; Diesing et al., 2014), we used this algorithm solely in order to minimize the noise in the original environmental data layers as a prior step to the subsequent clustering. It makes use of the software eCognition by Trimble.

eCognition operates a recursive algorithm on a set of input layers to obtain a series of hierarchical segmentations of a site (Benz et al., 2004). The algorithm starts with pixels taken as objects and recursively aggregate neighbouring objects based on the similarity of their properties in the input layers space. At the early stages of the process, the segmentation is made of a large number of small segments; at the later stages, it is made of a small number of large segments. Such process stage is identified by the parameter known as "scale".

The two important user-defined parameters of this process are the set of input layers chosen for the process, and the scale at which to stop the algorithm. We used Bathymetry, Backscatter, Fine BPI, Broad BPI and Complexity as input layers and used the eCognition ESP2 tool to select the segmentation scale.

Estimation of the scale parameter

A relatively objective methodology to estimate an "optimal" scale parameter for an object-based segmentation of multiple layers was designed and implemented in eCognition as the ESP2 tool (Drăguţ et al., 2014). The algorithm consists in running the object-based segmentation and measuring for each scale the average local variance and rate of change (ROC). The scale at which a first peak in the ROC appears is then selected as the "optimal" scale. We implemented this algorithm (Figure 5) on our choice of input layers (Bathymetry, Backscatter, Fine BPI, Broad BPI and Complexity). The first peak in ROC graph was found for a scale parameter of 20 (Figure 6).

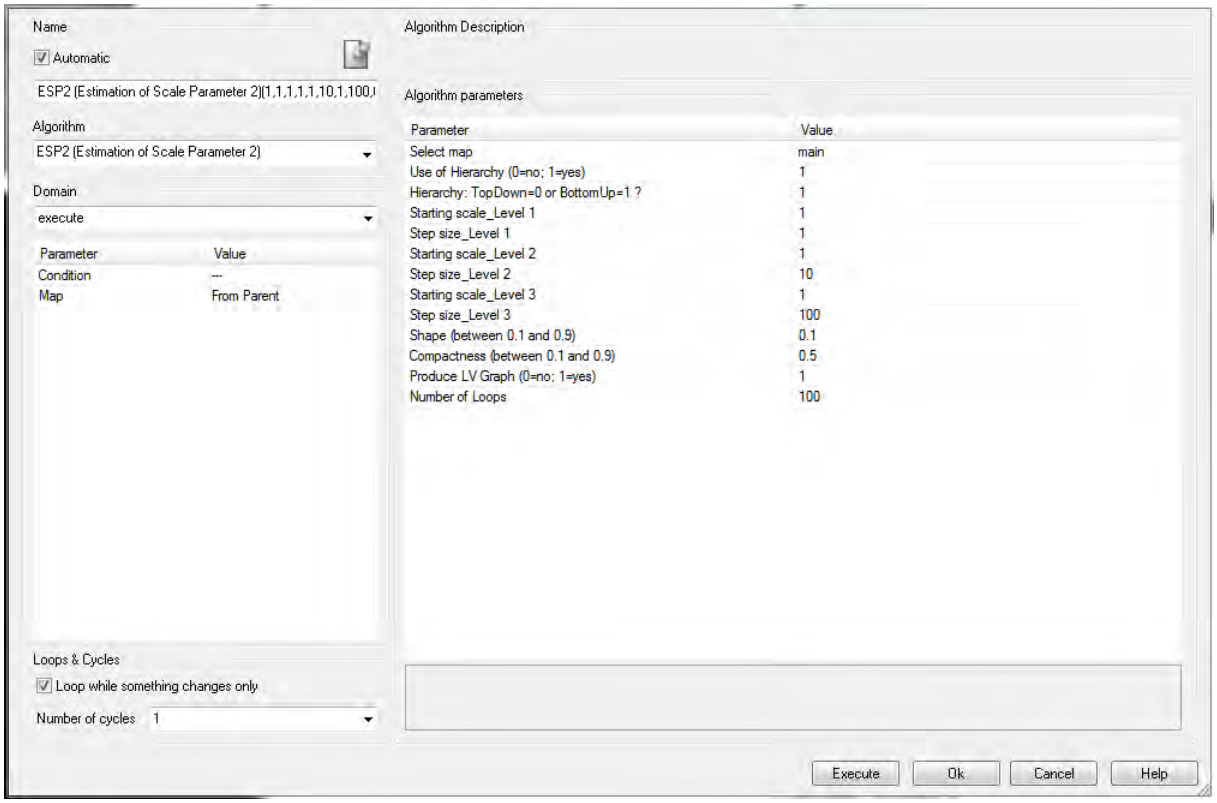

Figure 5 ESP2 tool settings in eCognition.

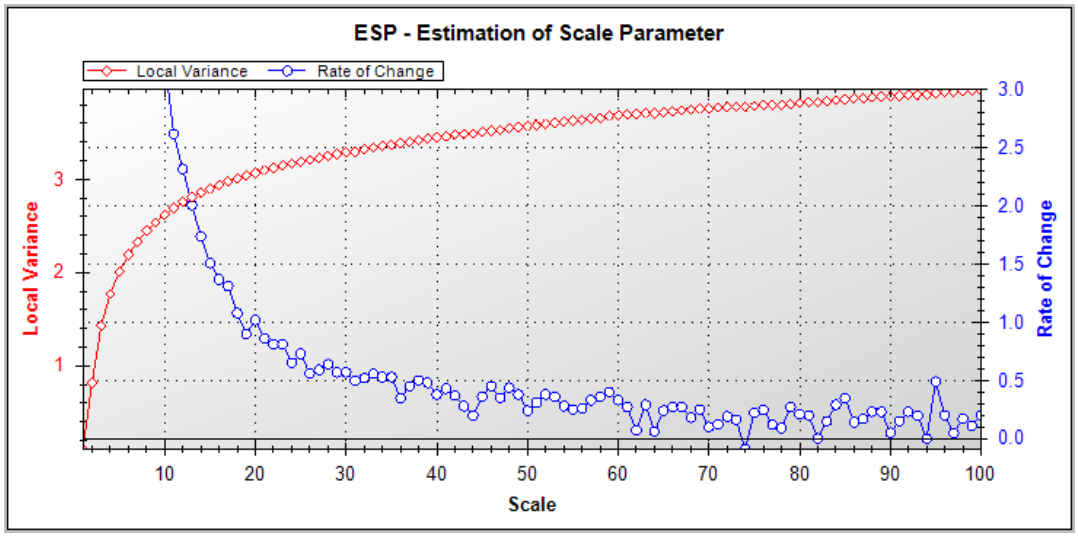

Figure 6 Result of ESP2 tool application to the dataset. The first peak in the Rate of Change indicate the Scale suggested as "optimal", here 20.

Segmentation

A multiresolution segmentation was then carried out with the same input layers as for the ESP2 tool above and a scale parameter of 20 (Figure 7).

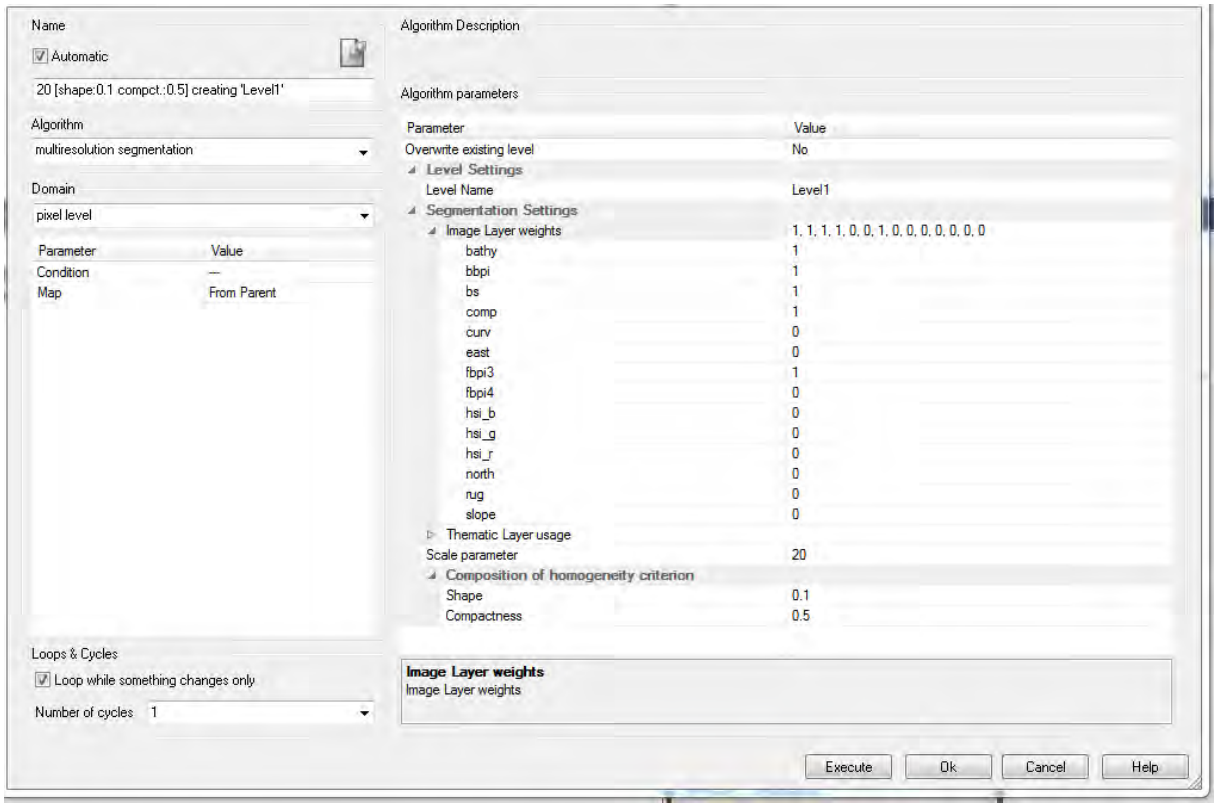

Figure 7 eCognition parameters for segmentation.

This process resulted in a relatively fine segmentation of the site in objects. We then calculated the mean, standard deviation, minimum and maximum value of each input layers for each object and exported the results as raster files. The main interest of this process is that the mean value of layers within each object appears as a de-noised version of the original layer that still conserves the boundaries of actual features. The other outputs (standard deviation, minimum and maximum) are additional layers that can be used for integration with ground-truth.

2.5.2 Clustering

We used the ArcGIS "Grouping Analysis" tool (Spatial Statistics Tools / Mapping Clusters, see Figure 8) to create ten classes meant to represent the main categories in the environmental datasets. We used the mean and standard deviation of Bathymetry, Backscatter mosaic and Complexity as layers (total of 6 layers). The choice of number of classes and layers were arbitrary. This process was completed with the "Dissolve Tool" (Data Management Tools / Generalization, see Figure 9) to group all segments belonging to the same class so as to create a polygon shapefile with only ten features, corresponding to each class.

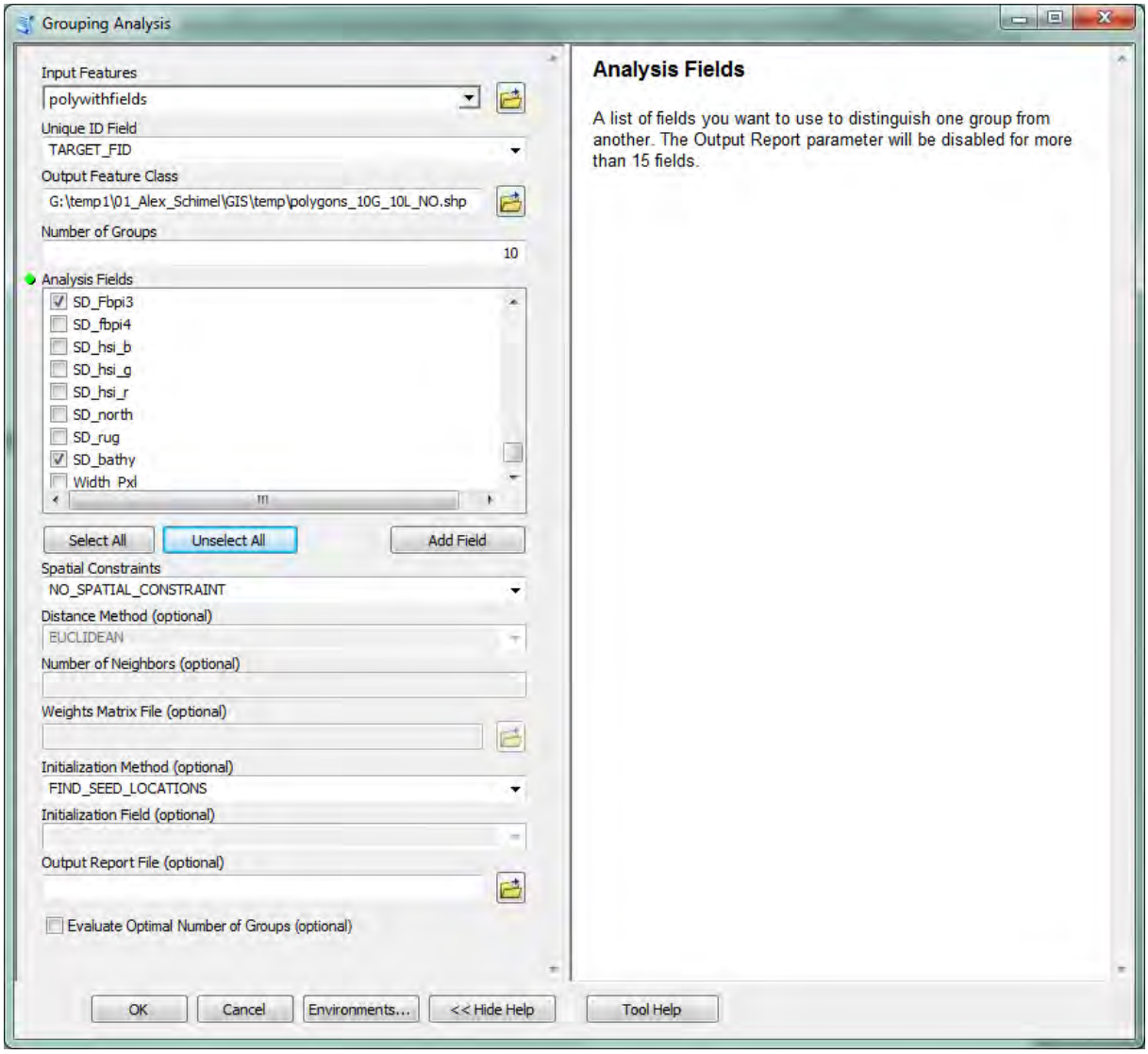

Figure 8 ArcGIS "Grouping Analysis" Tool.

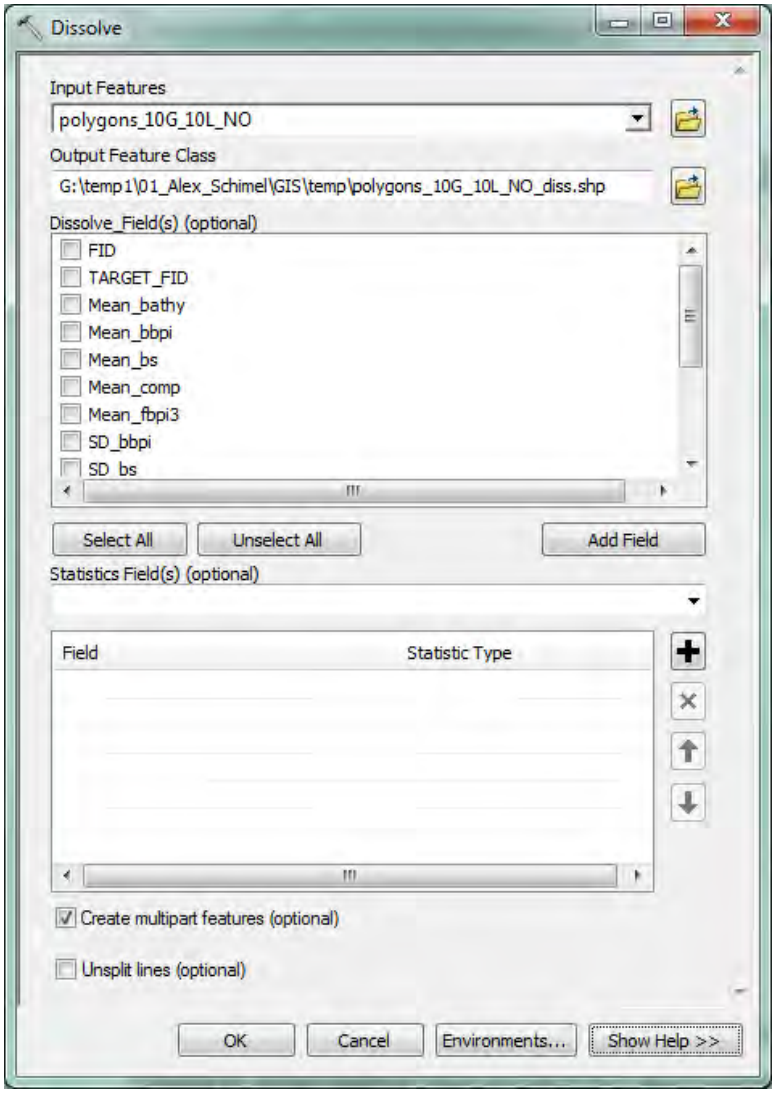

Figure 9 ArcGiS "Dissolve" Tool.

2.5.3 Point selection

Ten random points were created for each class using the ArcGIS "Create Random Points" tool (Data Management Tools / Feature Class, see Figure 10), leading to a total number of 100 sample locations.

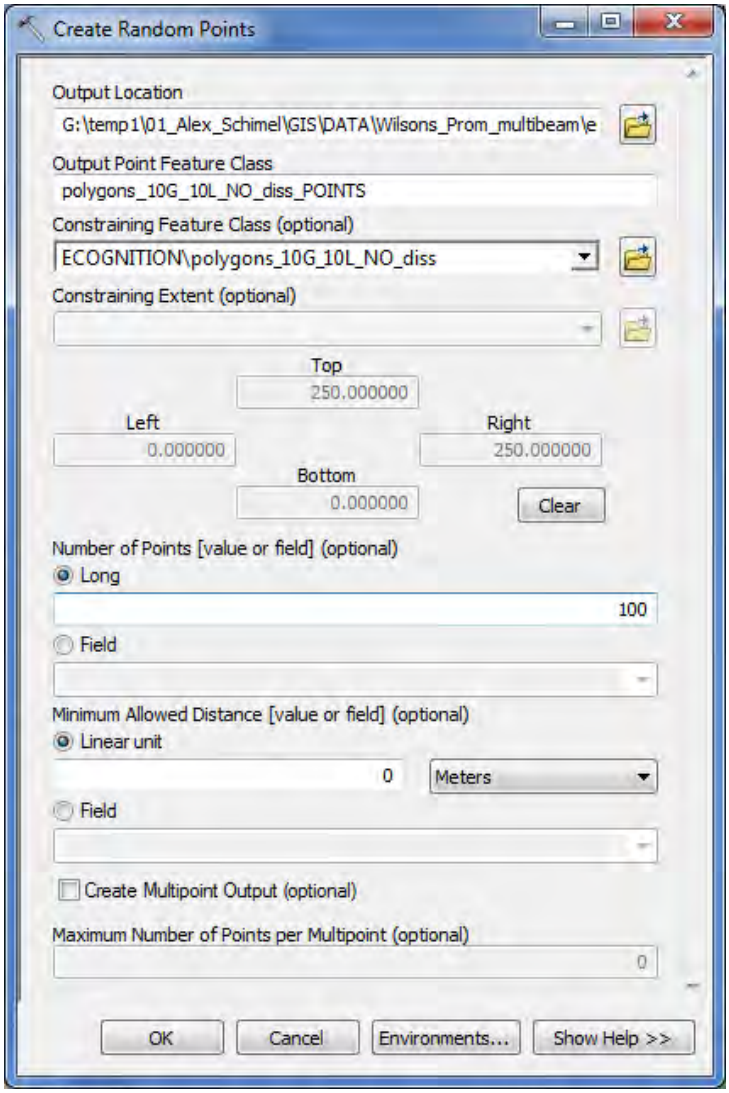

Figure 10 ArcGIS "Create Random Points" tool.

3. Results

3.1 Bathymetry and backscatter

Figure 11 and Figure 12 present the resulting bathymetry and backscatter maps, respectively. Analysis of these two original datasets provided major insights in the complex geomorphology of the WPMNP. It was found that the granitic outcrops visible on the shoreline and islands descend steeply to the seafloor to an average water depth of 40 m, with isolated areas near South East Point descending to around 90 m depth (Figure 11a). These granitic outcrops also occur underwater as isolated reefs 5.4–38.1 ha in area between 1 and 40 m depth (e.g. Figure 11b and Figure 11d). The seabed around the outcrops is characterised by a hard ground which is generally bare of sediment and has an average depth of 40–50 m (Figure 11d). On the eastern sides of the islands, large scour holes in the seafloor, up to 400 m wide, occur and descend to 90 m depth. Unconsolidated sediment sheets occur throughout the site, principally around the coastline and islands in relatively shallow waters down to 40 m (Figure 12c). The sediment sheet to the west of the Promontory, just north of the Anser Group cover 835 ha in area and is likely to be around 2–6 m thick, based on their height above the surrounding near-horizontal seafloor (Figure 11a). Sediment mounds are attached to all the islands and have a sculptured formation similar to shadow dunes found on land (Figure 11d and Figure 12b). An isolated transverse ridge composed of sediment extends from South East Point to the SE for 4.5 km rising to a height of 22 m above the seabed with an average width of 100 m (Figure 11c). All these sediment features appear to be active as they have steep slip faces present on their eastern sides as well as bedforms. A more detailed analysis of the geomorphology of the site based on this dataset was published (Kennedy et al., 2014) and can be found in Appendix C to this report.

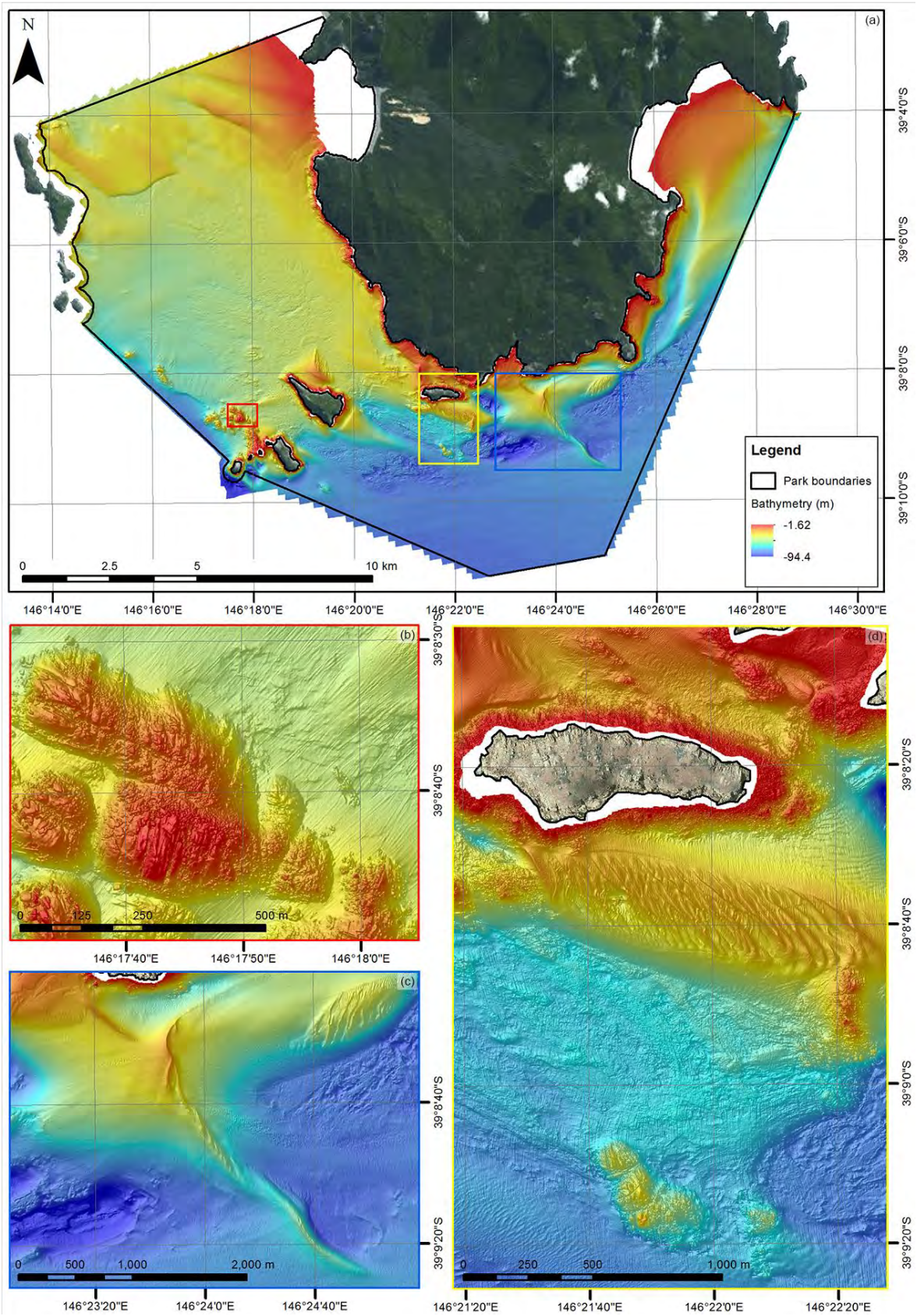

Figure 11 Bathymetry for the entire site (a) and for selected features including: a granitic outcrop with the wreck of the "Gulf of Carpentaria" nearby (b), an isolated transverse ridge of sediments (c) and a sediment mound (with bedforms) attached to Kanowna Island over an area of bare bedrock interspersed with granitic outcrops (d).

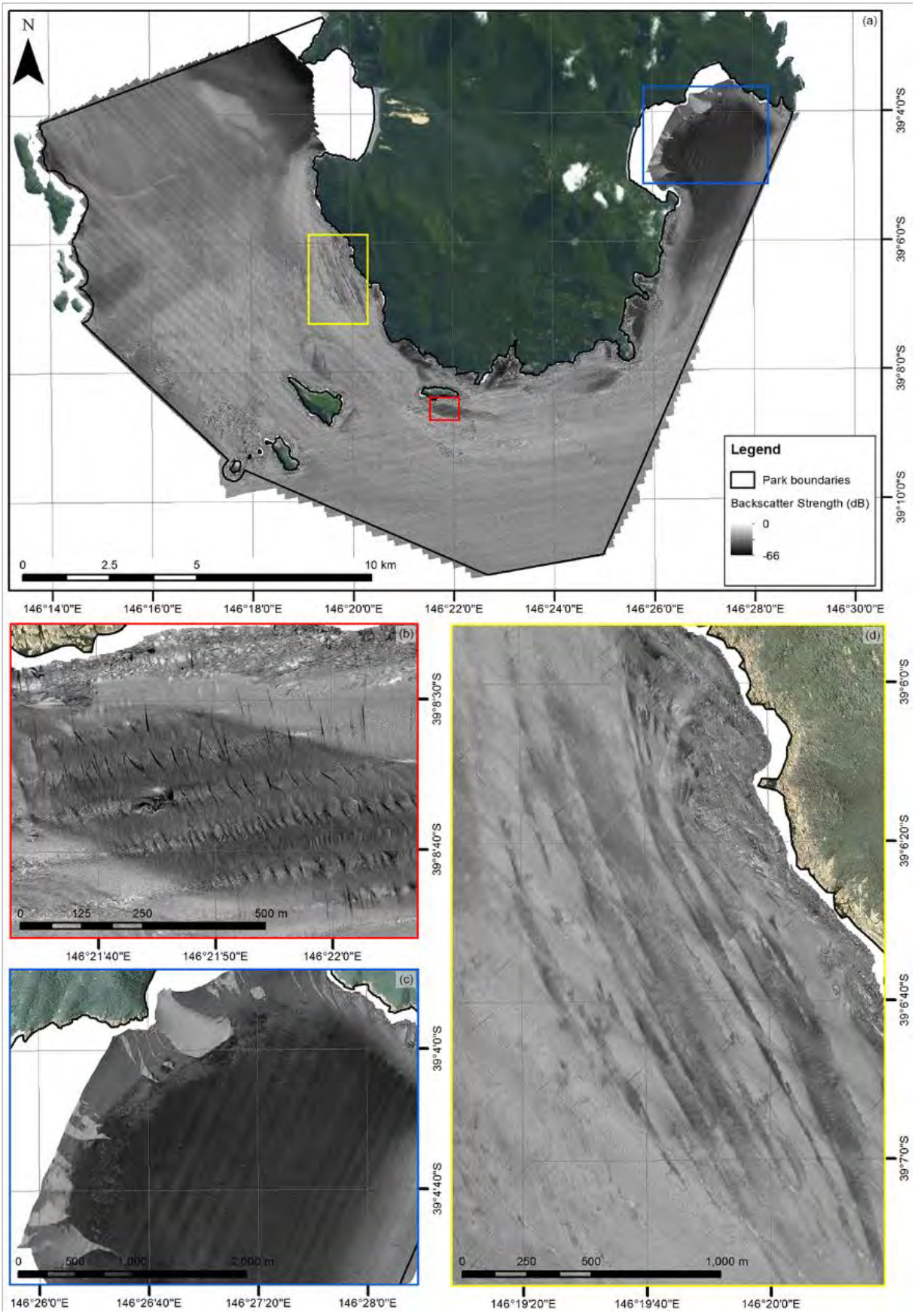

Figure 12 Backscatter mosaic for the entire site (a) and for selected features of interest (b, c and d).

3.2 Bathymetry derivatives

Figures 13 to 21 present the nine layers derived from bathymetry.

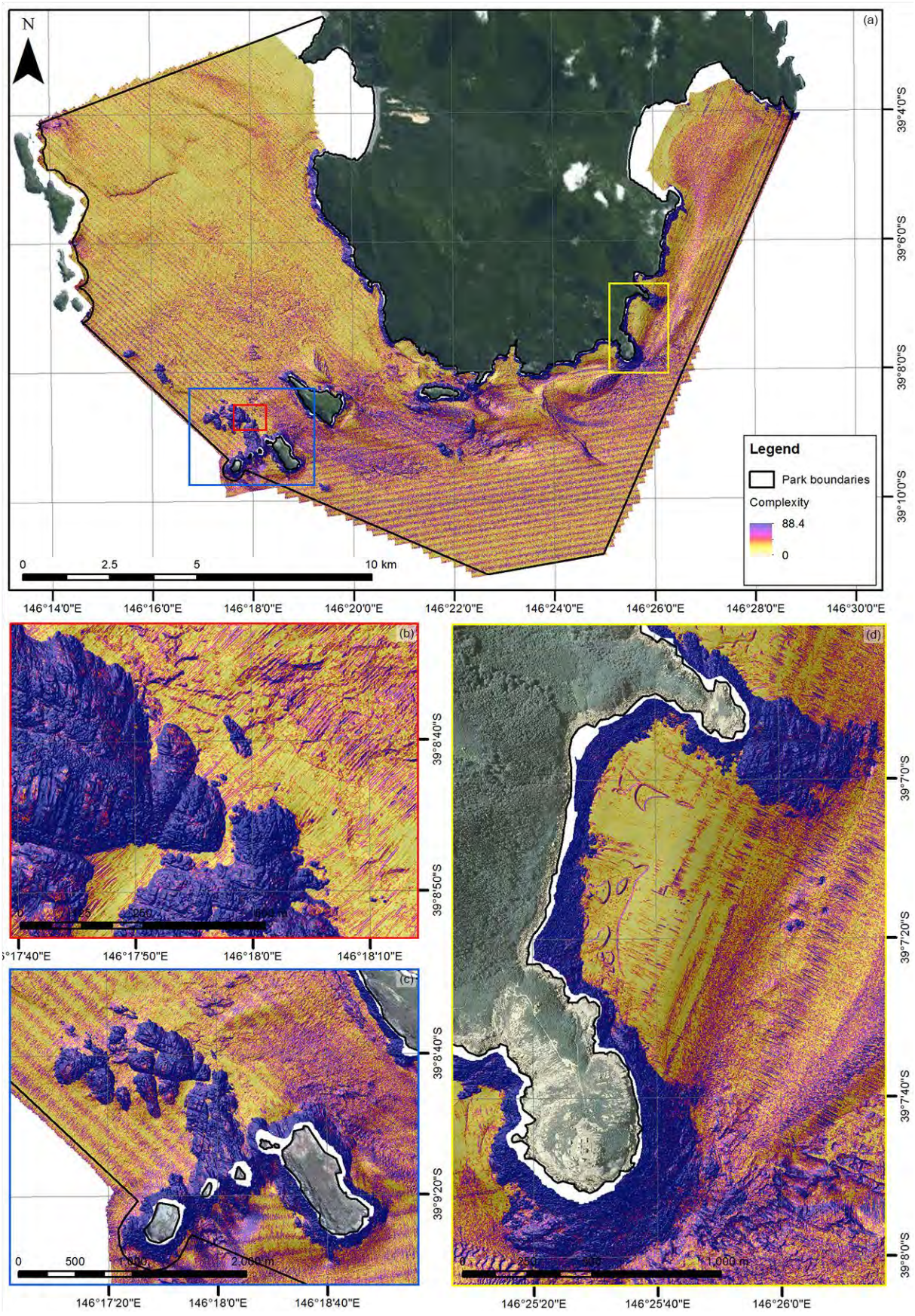

Figure 13 Complexity for the entire site (a) and for selected features of interest (b, c and d).

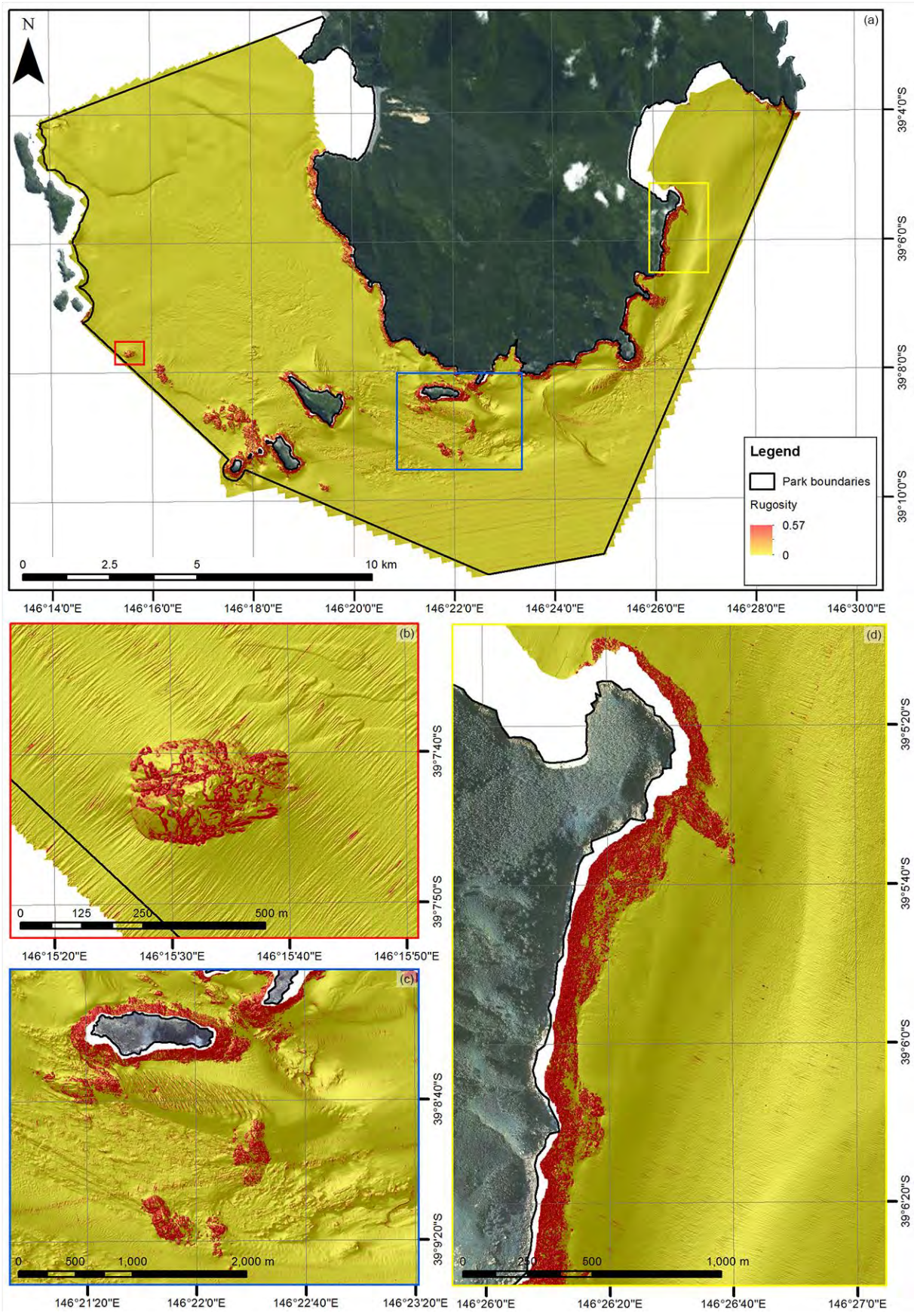

Figure 14 Rugosity for the entire site (a) and for selected features of interest (b, c and d).

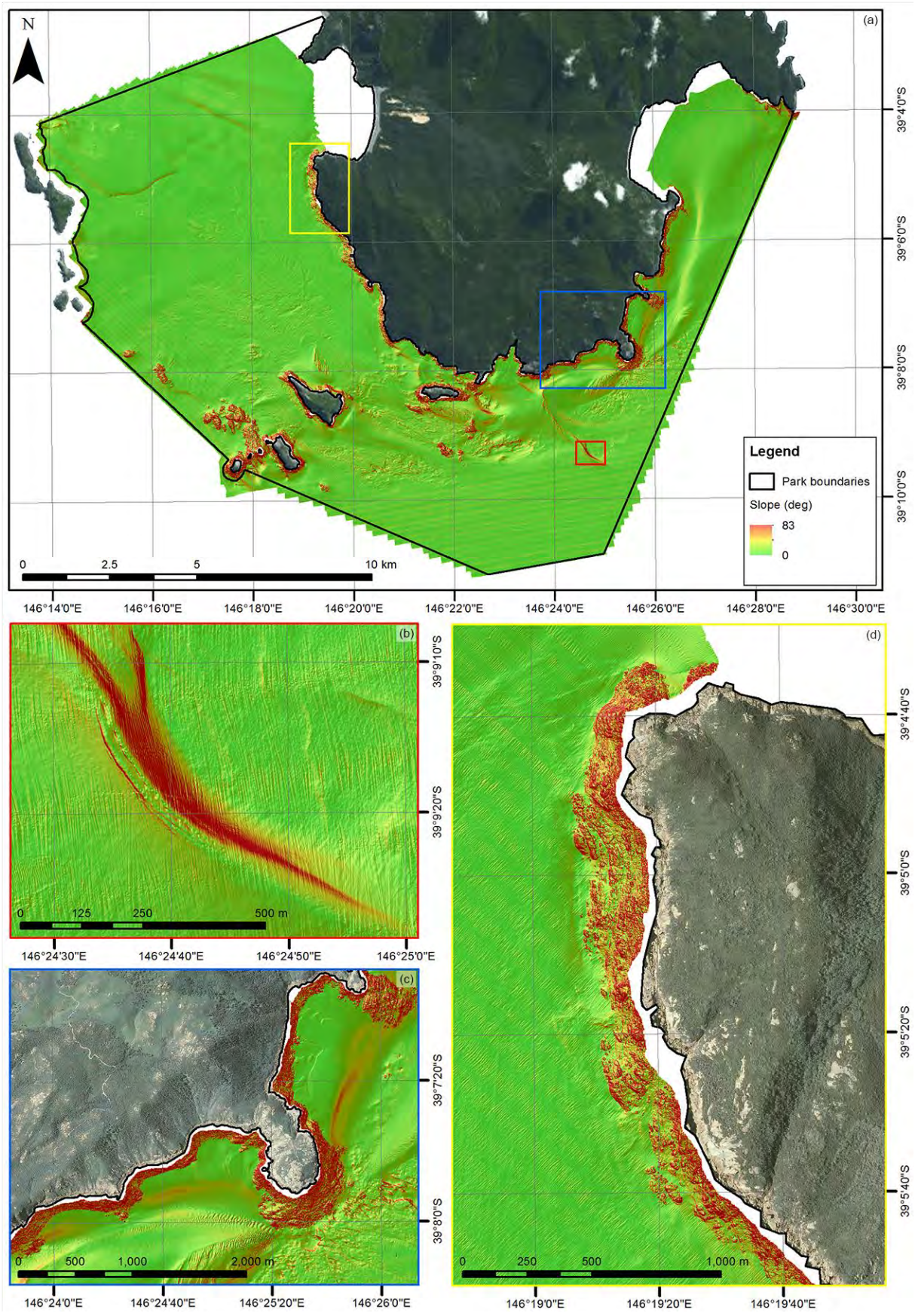

Figure 15 Slope for the entire site (a) and for selected features of interest (b, c and d).

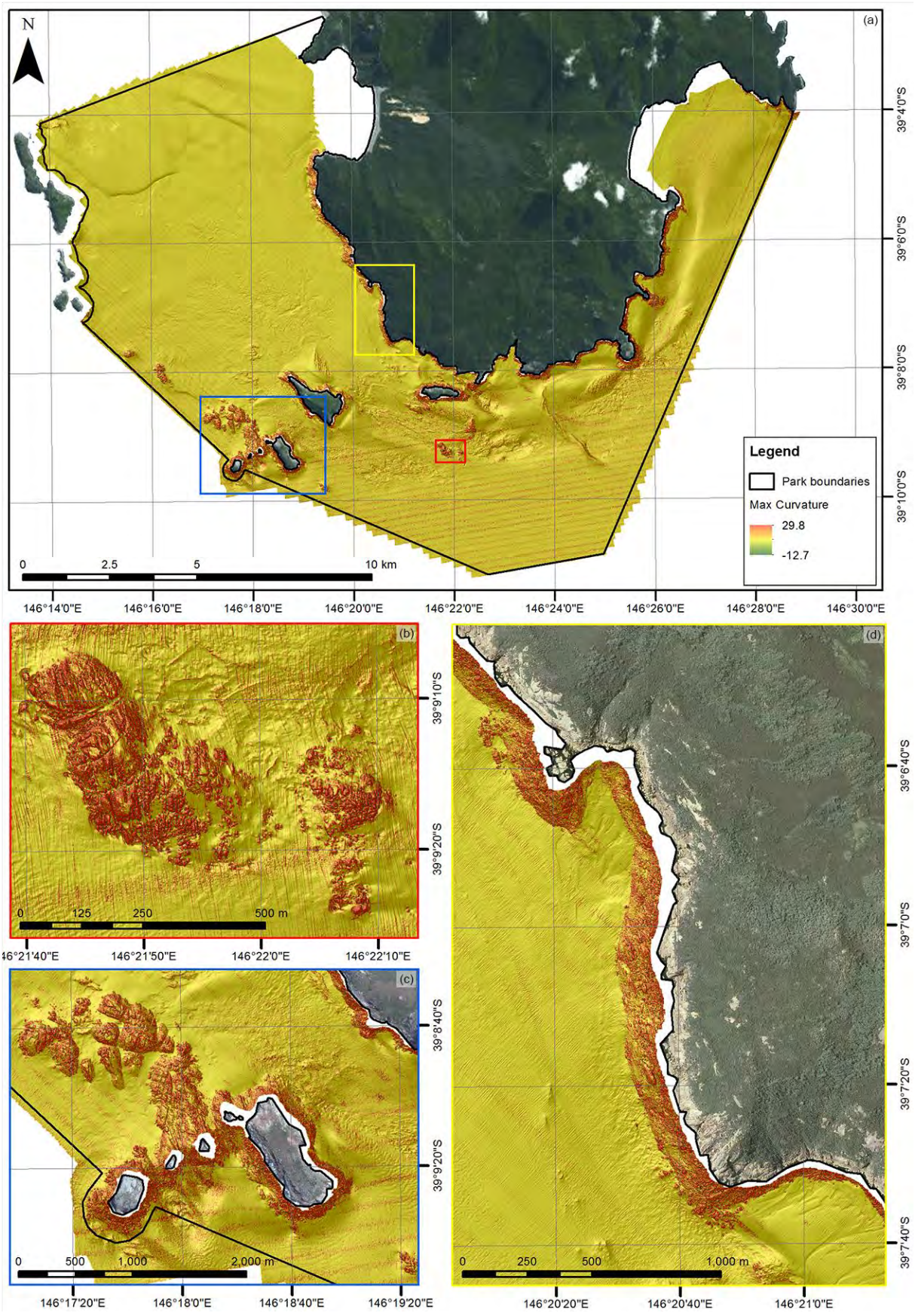

Figure 16 Maximum curvature for the entire site (a) and for selected features of interest (b, c and d).

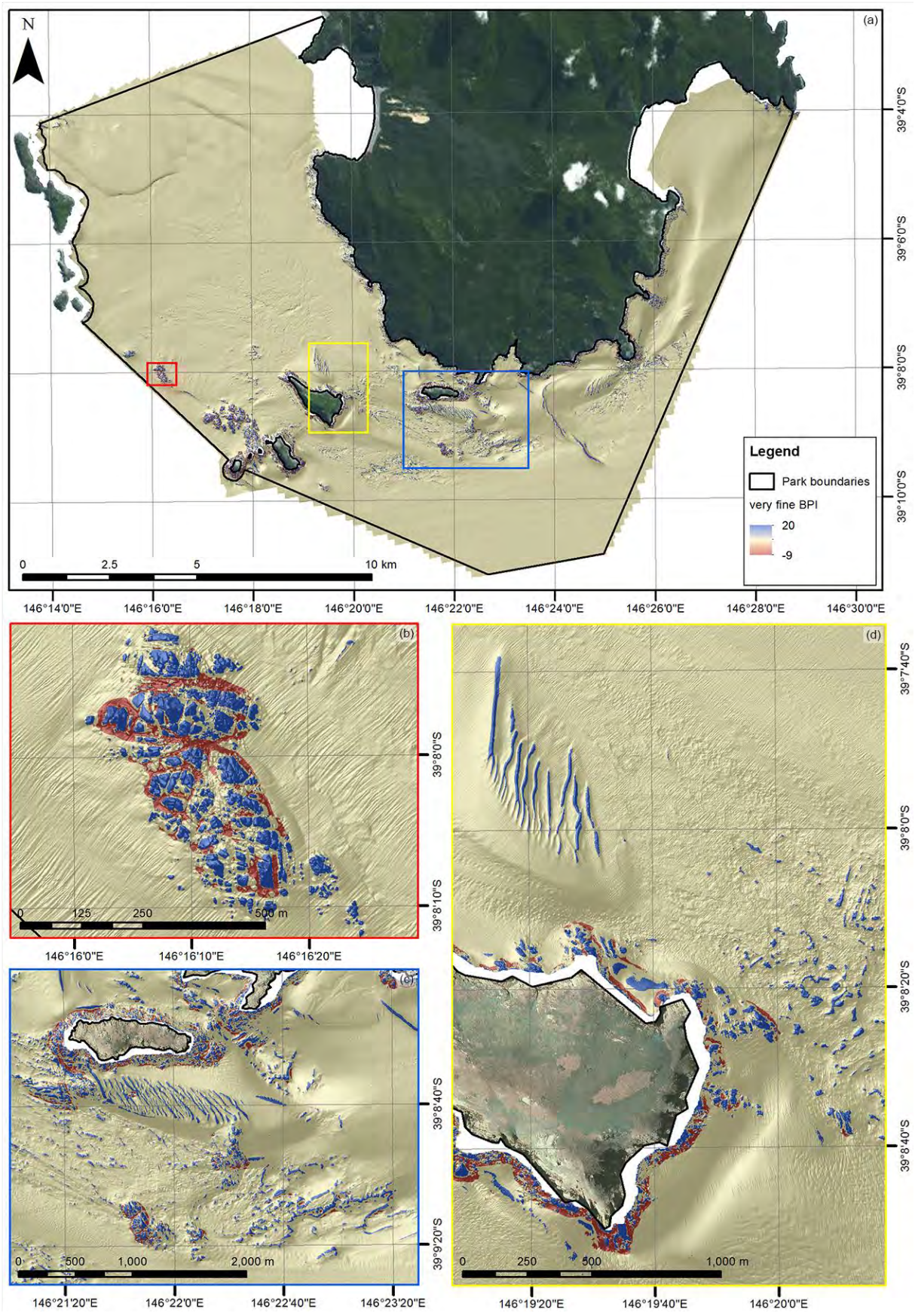

Figure 17 Very fine BPI for the entire site (a) and for selected features of interest (b, c and d).

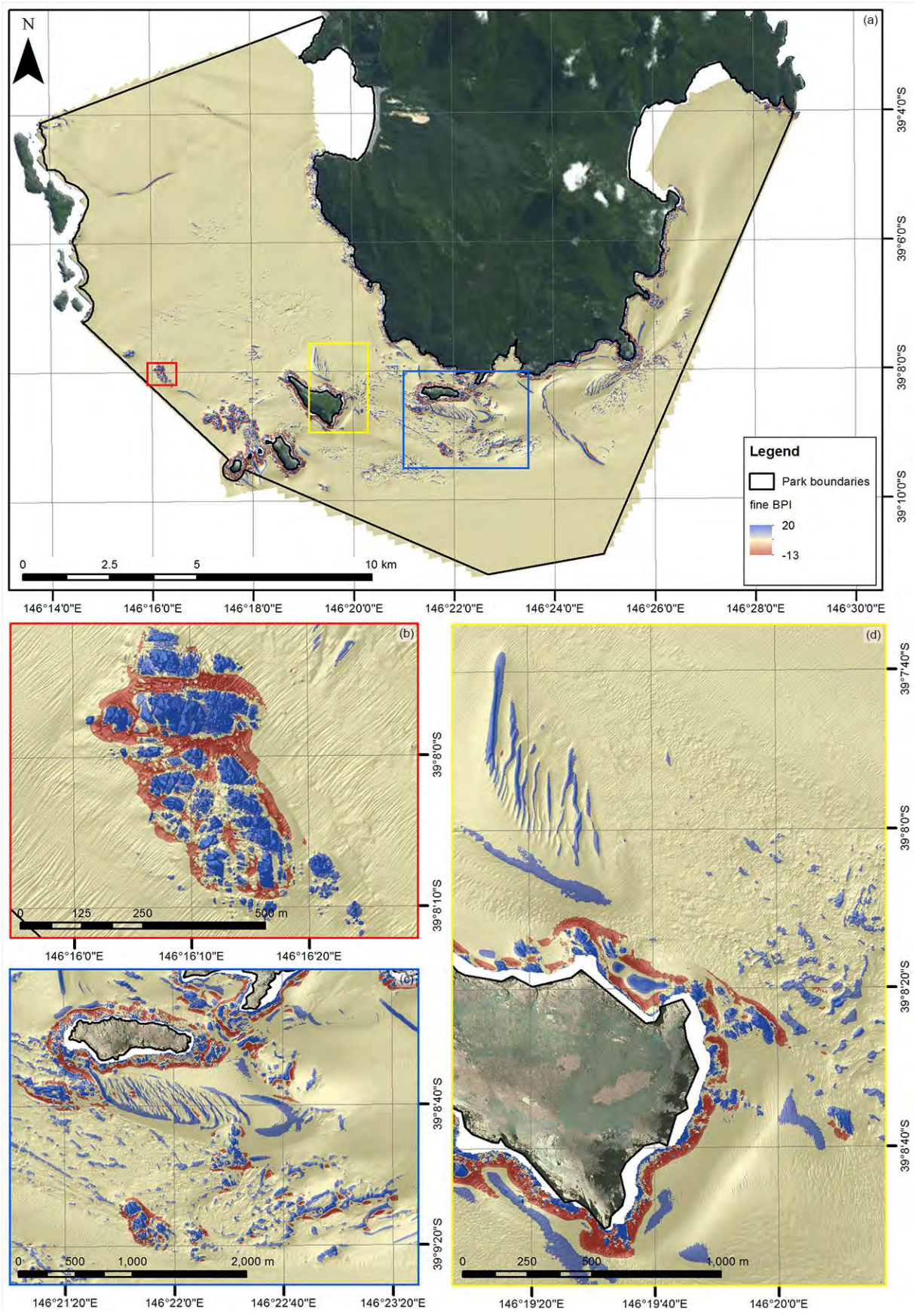

Figure 18 Fine BPI for the entire site (a) and for selected features of interest (b, c and d).

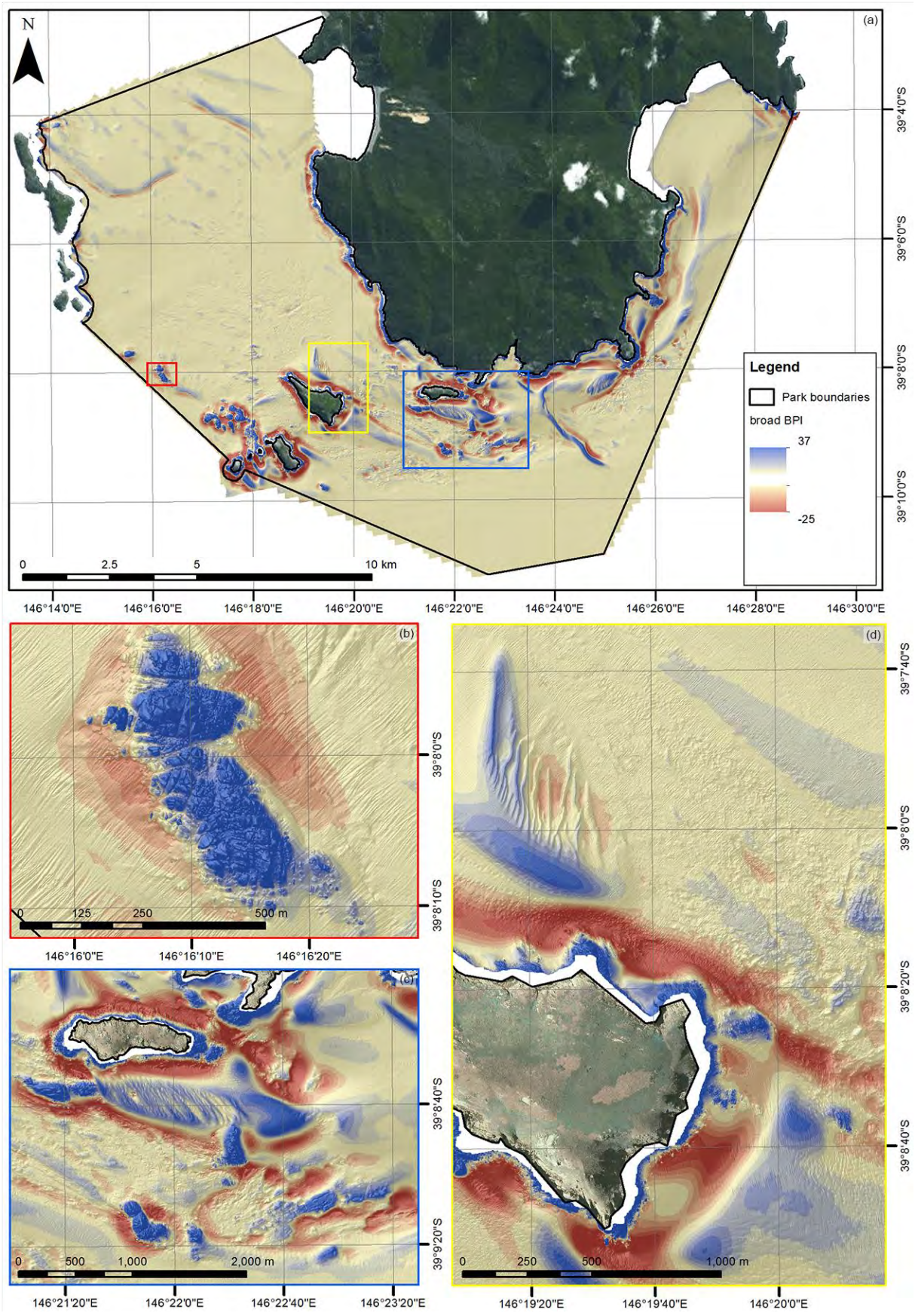

Figure 19 Broad BPI for the entire site (a) and for selected features of interest (b, c and d).

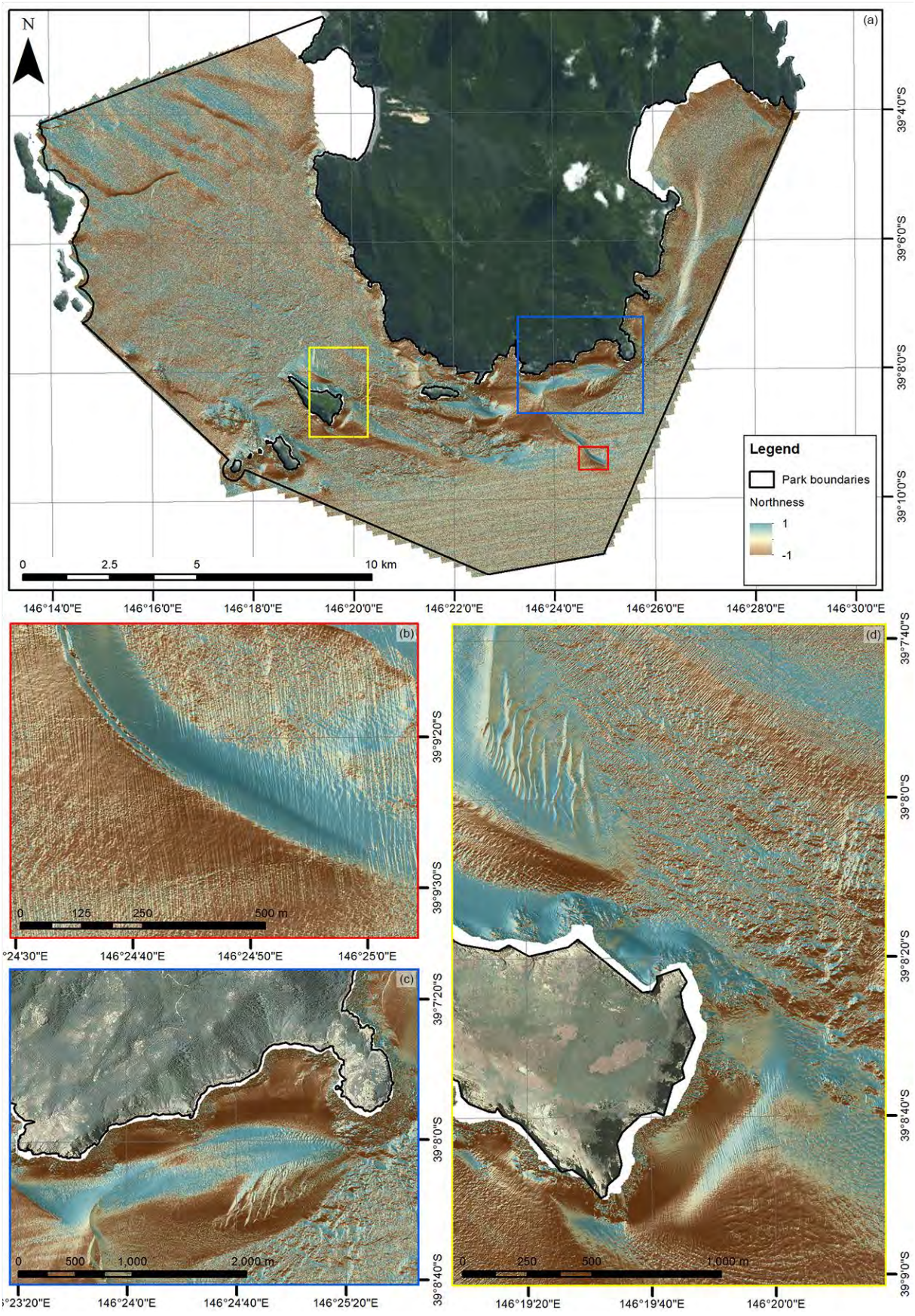

Figure 20 Northness for the entire site (a) and for selected features of interest (b, c and d).

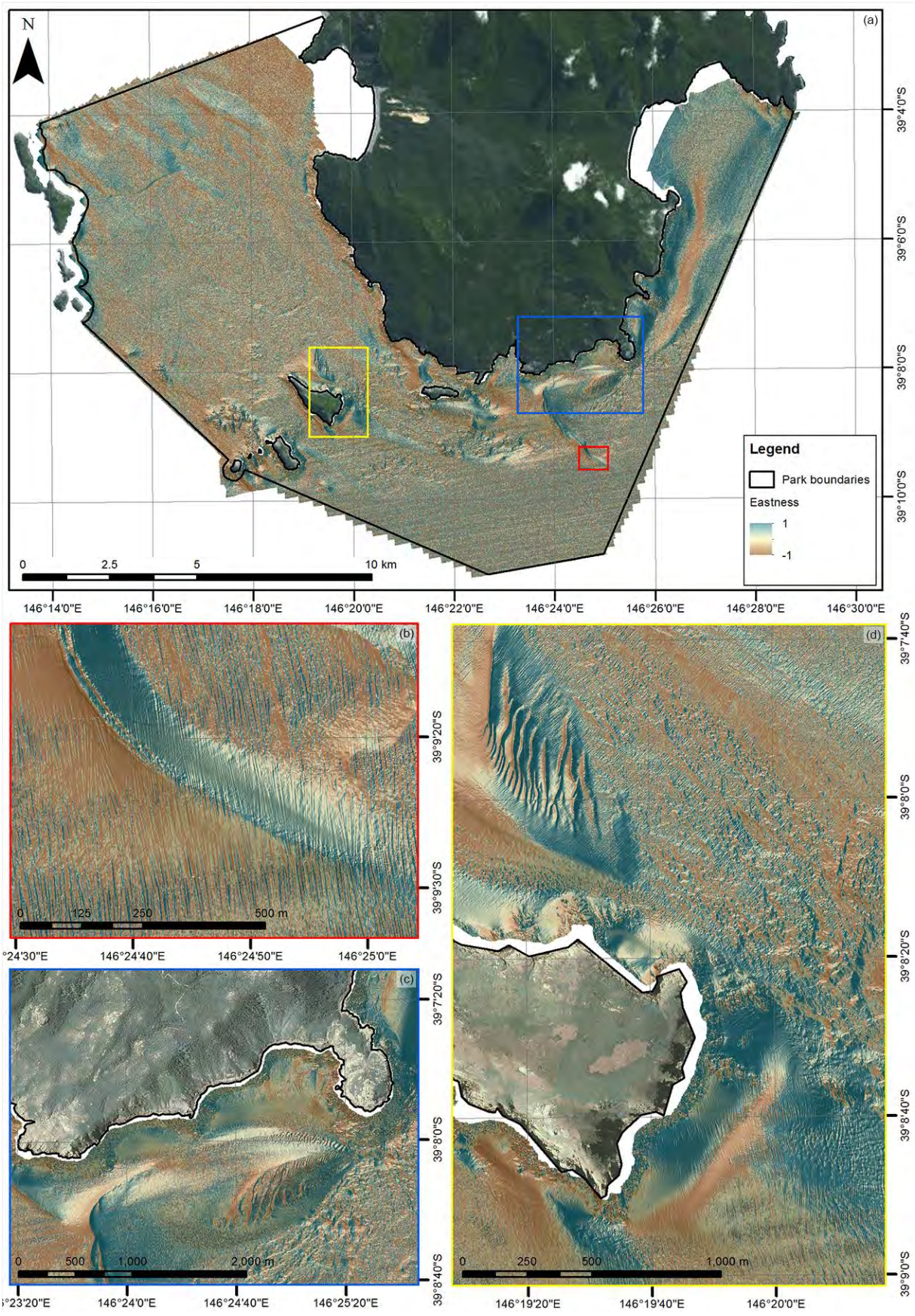

Figure 21 Eastness for the entire site (a) and for selected features of interest (b, c and d).

3.3 Backscatter derivatives

Figures 22 to 24 present the three layers derived from the coarse backscatter mosaic.

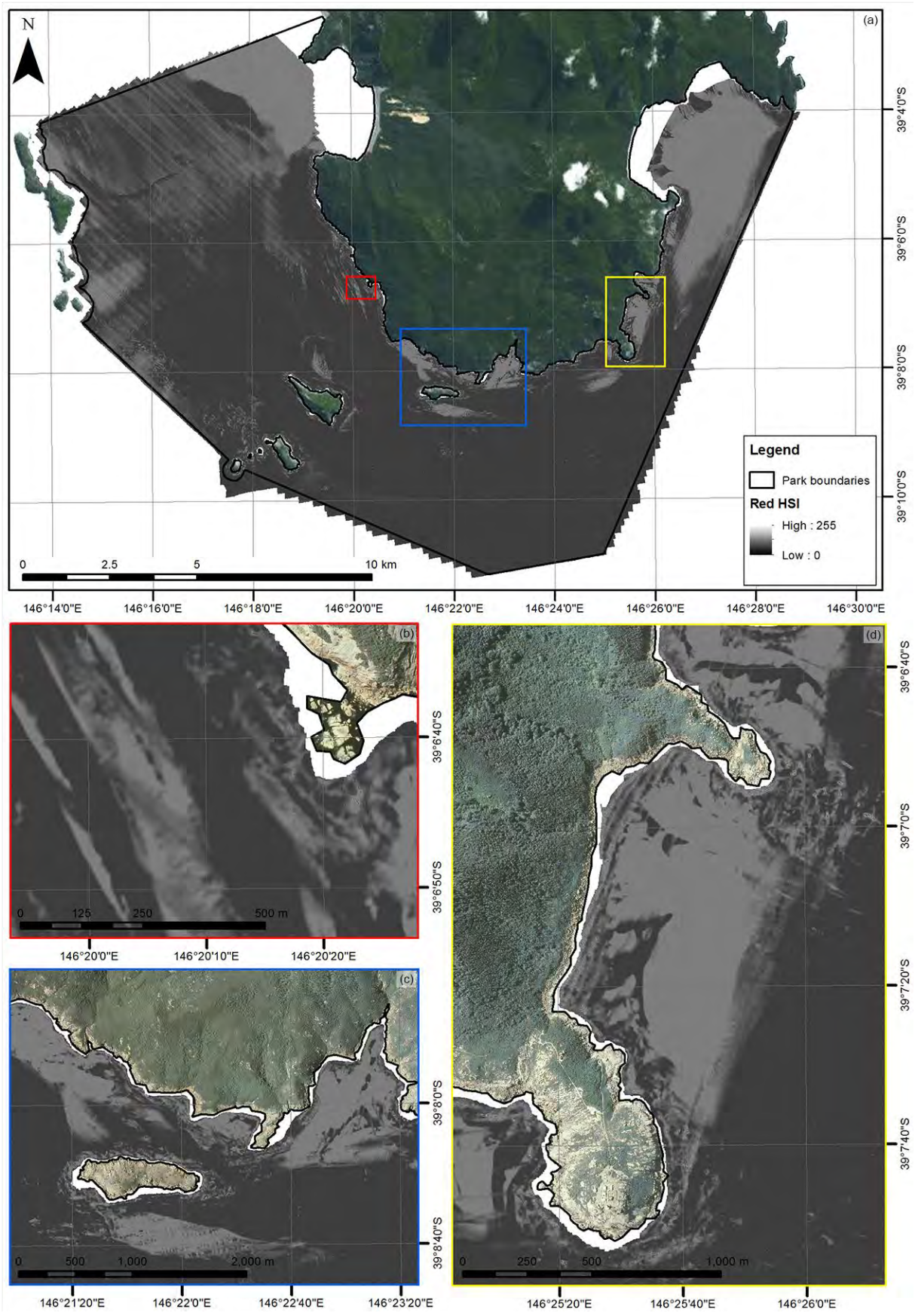

Figure 22 Red HSI for the entire site (a) and for selected features of interest (b, c and d).

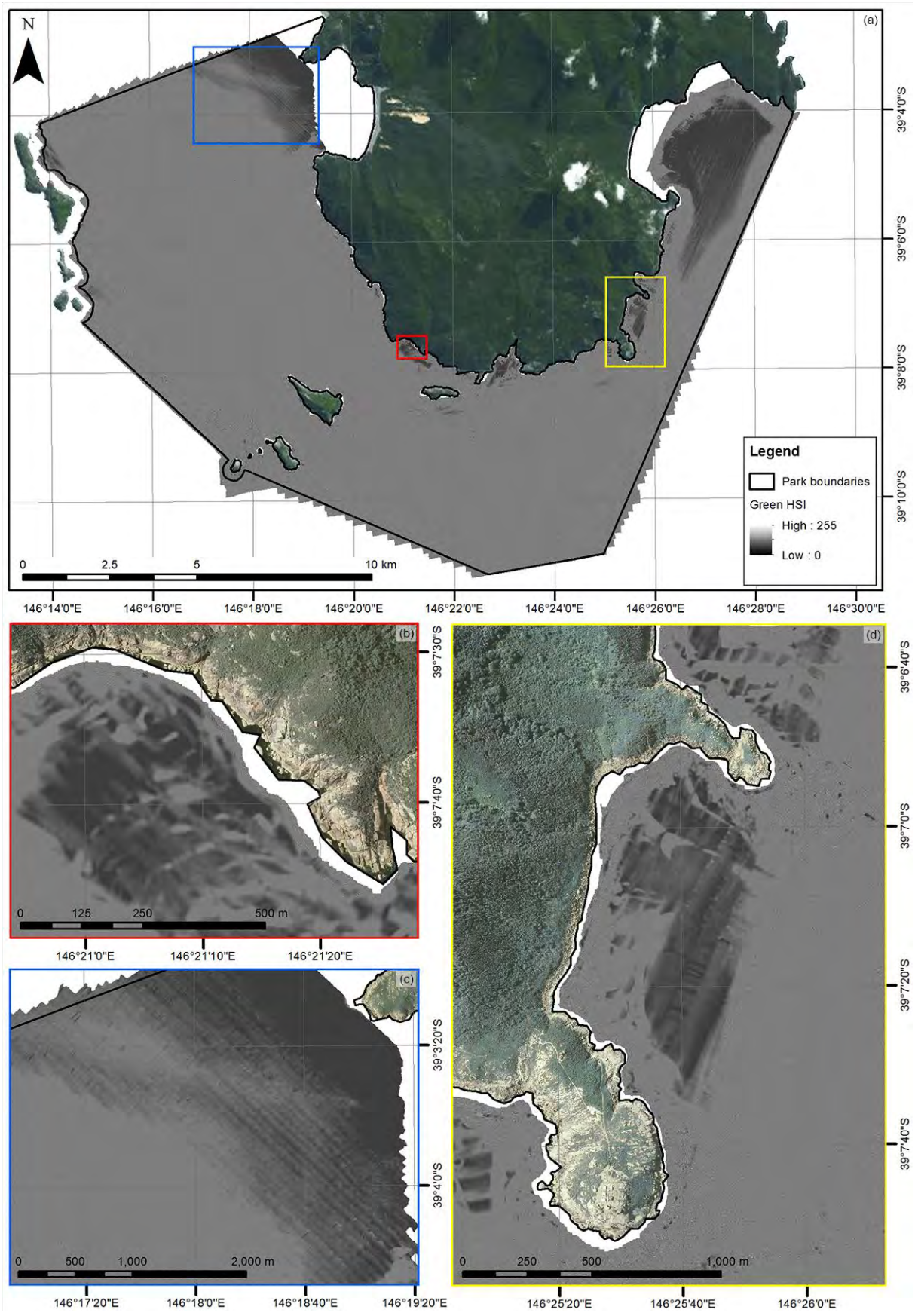

Figure 23 Green HSI for the entire site (a) and for selected features of interest (b, c and d).

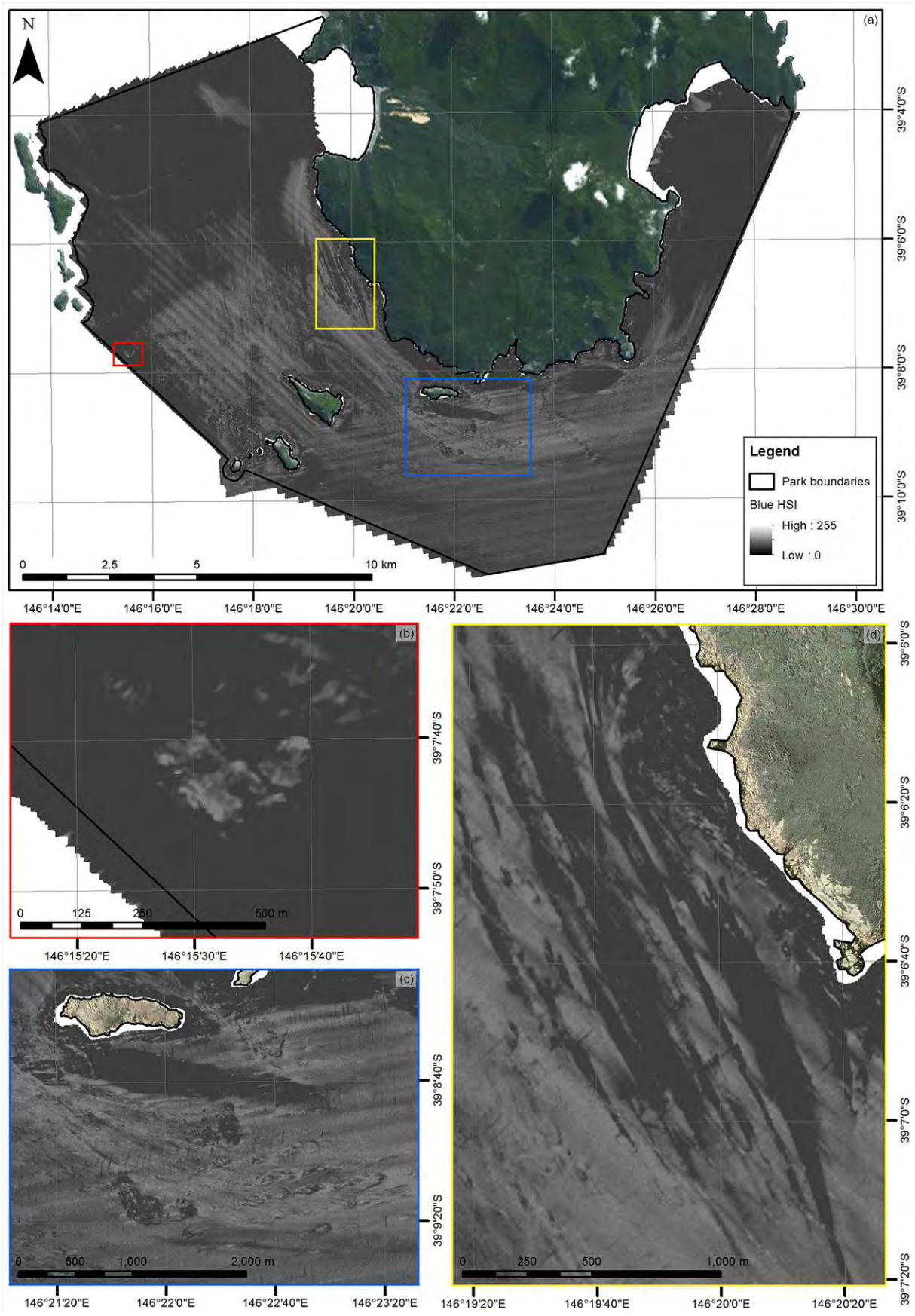

Figure 24 Blue HSI for the entire site (a) and for selected features of interest (b, c and d).

3.4 Object segmentation

Figure 25 presents the segmentation resulting from the eCognition process. The segmentation honours the boundaries of all features from the input layers, that is, any given segment is defined by an internally relatively consistent backscatter mosaic level (Figure 25b), depth (Figure 25c), complexity (Figure 25d) and bathymetric position indices (not shown on Figure 25). Figure 26 illustrates how computing the mean of a layer within each object results in a layer that is relatively similar to the original but without the spatial noise and artefacts.

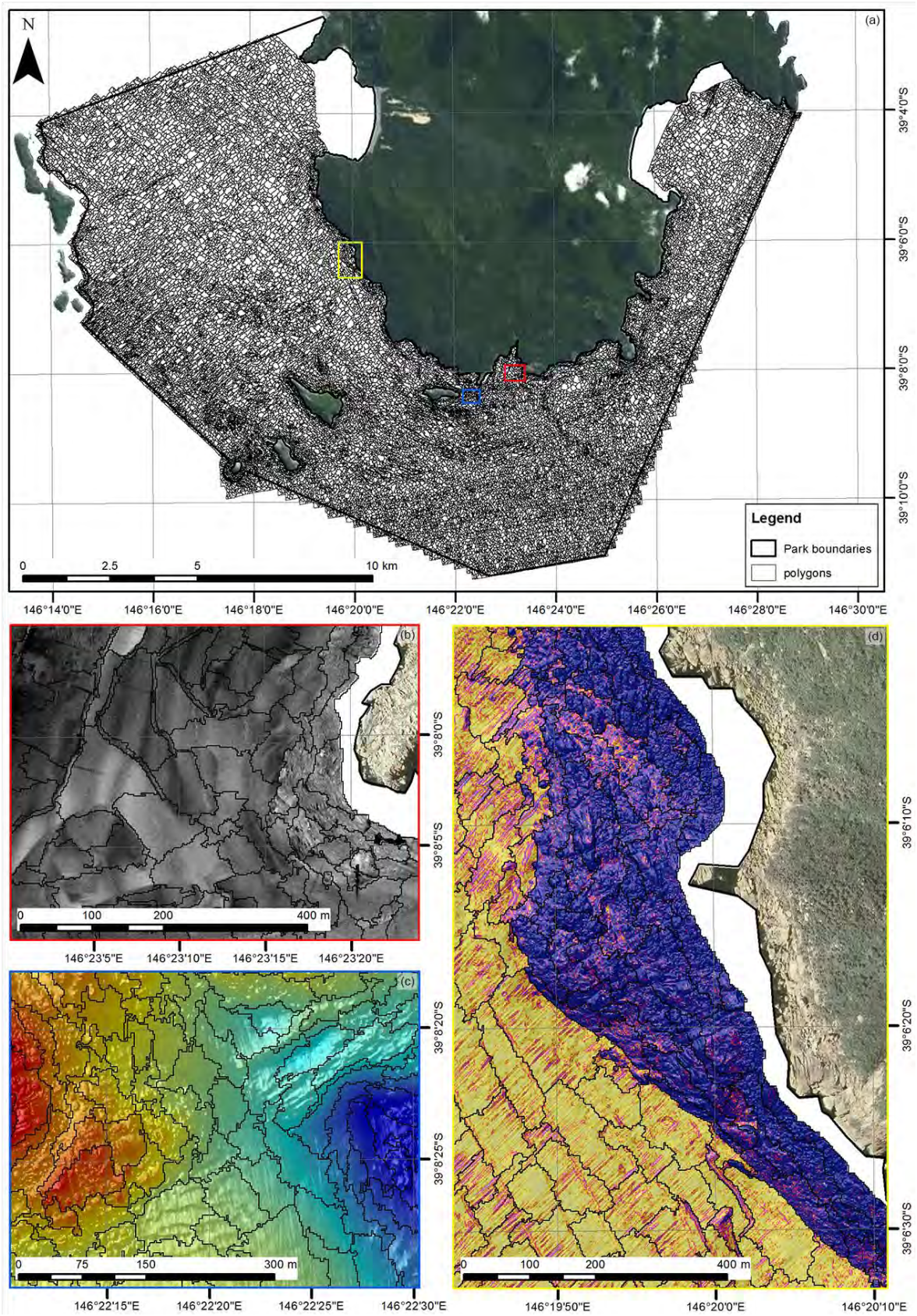

Figure 25 Result of the eCognition object-based segmentation (in plain black lines) for the entire site (a) and in selected areas over the backscatter mosaic (panel b, see Figure 12a for legend), bathymetry grid (panel c, see Figure 11a for legend) and complexity (panel d, see Figure 13a for legend).

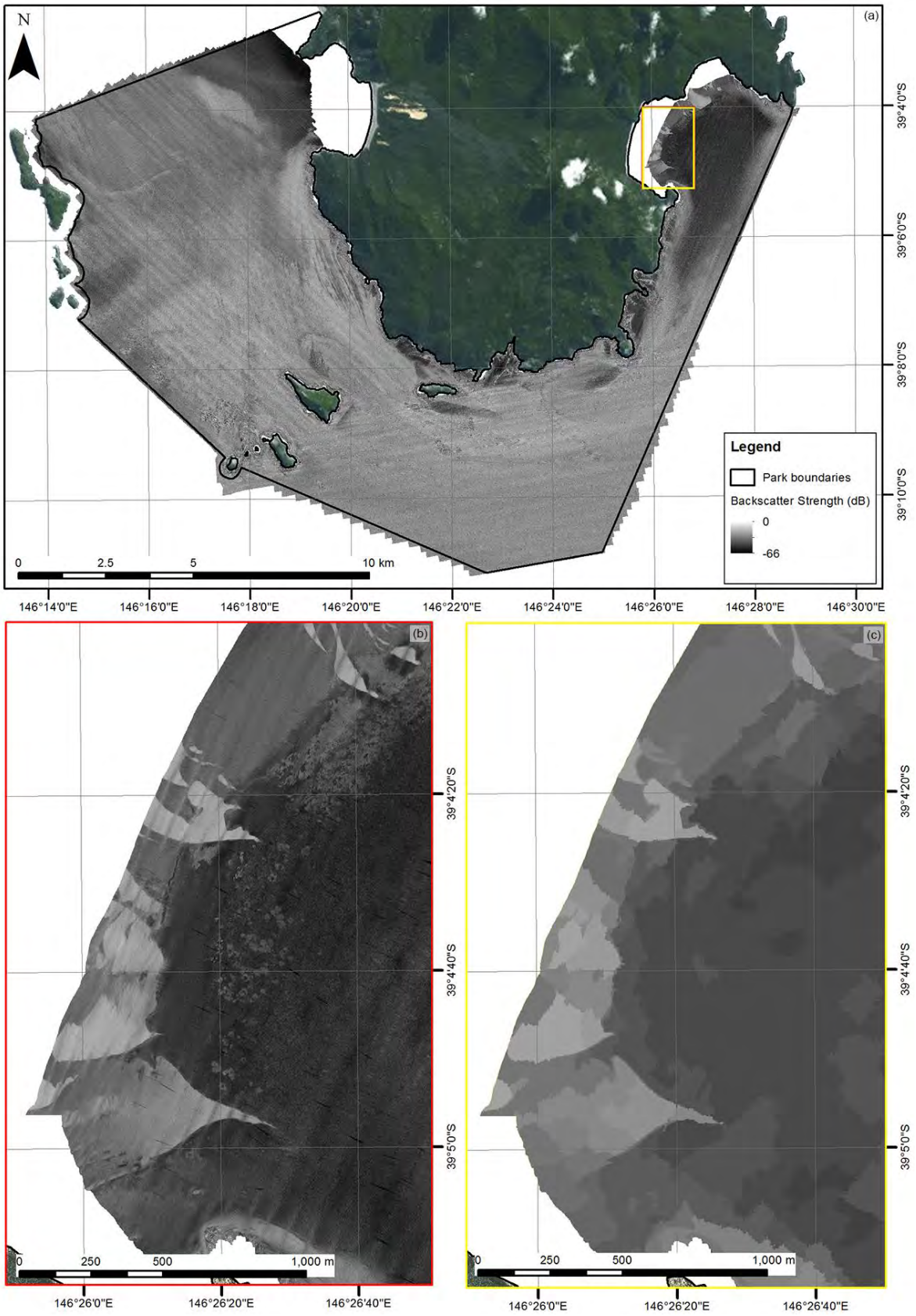

Figure 26 Original backscatter layer for the entire site (a) and a selected area in Little Waterloo Bay (b). Mean of backscatter per segment for that same selected area (c). Comparison of panels b and c illustrate how computing the mean level of the input layer per segment results in a similar layer relatively free from the artefacts in the original layer.

3.5 Clustering

Figure 27 presents the result of the process of clustering the segments from Figure 25 into ten classes on the basis of six layers (the mean and standard deviation of bathymetry, backscatter and complexity).

Many of the ten classes differ clearly on the basis of the input layers, resulting in classes delineating different habitats. For example, the shallow reefs are clearly delineated (in grey, class #8, and dark blue, class #9) from the surrounding flat, soft-sediment areas (in green, class #3, and brown, class #6), probably on the basis of the complexity and backscatter layers which represent seafloor structure (Figure 27c). Likewise, the shallow, flat areas of soft sediment are separated between the low backscatter strength areas (in light red, class #10) and high backscatter strength areas (in light blue, class #1) (Figure 27d).

However, the process is imperfect. First, some apparently artificial delineations are evident: the flat, deep, sandy southern part of the site appear as two classes (dark red, class #10 and yellow, class #4, Figure 27b), with the difference seemingly due to artefacts as demonstrated by the East-west lines patterns (Figure 27a). This artefact is likely driven by outer beams having a higher bathymetry standard deviation, affecting the complexity derivative. Second, any given class might not represent an individual seabed type or habitat. For example, class #7 in pink appears to cover the deep, complex bedrock (Figure 27c) as well as the sediment ridge in the South East of the site (Figure 27a).

These observations should not be mistaken as failures. This methodology is not a habitat mapping procedure; its only purpose is to target the variability of the environmental datasets in the subsequent ground-truthing. In this context, it is important that any variability induced by artefacts be targeted in ground-truthing so that they don't affect the subsequent habitat mapping procedure. Likewise, the fact that any class might cover several habitat types implies that these habitats are difficult to delineate on the basis of the environmental datasets. Therefore, it is important that these areas be targeted in the ground-truthing effort so that the future habitat mapping procedure can lift the ambiguity.

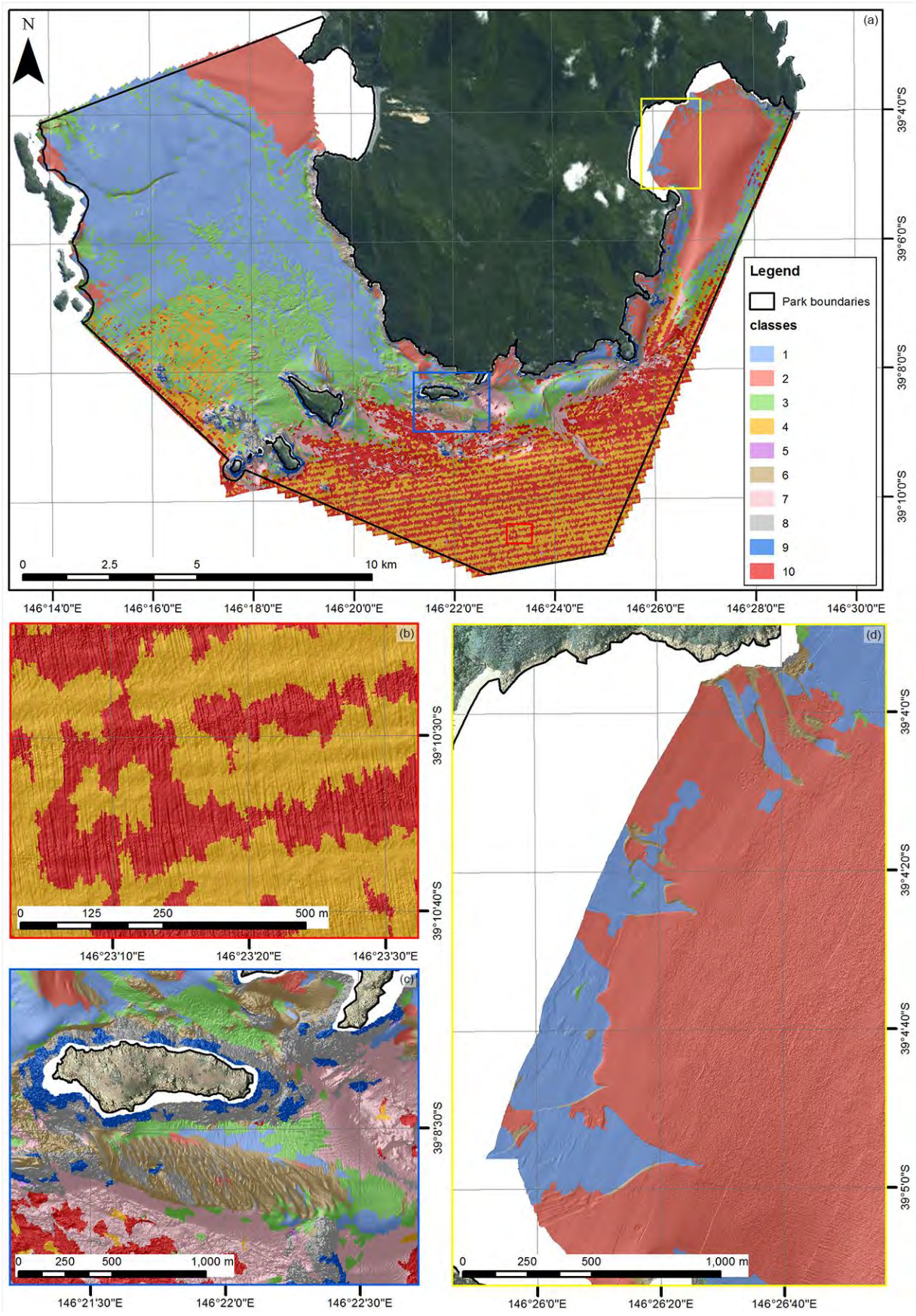

Figure 27 Clusters for the entire site (a) and for selected features of interest (b, c and d).

3.6 Ground-truth points

Figure 28 presents the points colour coded for each of the ten classes. The location of those points is provided in appendix B.

A visual analysis of the points created in that way reveals that most seafloor features of interest are represented in the survey design. Note that if a same habitat was represented by two (or more) classes because of artefacts impacting the process (such as the dark red and yellow classes—#10 and #4—discussed previously), this habitat type will get sampled twice as much (or more) as other habitats. Conversely, if a unique class overlapped two different habitats because they could not be delineated on the basis of the input layers, these two habitat types will get sampled half as much as other habitats. Hence the need for a maximum of locations being targeted for each class identified.

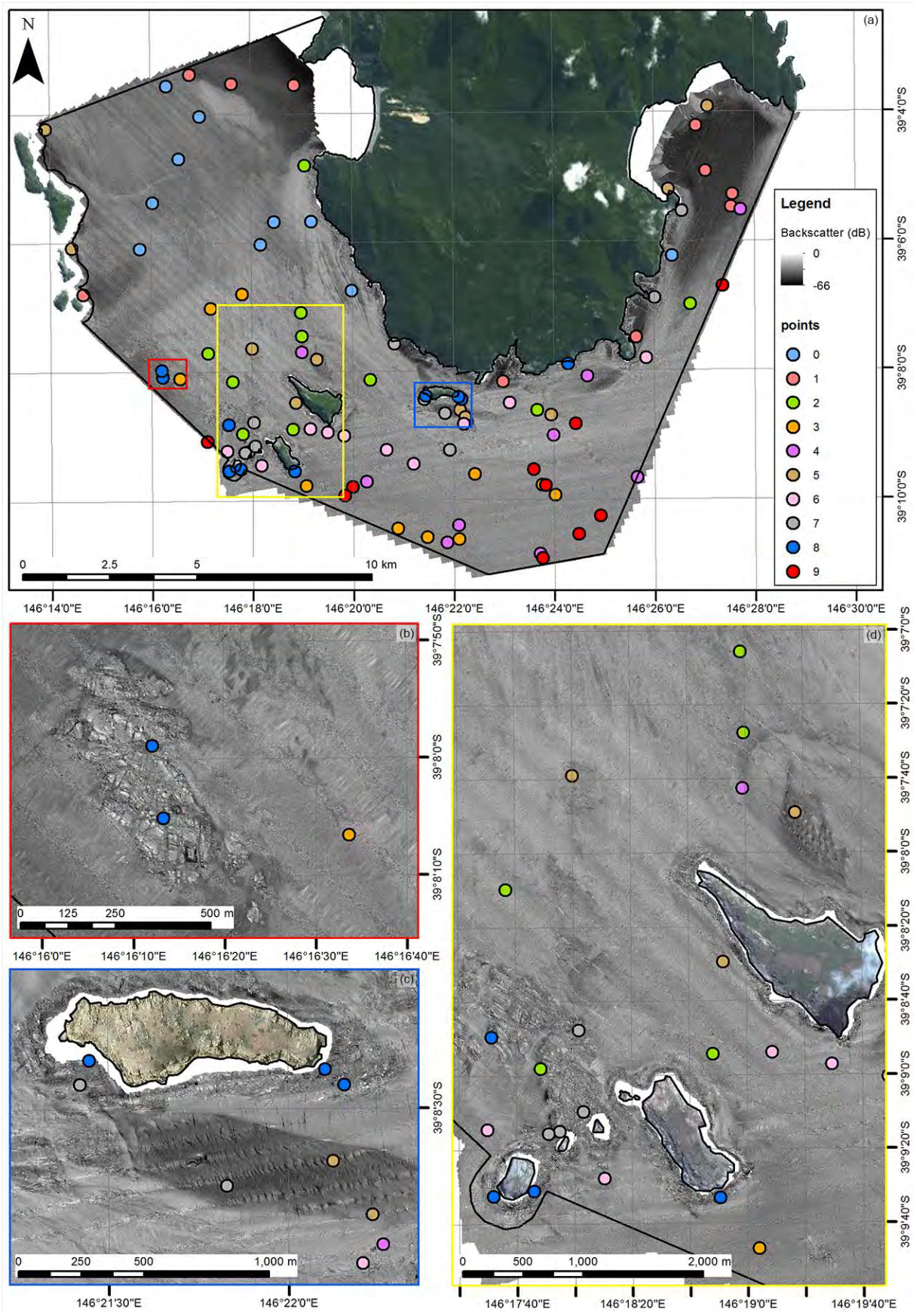

Figure 28 Ground-truthing suggested locations over backscatter mosaic for the entire site (a) and for selected features of interest (b, c and d).

4. Conclusion

Previous monitoring programs have observed that the WPMNP is composed of a wide range of habitats that support a high biodiversity due to the park's unique location in the mixing zone of warmer waters of the eastern Australian coast and the colder waters of western Bass Strait. Until now however, the WPMNP only had a small proportion of its seafloor area mapped. Parks Victoria required a complete MBES hydroacoustic survey of the seafloor of the WPMNP to be undertaken to provide a number of geographical products to be used for the purposes of future habitat mapping efforts.

The survey design was adapted to the exposed location and successfully resulted in the WPMNP being surveyed so as to achieve 100% coverage in combination with the Lidar bathymetric data (objective #1). The MBES data were then processed into a bathymetry grid and a backscatter mosaic at 1 m and 5 m resolution (objective #2). A suite of derivative products were developed from these original datasets to characterise the variability in acoustic terrain and acoustic facies and assist in future predictive modelling applications (objective #4). One immediate of such applications was the determination—through an automatic process—of a survey plan of 100 sampling locations to be used as guidelines/priorities for the future biological sampling (objective #5).

Water column data (objective #3) were not acquired during the survey of the WPMNP for three reasons. First, in the absence of ground-truth data, we had limited knowledge of the potential habitats to be detected with water-column data, with limited means of verification. Second, water-column data have a significantly higher volume than seafloor data (by a factor of 9 to 12), implying that a complete coverage of water-column data over the WPMNP would have led to significant issues in terms of management and backup of the resulting data volume (projected to be over one terabyte, instead of the final 120GB), especially given the remote conditions of the study site. Finally, with challenging weather conditions, the team elected to focus on the priority task of covering the entire site (objective #2). Water column data collection was later trialled in a known, controlled environment, with less data volume acquisition, in a less remote location, on the Hopkins Bank near Warrnambool, VIC. Appendix E is a presentation of the initial results of this research, presented at the GeoHab 2014 conference.

5. Acknowledgements

The MBES data were collected with the help of Sean Blake and Alex Rattray (Deakin University), and processed with the help of Richard Zavalas (Deakin University) and Marlus Diesing (CEFAS, Lowestoft, UK). We are deeply grateful for the assistance of Parks Victoria regional staff, in particular the supporting rangers at the Tidal River station in the Wilsons Promontory National Park for letting us use the Refuge Cove hut for the duration of the survey, and checking on our safety with daily call ins and constant radio contact. We also thank Gippsland Ports and the Port Welshpool coastguards for their assistance, opportunistic office and accommodation and their knowledge of local navigation and oceanographic conditions.

6. References

Benz U.C., Hofmann P., Willhauck G., Lingenfelder I. & Heynen M. (2004). Multi-resolution, object-oriented fuzzy analysis of remote sensing data for GIS-ready information. ISPRS Journal of Photogrammetry & Remote Sensing 58, 239–258.

Blaschke T. (2010). Object based image analysis for remote sensing. ISPRS Journal of Photogrammetry & Remote Sensing 65, 2–16.

Calder B.R. & Mayer L.A. (2003). Automatic processing of high-rate, high-density multibeam echosounder data. Geochemistry Geophysics Geosystems 4, 1048.

Che Hasan R., Ierodiaconou D., Laurenson L. & Schimel A.C.G. (2014). Integrating multibeam backscatter angular response, mosaic and bathymetry data for benthic habitat mapping. PloS One 9, e97339.

Daily M. (1983) Hue-saturation-intensity split-spectrum processing of Seasat radar imagery. Photogrammetric Engineering and Remote Sensing 49, 349–355.

Diesing M., Green S.L., Stephens D., Lark R.M., Stewart H.A. & Dove D. (2014). Mapping seabed sediments: Comparison of manual, geostatistical, object-based image analysis and machine learning approaches. Continental Shelf Research 84, 107–119.

Drăguţ L., Csillik O., Eisank C. & Tiede, D. (2014). Automated parameterisation for multi-scale image segmentation on multiple layers. ISPRS Journal of Photogrammetry and Remote Sensing 88, 119–127.

Ierodiaconou D., Burq S., Reston M. & Laurenson L. (2007) Marine benthic habitat mapping using multibeam data, georeferenced video and image classification techniques in Victoria, Australia. Journal of Spatial Science 52, 93–104.

Ierodiaconou D., Monk J., Rattray A., Laurenson L. & Versace V.L. (2011) Comparison of automated classification techniques for predicting benthic biological communities using hydroacoustics and video observations. Continental Shelf Research 31, S28–S38.

Kennedy D.M., Ierodiaconou D. & Schimel A.C.G. (2014). Granitic coastal geomorphology: applying integrated terrestrial and bathymetric LiDAR with multibeam sonar to examine coastal landscape evolution. Earth Surface Processes and Landforms 39, 1663–1674.

Lucieer V.L. (2008). Object-oriented classification of sidescan sonar data for mapping benthic marine habitats. International Journal of Remote Sensing 29, 905–921.

Lucieer V. & Lamarche G. (2011). Unsupervised fuzzy classification and object-based image analysis of multibeam data to map deep water substrates, Cook Strait, New Zealand. Continental Shelf Research 31, 1236–1247.

Lundblad E.R., Wright D.J., Miller J., Larkin E.M., Rinehart R., Naar D.F., Donahue B.T., Anderson S.M. & Battista T. (2006). A benthic terrain classification scheme for American Samoa. Marine Geodesy 29: 89–111.

Rattray A., Ierodiaconou D., Laurenson L., Burq S. & Reston M. (2009). Hydro- acoustic remote sensing of benthic biological communities on the shallow South East Australian continental shelf. Estuarine, Coastal and Shelf Science 84: 237– 245.

Schmidt J., Evans I.S. & Brinkmann J. (2003). Comparison of polynomial models for land surface curvature calculation. International Journal of Geographical Information Science 17, 797–814.

Weiss A.D. (2001). Topographic positions and landforms analysis (Conference Poster). ESRI International User Conference. San Diego, CA

Wilson M.F.J., O'Connell B., Brown C., Guinan J.C. & Grehan A.J. (2007). Multiscale terrain analysis of multibeam bathymetry data for habitat mapping on the Continental Slope. Marine Geodesy 30, 3–35.

7. Appendix A

Appendix A: Metadata for bathymetry and backscatter processing

Metadata. Alexandre Schimel 25th July 2014.

Location: Wilsons Promontory Marine National Park, Victoria, Australia

Equipment: Kongsberg EM2040c Multibeam sonar + Applanix POS MV Wavemaster, Yolla RV

Authors: Daniel Ierodiaconou, Alexandre Schimel, Sean Blake, Alex Rattray. DEAKIN UNIVERSITY

Acquisition Date: 9th to 18th April 2013, 27th May to 11th June 2013

Position processing: POSPAC MMS 6.2
- mode: Real-time Navigation (Marinestar)
- export: real time navigation in GDA94

Bathymetry processing: CARIS HIPS&SIPS 8.1.6
- heave: Delayed
- attitude/navigation: real-time
- BASE surface: CUBE (1A)
- resolution: 1m and 5m (generalized in filenames below as Xm)

#exports:
-> geotif/WP_Z_Xm_UTM55S_f.tif: BASE surface exported as a 24Bit compressed tiff file. Depth range 0-95m, vertical exaggeration x3
-> xyz/WP_Z_Xm_GDA94_f.txt: gridded xyz exported in geographical coordinates (8dp precision), vertical reference GDA94 ellipsoid.
-> xyz/WP_Z_Xm_UTM55S_GDA94_f.txt: gridded xyz exported in UTM projection zone 55 South, vertical reference GDA94 ellipsoid.

Backscatter processing: IVS FMGT 7.4.1
- AVG: Trend 300 pings
- sonar type: EM2040
- mosaic settings: Blend 50%
- resolution: 1m and 5m (generalized in filenames below as Xm)

exports:
-> geotif/WP_BS_Xm_UTM55S_f.tif: mosaic exported as a grayscale tif scaled between -31dB (low reflectivity, dark) and -8dB (high reflectivity, light).
-> fledermaus/WP_BS_Xm_UTM55S_f.sd: mosaic exported as a SD file

Other final products: IVS Fledermaus 7.4.1

#exports:

-> fledermaus/WP_Z_Xm_UTM55S_GDA94_f.sd: imported WP_Z_Xm_UTM55S_GDA94_f.txt, sign inverted (depth now negative).
-> fledermaus/WP_Zi_Xm_UTM55S_GDA94_f.sd: bathy interpolated (interpolation parameters simple,3,5)
-> fledermaus/WP_ZiBS_Xm_UTM55S_GDA94_f.sd: mosaic drapped on interpolated bathy
-> fledermaus/WP_ZiC_Xm_UTM55S_GDA94_f.sd: bathy contours at 0, -1, -2, -5, -10, -15, -20, -25, -30, -40, -50, -60, -70, -80 and -90m

-> googleearth/WP_Zi_Xm_UTM55S_GDA94_f.kmz: idem as above, exported to googleearth format
-> googleearth/WP_ZiBS_Xm_UTM55S_GDA94_f: idem as above, exported to googleearth format
-> googleearth/WP_ZiC_Xm_UTM55S_GDA94_f.kml: idem as above, exported to googleearth format

-> geotif/WP_Zi_Xm_UTM55S_f.tif: idem as above, exported to geotif format

-> arcgis/WPMNP_Xm.gdb: ArcGIS geodatabase containing the Z, Zi and BS layers

NOTE:
Fledermaus products (.sd files) are viewable with free software iView4d by QPS

(http://www.qps.nl/display/fledermaus/iview)

8. Appendix B

Appendix B: Suggested prioritized ground-truth point location (in UTM projection, zone 55S).

Class #	Easting (m)	Northing (m)
0	441181.6	5672489
0	442346.1	5670510
0	439724.6	5671827
0	437379.2	5674279
0	440119.2	5672483
0	437969.7	5675489
0	437015	5676360
0	451520.7	5671532
0	436277.4	5671694
0	436635.7	5673025
1	453213.2	5672947
1	440688.3	5676411
1	450510.2	5669204
1	438885.6	5676428
1	446690.5	5667921
1	452210.4	5675269
1	434660.8	5670372
1	452485.1	5673968
1	453249.7	5673302
1	437678.9	5676703
2	440895.9	5669877
2	440671.8	5666527
2	447674.9	5667104
2	440923.8	5669202
2	440989.6	5674096
2	442885.7	5667957
2	439235.1	5666400
2	452051.8	5670149
2	438230.4	5668710
2	438943.8	5667889
3	444533.9	5663446
3	443682.8	5663694
3	437430	5667975
3	439205.5	5670406
3	445882.2	5665264
3	445446.5	5663398
3	448196.7	5664662
3	438305	5669992
3	441059.2	5664911
3	447815.9	5664960
4	445095.7	5663298
4	453494.1	5672863
4	448143.6	5666385
4	449109.4	5668086
4	447767.5	5662980
4	445649.4	5666768
4	442793.4	5665033
4	445428.3	5663788
4	440914.6	5668743
4	450541.5	5665172

Class #	Easting (m)	Northing (m)
5	440754.5	5667293
5	451419.5	5673449
5	439498.4	5668841
5	434322.3	5671700
5	441352.5	5668540
5	448076.2	5666954
5	433561.2	5675118
5	445449.8	5667104
5	445607.5	5666888
5	452540.3	5675819
6	441163.9	5666544
6	445568.5	5666694
6	441661.3	5666446
6	443350.8	5665953
6	444127.4	5665547
6	439769.4	5665488
6	446875.8	5667304
6	442130.7	5666346
6	438793.7	5665890
6	450796.7	5668605
7	451807.9	5672824
7	443571	5669000
7	439397.1	5665877
7	445163.3	5665957
7	439303.7	5665858
7	451034.2	5670328
7	444435.2	5667407
7	439592.5	5666043
7	439553.8	5666719
7	445025.4	5667002
8	445492.7	5667407
8	448548.5	5668420
8	444473.3	5667502
8	439184.3	5665380
8	438846.2	5665335
8	436941.7	5668017
8	440732.6	5665331
8	438824.8	5666661
8	445415.5	5667470
8	436912.1	5668209
9	442390.3	5664888
9	448865.5	5663549
9	449488.4	5664074
9	447576.2	5665399
9	438216.9	5666178
9	447924.4	5664943
9	448773.7	5666715
9	452975.9	5670675
9	442168	5664641
9	447827.7	5662847

9. Appendix C

EARTH SURFACE PROCESSES AND LANDFORMS
Earth Surf. Process. Landforms **39**, 1663–1674 (2014)

Published online 9 July 2014 in Wiley Online Library
(wileyonlinelibrary.com) DOI: 10.1002/esp.3615

Granitic coastal geomorphology: applying integrated terrestrial and bathymetric LiDAR with multibeam sonar to examine coastal landscape evolution

David M. Kennedy,[1]* Daniel Ierodiaconou[2] and Alexandre Schimel[2]
[1] Department of Resource Management and Geography, The University of Melbourne, Parkville, VIC 3010, Australia
[2] Centre for Integrative Ecology, School of Life and Environmental Sciences, Deakin University, Warrnambool, VIC 3280, Australia

Received 21 January 2014; Revised 14 May 2014; Accepted 9 June 2014

*Correspondence to: David M. Kennedy, Department of Resource Management and Geography, The University of Melbourne, Parkville VIC 3010, Australia.
E-mail: davidmk@unimelb.edu.au

ESPL
Earth Surface Processes and Landforms

ABSTRACT: Coasts composed of resistant lithologies such as granite are generally highly resistant to erosion. They tend to evolve over multiple sea level cycles with highstands acting to remove subaerially weathered material. This often results in a landscape dominated by plunging cliffs with shore platforms rarely occurring. The long-term evolution of these landforms means that throughout the Quaternary these coasts have been variably exposed to different sea level elevations which means erosion may have been concentrated at different elevations from today. Investigations of the submarine landscape of granitic coasts have however been hindered by an inability to accurately image the nearshore morphology. Only with the advent of multibeam sonar and aerial laser surveying can topographic data now be seamlessly collected from above and below sea level. This study tests the utility of these techniques and finds that very accurate measurements can be made of the nearshore thereby allowing researchers to study the submarine profile with the same accuracy as the subaerial profile. From a combination of terrestrial and marine LiDAR data with multibeam sonar data, it is found that the morphology of granite domes is virtually unaffected by erosion at sea level. It appears that evolution of these landscapes on the coast is a very slow process with modern sea level acting only to remove subaerially weathered debris. The size and orientation of the joints determines the erosional potential of the granite. Where joints are densely spaced (<2 m apart) or the bedrock is highly weathered can semi-horizontal surfaces form. Copyright © 2014 John Wiley & Sons, Ltd.

KEYWORDS: rocky coast; cliff; shore platform; granite; LiDAR; multibeam; joint; sea level

Introduction

Granites produce spectacular landscapes. They are typically associated with inselbergs rising high above the surrounding landscape (Migon, 2006) or, on a smaller scale, form upstanding fields of rocky outcrops known as tors (Gunnell *et al.*, 2013). Granites are generally highly resistant to weathering and erosion (Twidale, 1982; Migon, 2006) and as a result they tend to evolve over long temporal scales. For example cosmogenic dating of granitic surfaces in southern and northern Australia indicate only decimetre erosion over the past million years (Bierman and Caffee, 2013) while on inselbergs in the Namib Desert rates were only slightly higher at 1–2 mm/kyr (Matmon *et al.*, 2013).

Bare granitic rock surfaces tend to erode at lower rates than those that are mantled by soil (Granger *et al.*, 2001; Jessup *et al.*, 2011). Chemical weathering is the principle factor of erosion of subaerial granitic landscapes occurring through the alteration of feldspar minerals to clay, a process which is facilitated by moisture (Migon, 2006, Twidale, 1982). This means surficial erosional features such as pits, overhanging rims and karren are formed in a two-stage process related to initial subsurface development at the weathering front followed by modification when exposed at the surface (Twidale and Vidal Romani, 1994; Johnson and Baarli, 2005). Although the fundamental processes of weathering and erosion are understood for inland landforms relatively little is known about the erosion of granite in coastal settings (Migon, 2006).

Due to the high erosional resistance of granite, shorelines developed within it undergo slow rates of change and therefore evolve over multiple eustatic cycles (Trenhaile, 1987). For example in Maine, USA, glacial striations on cliffs formed during the last glacial maximum are still observable today and can be traced below present sea level (Shepard and Wanless, 1971). This means erosional features, such as shore platforms, are rare on contemporary granitic shores (Jutson, 1940; Hills, 1949, 1971) only forming in circumstances where the erosional resistance has been significantly reduced through weathering or structural factors (Jutson, 1940; Trenhaile *et al.*, 1999; Blanco-Chao *et al.*, 2003). The general absence of shore platforms was noted by Twidale (1982) to be the 'principle oddity' of the granite coast.

The low rates of development of granitic cliffed coasts have hindered their study as their change cannot be observed over human timescales. An additional difficulty is that much of their morphology occurs below present sea level. As contemporary granitic shores have been exposed to multiple sea levels during

the Quaternary (Rohling *et al.*, 2009) the question arises as to whether erosion, and therefore shore platform development, have been concentrated at lower elevations than today.

Recent advances in aerial and underwater remote sensing technology provide new opportunities to answer this question. Airborne LiDAR can measure land elevation and seafloor depth over large geographic extents across the land–sea interface, allowing the production of high-resolution digital elevation models, surface complexity information layers and seamless coastal geomorphology maps (Vierling *et al.*, 2008). However, the depth range of LiDAR is limited by light attenuation in the water column. For example, a maximum underwater penetration of around 25 m was observed in the cool temperate waters of southeastern Australia (Quadros and Rigby, 2010). Ship-based multibeam echosounders (MBES) allow continuous and seamless coverage of the near-shore bathymetry, as systems specifically designed for mapping in shallow waters are able to measure high-resolution bathymetry beyond the range of optical sensors (Ierodiaconou *et al.*, 2011).

These technologies therefore provide the potential to quantify contemporary shoreline morphology and provide an opportunity for comparison with the submarine profile. Accordingly, this study sets out to (i) test the utility of these new data gathering technologies for quantifying coastal and submarine morphology, and (ii) assess the degree of erosion and platform development in granite at modern and past sea levels.

Regional Setting

Wilsons Promontory (39°S, 146°22′E) is located in Victoria, at the southern limit of mainland Australia (Figure 1). It rises to an elevation of 754 m and is composed of a series of S-type monzogranite domes of middle to upper Devonian age (*c.* 380 ma) which forms part of the Central Superprovince granites and are assigned to the Bassian Basement Terrane (Rossiter, 2003). The granite is relatively high in Rb and low in Ba and Sr with occasional concentrations of garnet (Chappell *et al.*, 1988). Weathering of the granite during the Mesozoic occurred to depths of over 300 m with much of this regolith being subsequently eroded, especially at the coast (Hill and Joyce, 1995; Hill *et al.*, 1995). The topography of Wilsons Promontory is strongly influenced by tectonic activity dating after the early-Cretaceous with vertical fault movement contributing to the elevation of palaeoerosion surfaces (Hill *et al.*, 1995). There appears to be little vertical movement of the landscape during the Quaternary (Cupper *et al.*, 2003).

Wilsons Promontory is located within the shallow sea of Bass Strait connecting the Pacific Ocean in the east, Indian Ocean in the west and the Southern Ocean. Bass Strait marks the confluence of the warm waters of the Eastern Australian Current (EAC) that flow further south seasonally along the east coast and the colder waters of western Bass Strait from the South Australian Current (Edmunds *et al.*, 2012). In winter, cooler subantarctic waters are forced eastward into Bass Strait (James and Bone, 2011). Currents approaching speeds of 5.5 km/hr have been observed off Wilsons Promontory using acoustic Doppler current profilers (Lindsay, 2013). Granitic domes rising as islands off the mainland likely funnel this flow generating higher velocities between the islands and the mainland. During winter, winds are predominantly from the south-west, driving a south-westerly swell of up to 8 m in height (mean 2 m) on the west and south coast of the promontory (Figure 2). South-westerly swell dissipates as it rounds the promontory towards the east coast (maximum ~5 m). The east coast of the promontory is exposed to easterly and south-easterly swells of up to 6 m in height driven by south-easterly wind patterns in summer months (Figure 2). The region is microtidal.

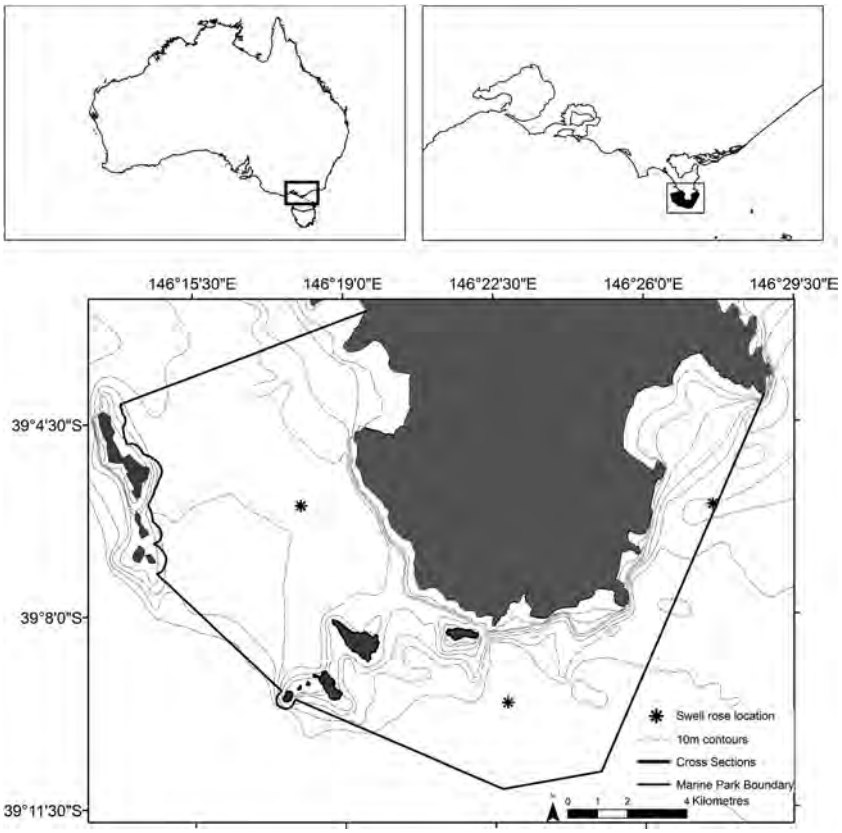

Figure 1. Location of Wilsons Promontory showing the boundaries of the Marine National Park and location of profiles derived from the LiDAR and MBES datasets.

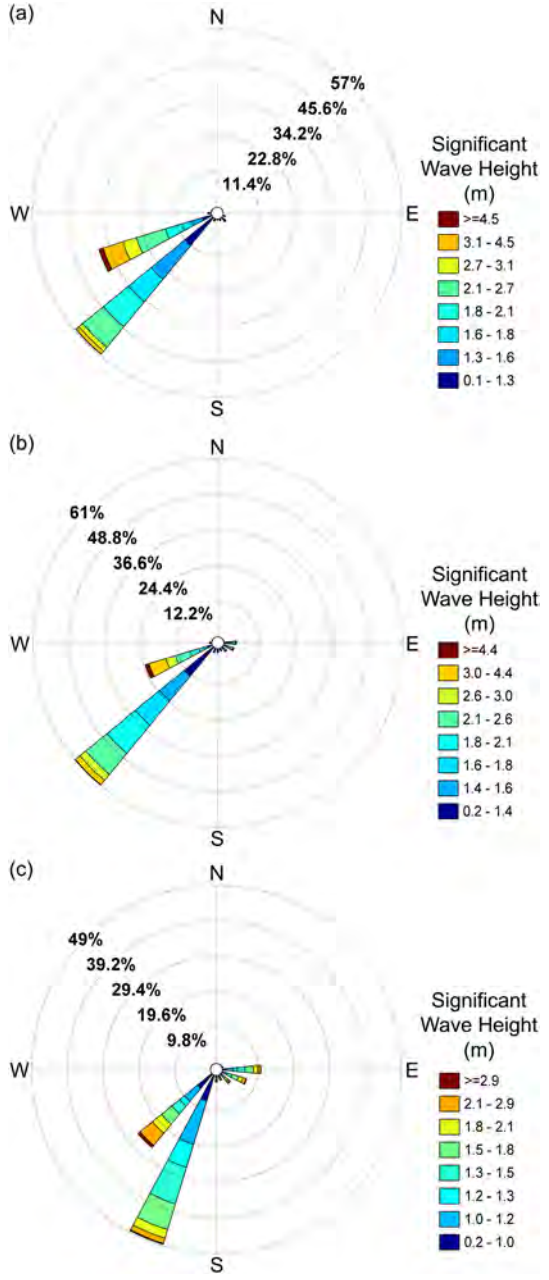

Figure 2. Directional plots of significant wave height for three locations (a) west, (b) south and (c) east of the Promontory, as indicated on Figure 1. Data were obtained from a 30-year-long wave hindcast model (1979–2009). This figure is available in colour online at wileyonlinelibrary.com/journal/espl

Methods

LiDAR data were collected in 2007 using a LADS Mk II system coupled with a GEC-Marconi FIN3110 inertial motion sensing system and a dual frequency kinematic geographic positioning system (kGPS). This dataset includes seamless terrestrial–marine mosaics from elevations of +10 m to depths of –25 m, for a surface coverage exceeding 10 000 km^2 (Quadros and Rigby, 2010). LiDAR penetration into the water column was reported to be typically 2–3 times the Secchi depth (Wang and Philpot, 2007); this information was impaired in certain areas by high turbidity and breaking waves. Flight lines for the mapping survey were spaced at approximately 220 m, with a swath width of 240 m, leading to a lines overlap of 10 m. Final raster grid comprised a continuous 5 m resolution topographic and bathymetric surface. No vegetation removal was applied to the terrestrial component. Vegetation was scarce on the field site thus we expect a limited impact on the derived LiDAR parameters and the characterization of boulders on the terrestrial slopes.

The MBES survey was conducted between the 10th of April and the 10th of June 2013 using a Kongsberg Maritime EM2040C MBES integrated with an Applanix POS MV WaveMaster fitted to a 9.2 m research vessel. The MBES was operated at a constant frequency of 300 kHz, a varying ping rate and pulse length (resp. up to 50 Hz and down to 0.025 ms) automatically adjusting to water depth, in high-density equidistant mode (400 soundings per ping) and with a constant sector coverage of +-65° athwartships. One sound speed profile was captured at the start of each day of survey with a Valeport Monitor Sound Velocity Profiler and imported in Kongsberg Maritime's acoustic data acquisition software SIS to correct soundings for variation of sound velocity in the water column. The POS MV WaveMaster measured the position of the vessel in Differential GNSS mode using GPS/GLONASS corrections received by radio from the Fugro MarineStar satellite positioning service. The POS MV WaveMaster also measured precise vessel motion data (roll, pitch, yaw, true heave). A post-processed kinematic (PPK) solution was later obtained from these position and motion data using Applanix software POSPac Mobile Mapping Suite (MMS). This solution was then integrated with the bathymetry data in CARIS software HIPS and SIPS 8.1. The soundings were manually cleaned in HIPS and SIPS and gridded at a resolution of 0.5 m.

Further spatial analysis was conducted in ArcGIS (version 10.1). Slope and terrain ruggedness were derived from the combined LiDAR and MBES bathymetry datasets. Slope is a function derivative that denotes the maximum rate of change between each pixel and its neighbours (Wilson *et al.*, 2007), while terrain ruggedness or rugosity provides a measure of the three- dimensional orientation of a grid cell, effectively capturing aspect and slope in a single measure (Sappington *et al.*, 2007). These measures were used to determine whether high ruggedness and slope values correlate to more jointing on granite outcrops. Transects were haphazardly placed across granitic features with bathymetry, slope and ruggedness values extracted at 1 and 5 m intervals for MBES and LiDAR underlying coverage, respectively to provide bedform profiles. In areas of overlap between the two datasets, data points are extracted from the MBES survey due to its higher spatial resolution. Fixed point values were extracted every 100 m along contours at 5 m intervals to determine the average bedrock slope between 10 m above and below MSL.

Only in locations where waves are breaking do data gaps exist in the otherwise seamless dataset combination as LiDAR cannot penetrate the turbulent water and the depth is too shallow for ships to safely survey. The MBES bathymetry has a resolution of 0.5 m, the LiDAR grid has a much coarser resolution of 5 m. This implies that small scale features only a few metres wide at current sea level are not represented in the dataset and are therefore missed in the analysis. In order to account for this potential error, we conducted a visual examination of 50 cm resolution aerial photographs of the shore taken in 2010 as part of the Department of Environment and Primary Industries coordinated imagery program.

Results

General submarine geomorphology

The granitic outcrops of Wilsons Promontory descend steeply (up to 70º) to the seafloor to an average water depth of 40 m, with isolated areas near South East Point descending to around 90 m depth (Figure 3). Granitic outcrops occur offshore of the

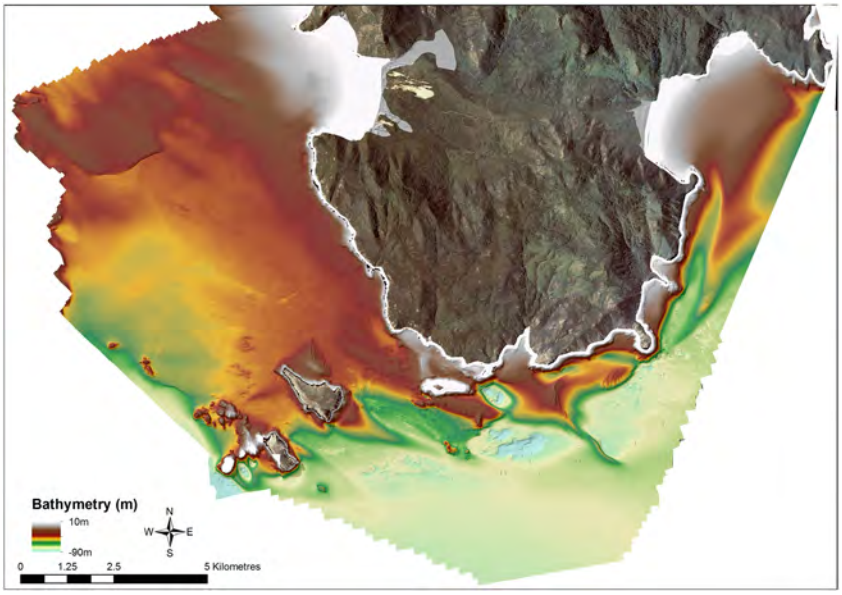

Figure 3. Combined digital elevation model of Wilsons Promontory and its Marine National Park utilizing the bathymetric and terrestrial LiDAR datasets as well as the MBES bathymetry dataset. This figure is available in colour online at wileyonlinelibrary.com/journal/espl

Promontory on Wattle Island and the Anser Group islands as well as below the sea surface as isolated outcrops 5.4–68.1 ha in area between 1 and 40 m depth. The seabed around the outcrops is characterised by a hard ground which is generally bare of sediment and has an average depth of 40 - 50 m. On the eastern sides of the islands large scour holes in the seafloor, up to 400 m wide, occur and descend to 90 m depth (Figure 3). Hillshade modelling of this surface indicates bedded sedimentary layers which have been folded (Figure 4). This likely represents the tightly folded shales and sandstones of Ordovician age in which the Wilsons Promontory granites are intruded (Hill and Joyce, 1995). Unconsolidated sediment sheets are present to the west of the Promontory, just north of the Anser Group. These sheets are over 835 ha in area and are likely to be around 2 – 6 m thick, based on their height above the surrounding near-horizontal seafloor. Sediment mounds are attached to all the islands in the marine park and have a sculptured formation similar to shadow dunes found on land (Figure 4). An isolated transverse ridge composed of sediment extends from South East Point to the SE for 4.5 km rising to a height of 22 m above the seabed with an average width of 100 m. All these sediment features appear to be active as they have steep (13–22°) slip faces present on their eastern sides.

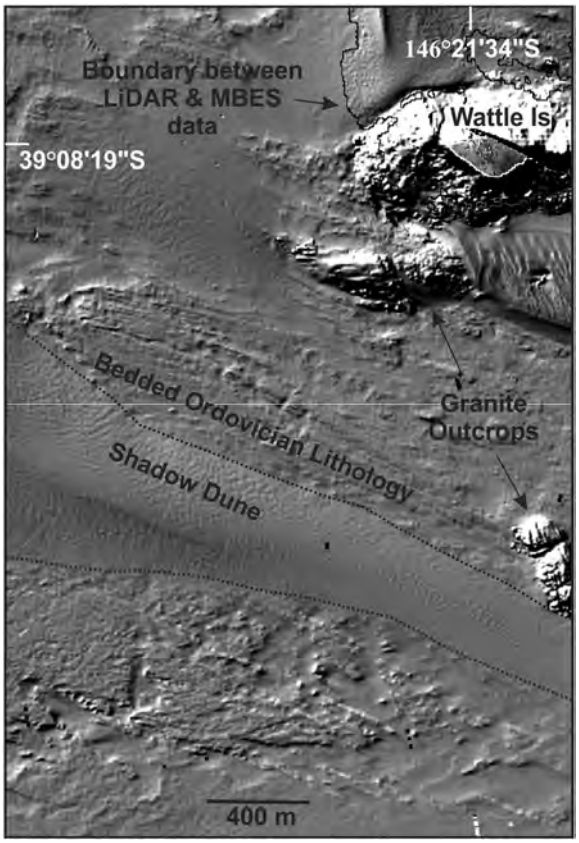

Figure 4. A hillshade model of the seafloor where the bedded Ordovician sediments are partly buried by a large dune feature in the lee of the Anser Group Islands.

Shoreline morphology

The shoreline on the western side of Wilsons Promontory is generally concave in profile descending steeply from 40−60 m above sea level to close to −10 m elevation from where the slope decreases towards the seabed where it is near horizontal (<1°) at between 30 and 40 m depth (Figure 5). The steepest parts of the slope occur above sea level, between +10 and +50 m where the slopes are almost always over 25° but in some cases may be up to 70°. Cross-sectional profiles of the shore can be subdivided into three main zones, an upper steeper zone with a stepped morphology, a central undulating zone of lower slope and a lower uniform near-horizontal zone (Figure 6). The upper zone is characterized by bedrock and descends from the upper limit of terrestrial LiDAR surveys (40–60 m) to between −0.2 (profile 2) and −20.9 m (Profile 4). Above sea level the granite outcrops have a convex slope (e.g. profile 4, 5), with vertical (e.g. profile 6) and sheet jointing (profile 5) leading to small steps (10 m relief) or undulations in the cross-sectional profile (Figure 5). The vertical joints are spaced at approximately 20 m intervals while the sheet joints are 6–7 m apart when exposed.

The central zone extends to between 30 and 40 m depth and is likely composed of a combination of bedrock and talus material derived from the upper slopes. A relief of 2–5 m occurs in this zone with the profile generally concave up in shape and

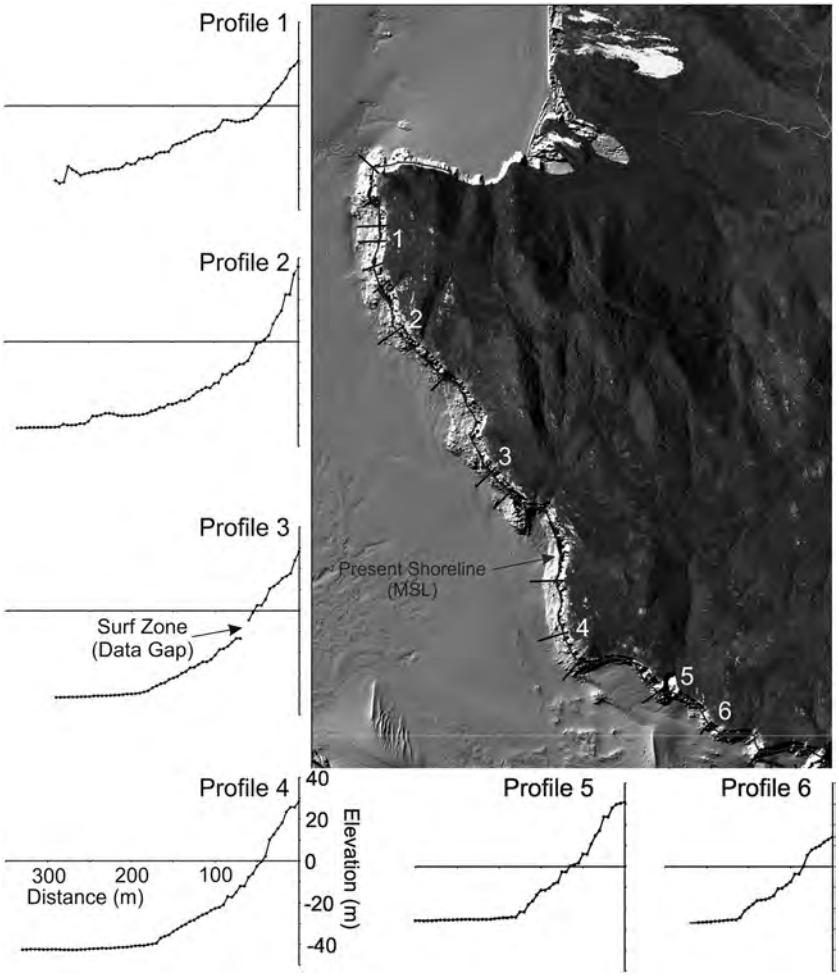

Figure 5. Cross-sections of the western side of Wilsons Promontory derived from the terrestrial and marine LiDAR datasets. The position of MSL on the coast is marked by a dark line. On profile 3 a data gap exists in the LiDAR surveys resulting from signal loss due to wave breaking.

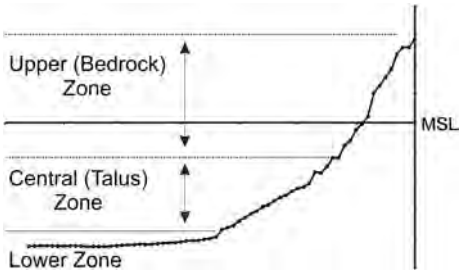

Figure 6. A schematic cross-section of the granitic shore showing the three major morphological zones.

likely being composed of loose boulders lying on the slope. The transition between these two zones usually occurs within 55 m of the shoreline. The lower zone is generally classified when the slope falls below 5° and occurs between 125 and 165 m from the shore. This area marks the transition between the granite dome and the surrounding seabed and often the transition is sharp with the slope values decreasing by around 10° over a distance of 5 m.

On the southern and eastern sides of the promontory a similar cross sectional morphology is found. In the case of profile 7, a large granitic block (17 × 25 m) representing detached sheet jointing occurs at the base of the cliff at sea level producing a near-horizontal surface (Figure 7). Profile 8 is the only example where a shore platform feature is found, located on the eastern side of South East Point. The surface is semi-horizontal, 25 m wide with an average elevation of −0.59 m before sloping seaward at an average angle of 15.8° for 15 m to a depth of −4.2 m from where it descends to the seafloor at angles of up to 22.2° (Figure 7). The platform appears to be formed in an area of highly jointed bedrock and, based on aerial photography, is covered in boulders 3−7 m long and 1−5 m wide.

On Wattle Island, 600 m due south of the Promontory, the granite is more highly jointed than on the mainland with vertical joint sets spaced at < 5 m apart. Domal outcrops with vertical joints spaced between 10 and 50 m apart occur on the southern edge of the island (Figure 8(a)). Cross- sectional profiles in the north–south orientation are similar to the mainland, with a steep upper, bedrock-dominated, section dipping steeply to the lower, sea floor, zone at between 30 and 40 m depth. A profile across the island (west to east) highlights the dissection of the island caused by vertical jointing leading to a relief of over 20 m in places (profile 9). Shore platforms are generally absent from the shore, although semi-horizontal surfaces are apparent close to sea level on the north side of the island (e.g. profile 10 and 11). This surface slopes at between 0.7° (profile 11) and 1.5° (profile 10) and is formed on highly jointed bedrock or on the top of a domal outcrop on each profile respectively (Figure 8(b)).

Hypsometry

Through taking fixed points at 100 m intervals on the contours around the entire coast it is calculated that the average bedrock slope between 10 m above and 10 below MSL, is

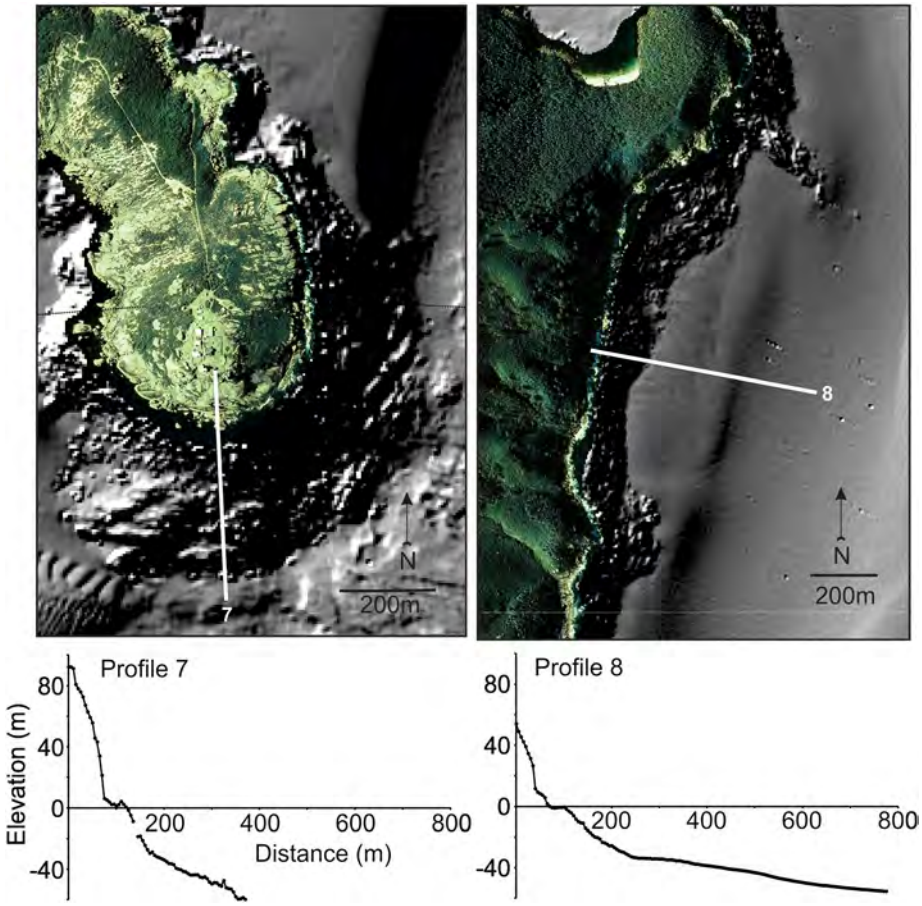

Figure 7. Profiles of South East Point and the eastern side of Wilsons Promontory. These areas are the only locations to have a semi-horizontal surface present at sea level. This represents a large detached sheet joint on profile 7 observable in the aerial image, while on profile 8 the shoreline is dominated by boulders. This figure is available in colour online at wileyonlinelibrary.com/journal/espl

26.4 +/− 14.5° with a median of 18° (Figure 9). The lowest slopes occur at MSL with an average angle of 17.6 +/− 11.6° compared with more than 20° at 5 and 10 m below sea level and 30–40° at +5 and +10 m respectively (Figure 10(a), Table I). There is a significant difference between the slope angle at MSL and those at +/− 5 m elevation, and there is also a significant difference between the slopes at +5 and +10 m (Table II). Levene's test for equality of variances between the datasets (Table II) does however indicate that the variability of the two conditions is also significantly different. In part this is likely due to the degree of indentation with the shore which is reflected in the number of measurements taken. Specifically the MSL contour is almost double the length of the −10 m contour.

Where joints occur they lead to metre-scale vertical relief in the landscape and this can be quantified in the LiDAR dataset through calculations of terrain ruggedness. There is little variation between ruggedness values above and below mean sea level (Figure 10(b)) and in addition there is little relation between slope and ruggedness ($r^2 = 0.147$). The lack of correlation likely relates to the resolution of the LiDAR dataset. The 5 × 5 m grid means that variation in relief between adjacent pixels can be driven by a range of factors and not just vertical joints. For example the high slopes of the domal outcrops often result in a high ruggedness value despite these surfaces being virtually free from joint planes. The higher resolution 0.5 × 0.5 m grid obtainable with the MBES data shows that areas of high ruggedness correspond well to the joint surfaces (Figure 8(a) and 8(c)). Areas with a low ruggedness within the MBES data correspond to the top of granite domes.

Bathymetry

Between 7 and 9 km to the north-west of Kanowna Island a series of granitic outcrops rise to 31 m from the seafloor. All these reefs are bare of sediment and both vertical and sheet jointing can be observed across the domed surface (Figure 11(a), (b)). These are interpreted to represent granitic outcrops. Cross-sections across these reefs are characterized by a convex profile characteristic of a granitic dome with slopes ranging up to 25.7° (profiles 12 and 13) (Figure 11(c)). Small steps in the profile cause isolated areas of relief up to 2 m and relate to the erosion of slabs along the sheet jointing planes (Figure 12 and 13(a), (b)). In some instances the sheets have broken into individual blocks up to 32.4 m^2 in size.

Immediately adjacent to Kanowna Island, submarine outcrops of granite 76.7 ha in size occur rising from almost 50 m depth to the intertidal zone (Figure 13(a)). These outcrops have a typical domal morphology with bare convex slopes with angles of up to 56° (Figure 13(b)). In areas with a higher joint density (<10 m spacing) the profiles also have bare convex slopes although the crest of the domes tend to have a lower slope and to be less smooth (e.g. profile 16) (Figure (12)). In some cases (e.g. profile 15) the flanks of the granitic domes appear to be covered in a veneer of large boulders around 1 m in size (Figure 12 and 13(a)). The central undulating zone of the profiles found on the mainland tends to be absent from the submarine outcrops.

Discussion

The combined terrestrial and bathymetric LiDAR with MBES surveys provides a seamless dataset from which the morphology

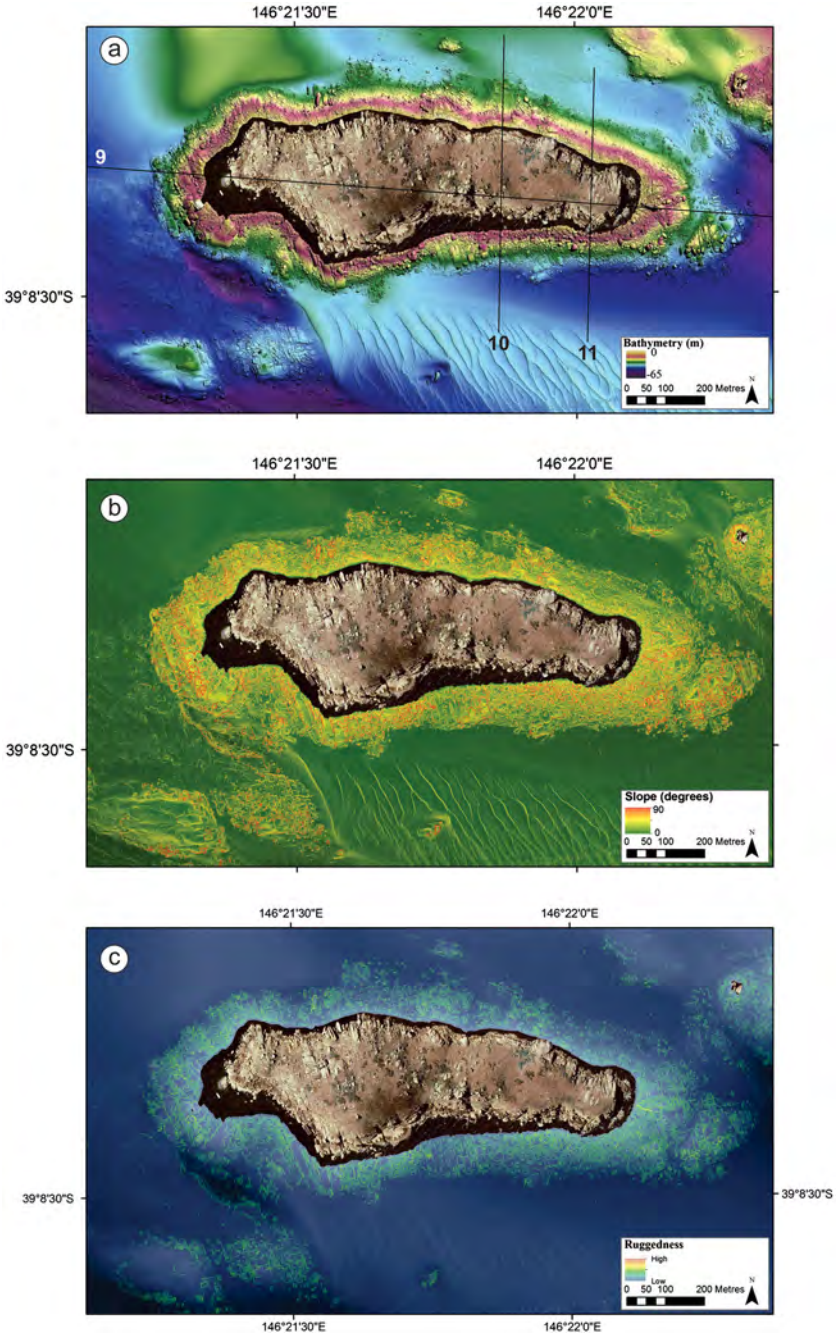

Figure 8. (a) MBES bathymetry around Wattle Island showing the repetition of the jointed domal granitic surfaces present above sea level down to 65 m water depth. (b) Slope derived from MBES bathymetry. Areas of near vertical slopes correspond to joints and there appears to be little truncation of the slopes associated with a past lower sea level. (c) Rugosity values for Wattle Island derived from MBES bathymetry. This figure is available in colour online at wileyonlinelibrary.com/journal/espl

of the coast can be examined above and below MSL. The steepness of the granite profiles is particularly advantageous as MBES data can be efficiently collected in deep water very close to the shoreline allowing for overlap with the LiDAR datasets.

Bedrock erosion

Erosional processes acting on rocky shores can be expected to cause the profile to become truncated at or close to sea level over Quaternary timescales (Trenhaile, 2001, 2008). Rock structure, especially jointing, is the key determinate of erosional potential on many rocky shores with areas of higher density often eroding at greater rates than unjointed surfaces (Kennedy and Dickson, 2006; Kennedy, 2010) and this is especially the case for granitic lithologies (Twidale, 1982; Migon, 2006). In highly jointed lithologies waves can directly erode the bedrock through rock plucking (Kennedy and Beban, 2005; Paris *et al.*, 2011); however, it is more often the case that a degree of weathering is required to prepare a surface through widening and loosening joints (Naylor and Stephenson, 2010; Stephenson and Naylor, 2011). In granitic settings where there is a high density of joints (spaced < 1 m apart) shore platforms can form. For example in western Galicia, Spain, platforms sloping up to 2° and over 100 m wide are found (Blanco-Chao *et al.*, 2003, 2007; Feal-Pérez and Blanco-Chao, 2013) while in NW Ireland platforms up to 80 m wide occur (Knight *et al.*, 2009; Knight and Burningham, 2011).

On the granite of Wilsons Promontory joint sets are both vertical and horizontal in orientation with sheet jointing several metres thick and orientated parallel to the domed surface being the most common (Figure 14). The coastline is dominated by

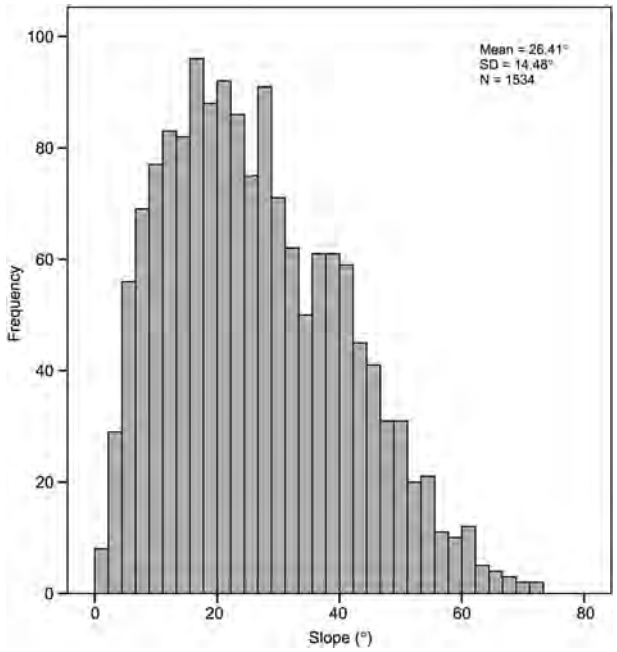

Figure 9. Frequency histogram of slope from the +10 to −10 m contour in 5 m intervals. The lack of a peak of slope at 0° highlights the lack of shore platform development at modern sea level.

plunging convex-shaped cliffs and only in a few isolated areas do shore platforms form such as between South East and Waterloo Points as well as on Wattle Island. In the former area, the platforms are around 25 m wide (Figure 7) and correspond to areas of high joint density (spaced < 2 m apart). In the case of Wattle Island a semi-horizontal surface corresponds to a bare granitic outcrop where the sheet jointing appears to form a circular pattern. The platform here is interpreted as representing the top of a sheet joint. Such an exposure of a sheet jointing plane at sea level may also explain the existence of steeply-sloping (8−10°) platforms in Ireland which are orientated at a similar angle to the joints (Knight and Burningham, 2011).

The lack of platforms on granitic domes appears to be primarily due to the widely spaced jointing inhibiting erosion. This is would also explain the absence of shore platforms in other locations globally such as in Abel Tasman National Park, New Zealand (Rattenbury *et al.*, 1998), the Seychelles (Johnson and Baarli, 2005) and the Pearson Islands in the Great Australian Bight (Twidale and Romani, 2005).

Erosion of the weathered mantle

Even though shore platforms are generally absent analysis of the hypsometry and bathymetry indicates there is a distinct truncation of the slope at MSL. The zero-contour is significantly lower in slope when compared with the contours between 10 m above and below MSL (Figure 10(a)). This suggests that processes occurring at present sea level are causing the shoreline to erode. The dominance of bare bedrock at MSL and the absence of shore platforms suggests that stripping of the weathered regolith from the hillslopes is the dominant processes.

Chemical weathering is the principle mechanism of erosion of granitic landscapes and it tends to be concentrated along joints and fractures (Twidale, 1982; Migon, 2006). Small-scale morphological features such as kluftkarren and flared sidewalls are found on shore platforms formed in granite in South Australia (Twidale *et al.*, 2005) which contribute to their development (Twidale *et al.*, 2005). In the Seychelles, fluted rillenstein found on the surface of convex plunging cliffs (Johnson and Baarli, 2005) are also evidence of chemical weathering; however, these erosional forms are not observed on Wilsons Promontory. Chemical weathering has occurred on Wilsons Promontory since the Cretaceous, resulting in a weathered layer up to 300 m deep (Hill, 1994; Hill *et al.*, 1995). In some instances such as Mt Martha, Port Philip Bay, Australia (Jutson, 1940) or western Galicia, Spain (Trenhaile *et al.*, 1999; Blanco-Chao *et al.*, 2003) shore platforms are formed within weathered granite, but in the case of Wilsons Promontory much of this layer has been removed exposing fresh bedrock at the shore. This erosion also results in the widespread occurrence of remanent tors (Hill and Joyce,

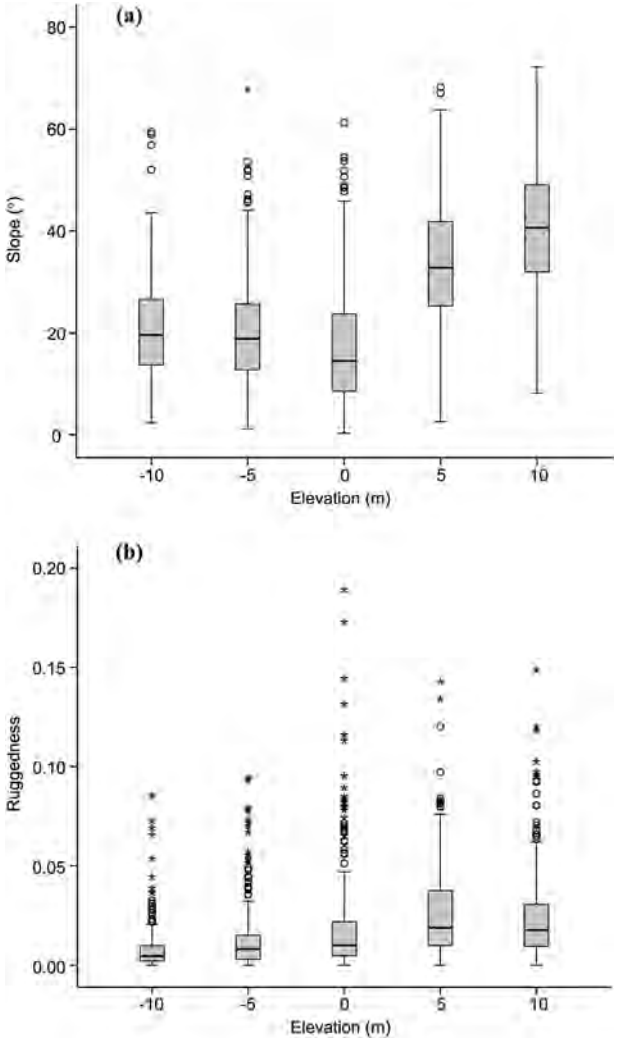

Figure 10. Box plots of (a) slope and (b) ruggedness at different elevations along Wilson Promontory. While the lowest slope occur at 0 m elevation they are not significantly different from the slope below sea level and much higher than the angle of contemporary shore platforms around the globe. There is also little relation between ruggedness and elevation.

Table I. Summary statistics of slope and ruggedness for contours above and below mean sea level. Statistics are based on point data taken at 100 m intervals along each contour line

Elevation (m)	n	Slope (°)	Ruggedness
10	284	40.68 +/− 12.48	0.02 +/− 0.02
5	338	33.54 +/− 11.79	0.03 +/− 0.02
0	401	17.55 +/− 11.48	0.02 +/− 0.00
−5	296	20.65 +/− 10.50	0.01 +/− 0.02
−10	215	20.85 +/− 10.17	0.01 +/− 0.01

Table II. Test of significance for slope and ruggedness for 5 m contour intervals between 10 m above and below mean sea level

Depth	(m)	+10 to +5		+5 to 0		0 to −5		−5 to −10	
Equal variance assumed		Sig.	Sig. (2-tailed)	Sig.	Sig. (2-tailed)	Sig.	Sig. (2-tailed)	Sig.	Sig. (2-tailed)
Slope	Y	0.576	0.000	0.393	0.000	0.027	0.000	0.775	0.826
	N		0.000		0.000		0.000		0.826
Ruggedness	Y	0.179	0.333	0.073	0.000	0.000	0.001	0.003	0.003
	N		0.333		0.000		0.000		0.002

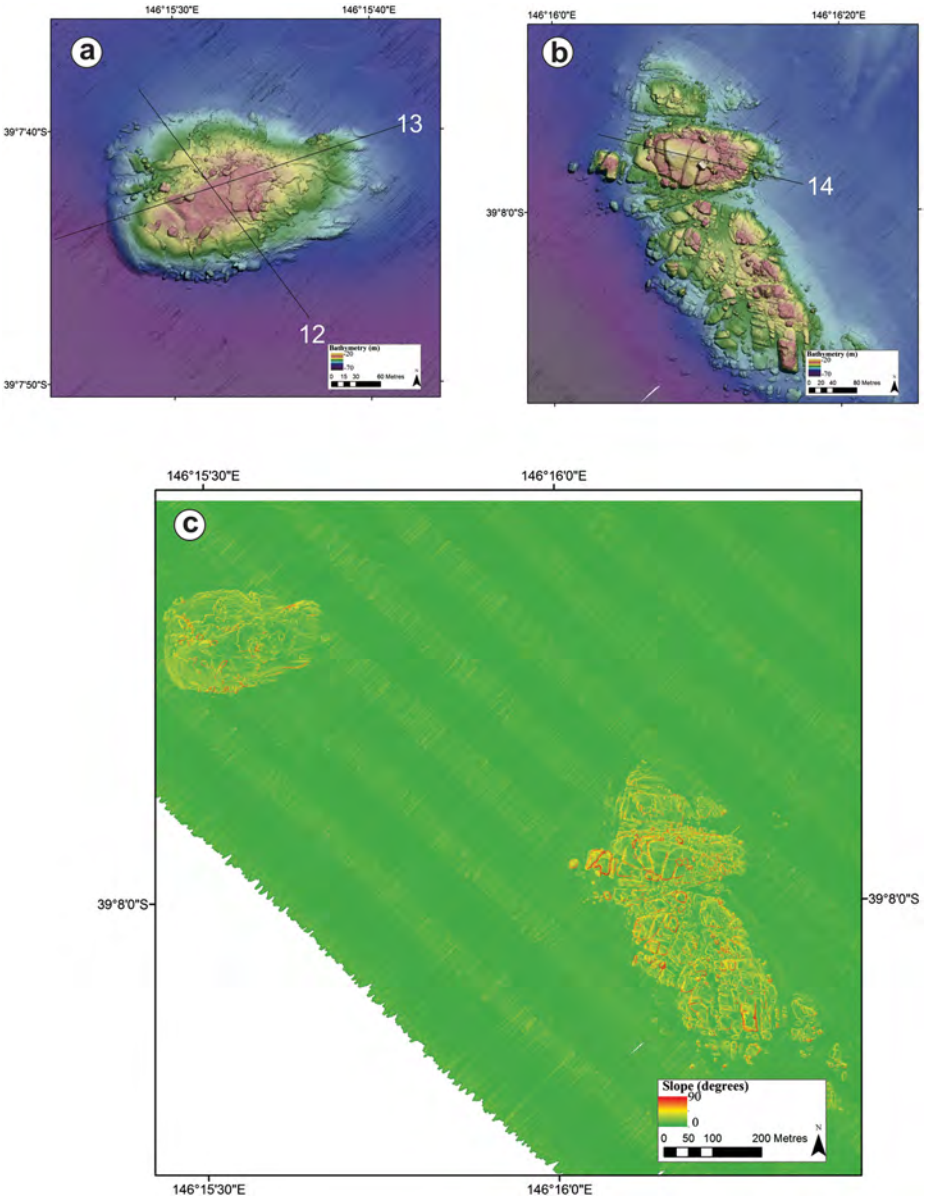

Figure 11. MBES bathymetry of two granitic reefs (a and b) showing distinct vertical and sheet jointing with detached boulders being found on the seafloor adjacent to the outcrops. Slope values derived from the MBES data for the granitic reefs (c). This figure is available in colour online at wileyonlinelibrary.com/journal/espl

1995) which increase in height with decreased elevation as the greatest erosion occurs at sea level (Hill, 1994; Hill *et al.*, 1995).

The weathered alluvium does not appear to be entirely broken down to sand-sized material, with large blocks, derived from both broken tors and sheet jointing, prevalent in some areas of the shore (Figure 14). This debris appears to also dominate the undulating middle sections of the profiles (Figure 5). It can therefore be postulated that under contemporary climatic conditions landscape change is driven by physical rather than chemical processes; however, erosion at sea level acts to only remove already weathered material rather than directly removing bedrock.

Erosion during the Quaternary

The present elevation of sea level is, however unusual during the Quaternary, with a mean elevation of −50.9 +/− 30.1 m

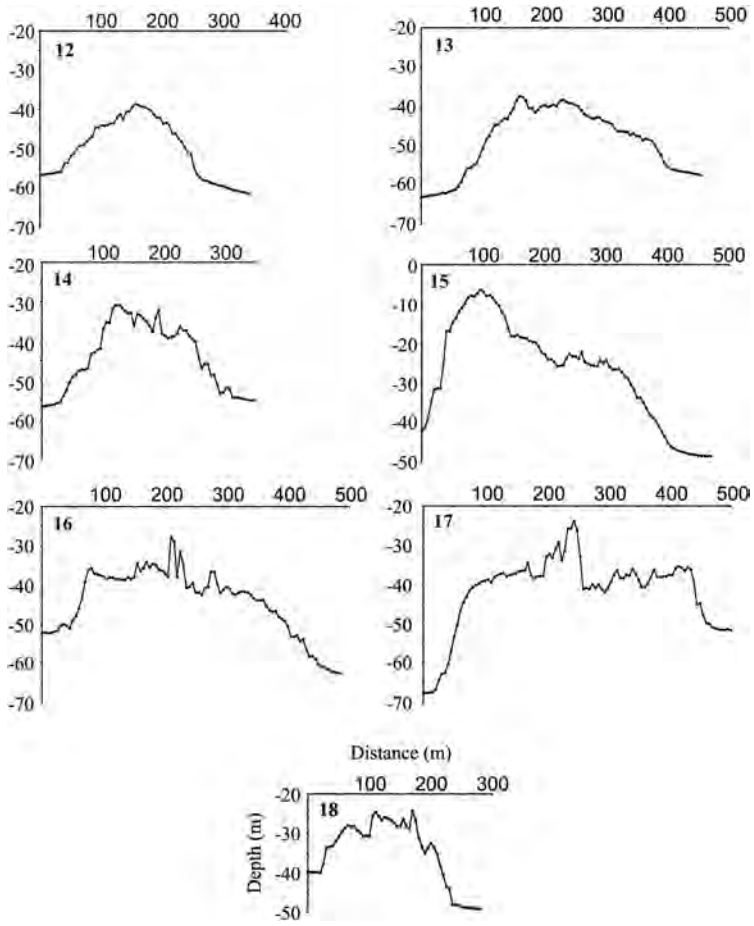

Figure 12. Cross-sectional profiles across the granitic reefs within the Marine National Park. The domal form of the granite and its vertical joints are the main determinates of the profile shape.

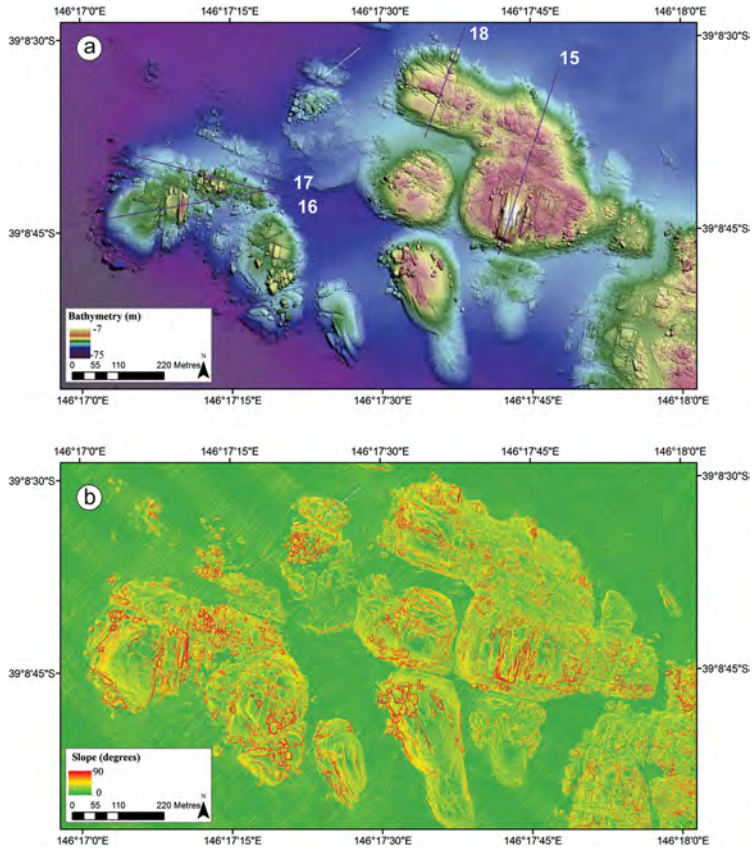

Figure 13. (a) MBES bathymetry map of the Carpentaria Rock granitic reef immediately adjacent to the Anser Group. The wreck of the MV Carpentaria, which struck the reef in the late 19th century, is observable on the seafloor on the eastern side of the image. (b) Slope angles for the Carpentaria Reef complex derived from MBES bathymetry. This figure is available in colour online at wileyonlinelibrary.com/journal/espl

Figure 14. (a) Typical shoreline of the western side of Wilsons Promontory where domal outcrops descend to sea level with little change in slope. (b) Large boulders, likely remanent tors at sea level with eroded sheet jointing slabs accumulated at its base. Person for scale in the centre of the boulders. This figure is available in colour online at wileyonlinelibrary.com/journal/espl

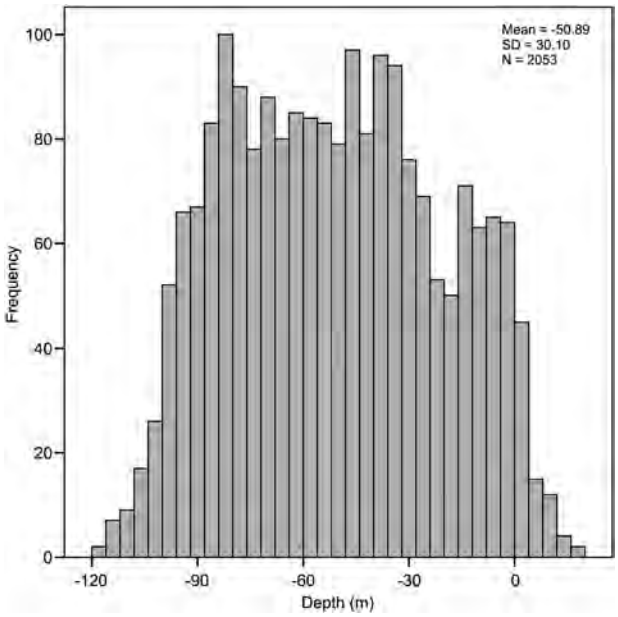

Figure 15. Histogram of global sea level elevations for the past 500 ka. Data from Rohling *et al.* (2009).

for the past 500 ka (Rohling *et al.*, 2009). The mean depth of the sea floor in the study area is 40–50 m which corresponds to a peak in sea level elevations where several small interstadial shorelines are likely to have occurred (Figure 15). No distinct break in slope corresponding to an interstadial sea level position can be identified on the Promontory profiles below MSL which are often mantled by debris. The submarine granitic outcrops on the other hand are almost entirely bare dome surfaces with their cross sectional profiles reflecting the orientation of the joint planes (Figures 11 and 13). Any pre-existing weathered mantle has been completely eroded with debris being present only as large bedrock clasts on the seabed representing detached sheet joints. Rock structure therefore appears to determine the cross- sectional morphology with sea level only acting to remove the weathered mantle. It is not apparent whether there is a cyclic process of weathering during lowstands and erosion at highstands on the granitic shores of Wilsons Promontory. Long-term temporal scales are required to weather granites (Migon, 2006), but the erosional features observed could still have been formed during the Holocene. Landform evolution can therefore be considered to be a weathering-limited system where the rates of chemical erosion determine the degree of landscape change.

Conclusions

Combined marine and terrestrial data sets derived from aerial LiDAR and MBES mapping represent the new frontier in understanding coastal geomorphology. In this study these data allowed for seamless mapping of rocky coast profiles above and below sea level. The low turbidity and deepness of the seabed close to shore are particularly suitable for seamless joining of MBES and LiDAR data. The shape of the granitic shoreline of Wilsons Promontory appears to be primarily determined by joint density and orientation. The joints are generally resistant to physical erosion with shore platforms forming only where the joints were spaced < 2 m apart, or where the top of a dome coincided with contemporary sea level. Erosion at current sea level elevation appears to be focused on the removal of the weathered mantle with the transfer of large blocks to the lower parts of the submarine slopes also occurring. Rocky coast evolution can therefore be considered to occur over long timescales on granitic lithologies.

As joint structure is the primary control on shore platform development in granitic settings, in areas of low joint density reconstruction of past sea levels can be difficult. Evidence of past interglacial and interstadial sea levels was not found on Wilsons Promontory with submarine granitic outcrops being characterized by the domal shape of the bedrock. Contemporary sea levels therefore appear to be efficient at removing weathered material but unable to cause significant bedrock erosion. Such landscapes are therefore poor environments for the reconstruction of past sea levels.

Acknowledgements—We thank Parks Victoria for funding the capture of the multibeam sonar data used in this study. We thank members of the crew Sean Blake and Dr Alex Rattray of Deakin University's research vessel Yolla for assistance in the collection of the multibeam sonar data. We also thank Parks Victoria staff at Tidal River for their logistical support and use of their field station at Refuge Cove. We thank the Department of Environment and Primary Industries Department of Environment and Primary Industries coordinated imagery program for access to the georegistered aerial photography and the Future Coasts Program for access to the LiDAR data. We thank Ian Atkinson from Geoscience Australia and Nicole Bergersen from Acoustic Imaging Pty Ltd for technical support provided during MBES data capture and analysis. We thank Dr David Johnson from Metocean Solutions Ltd

for providing the hindcast swell data. GIS laboratory facilities at Deakin University, Warrnambool, Victoria were used for spatial analyses. Comments by Jasper Knight and an anonymous reviewer were appreciated.

References

Bierman PR, Caffee M. 2013. Cosmogenic exposure and erosion hisotry of Australian bedrock landforms. *Geological Society of America Bulletin* **114**: 787–803.

Blanco-Chao R, Costa Casais MC, Martinez Cortizas AM, Perez Alberti AP, Trenhaile AS. 2003. Evolution and inheritance of a rock coast: Western Galicia, Northwestern Spain. *Earth Surface Processes and Landforms* **28**: 757–775.

Blanco-Chao R, Perez Alberti AP, Trenhaile AS, Costa Casais MC, Valcarcel DM. 2007. Shore platform abrasion in a para-periglacial environment, Galicia, northwestern Spain. *Geomorphology* **83**: 136–151.

Chappell BW, White AJR, Hine R. 1988. Granite provinces and basement terranes in the Lachlan Fold Belt, southeastern Australia. *Australian Jounral of Earth Sciences* **35**: 505–521.

Cupper ML, White S, Neilson JL. 2003. Quaternary: Ice ages - environments of change. In *Geology of Victoria*, Birch WD (ed). Geological Society of Australia (Victoria Division): Sydney; 337–359.

Edmunds M, Pritchard K, McArthur M. 2012. Victorian Subtidal Reef Monitoring Program: the reef biota at Wilsons Promontory Marine National Park, November 2010. In *Parks Victoria Technical Series No. 71*: Melbourne.

Feal-Pérez A, Blanco-Chao R. 2013. Characterization of abrasion surfaces in rock shore environments of NW Spain. *Geo-Marine Letters* **33**: 173–181.

Granger DE, Riebe CS, Kirchner JW, Finkel RC. 2001. Modulation of erosion on steep granitic slopes by boulder armoring, as revealed by cosmogenic Al-26 and Be-10. *Earth and Planetary Science Letters* **186**: 269–281.

Gunnell Y, Jarman D, Braucher R, Calvet M, Delmas M, Leanni L, Bourlès D, Arnold M, Aumaître G, Keddaouche K. 2013. The granite tors of Dartmoor, Southwest England: rapid and recent emergence revealed by Late Pleistocene cosmogenic apparent exposure ages. *Quaternary Science Reviews* **61**: 62–76.

Hill SM. 1994. Some granite landforms of Wilsons Promontory, Southern Victoria. *The Victorian Naturalist* **111**: 184–190.

Hill SM, Joyce EB. 1995. Granitic regolith and landscape evolution of Wilsons Promontory, Victoria. *Proceedings of the Royal Society of Victoria* **107**: 1–10.

Hill SM, Ollier CD, Joyce EB. 1995. Mesozoic deep weathering and erosion: an example from Wilsons Promontory, Australia. *Zeitschrift für Geomorphologie* **39**: 331–339.

Hills ES. 1949. Shore platforms. *Geological Magazine* **84**: 137–154

Hills ES. 1971. A study of cliffy profiles based on examples in Victoria, Australia. *Zeitschrift für Geomorphologie* **15**: 137–180.

Ierodiaconou D, Monk J, Rattray A, Laurenson L, Versace VL. 2011. Comparison of automated classification techniques for predicting benthic biological communities using hydroacoustics and video observations. *Continental Shelf Research* **31**: 28–38.

James NP, Bone Y. 2011. *Neritic Carbonate Sediments in a Temperate Realm*. Springer: New York

Jessup BS, Jesse Hahm W, Miller SN, Kirchner JW, Riebe CS. 2011. Landscape response to tipping points in granite weathering: The case of stepped topography in the Southern Sierra Critical Zone Observatory. *Applied Geochemistry* **26**, Supplement: S48–S50. DOI: 10.1016/j.apgeochem.2011.03.026

Johnson ME, Baarli BG. 2005. Erosion and burial of granite rocky shores in the Recent and Late Plesitocene of the Seychelles Islands: physical and biological perspectives. *Journal of Coastal Research* **21**: 867–879.

Jutson JT. 1940. The shore platforms of Mt Martha, Port Phillip Bay, Victoria, Australia. *Proceedings of the Royal Society of Victoria* **52**: 164–175.

Kennedy DM. 2010. Geological control on the morphology of estuarine shore platforms: Middle Harbour, Sydney, Australia. *Geomorphology* **114**: 71–77.

Kennedy DM, Beban JG. 2005. Shore platform morphology on a rapidly uplifting coast, Wellington, New Zealand. *Earth Surface Processes and Landforms* **30**: 823–832.

Kennedy DM, Dickson ME. 2006. Lithological control on the elevation of shore platforms in a microtidal setting. *Earth Surface Processes and Landforms* **31**: 1575–1584.

Knight J, Burningham H. 2011. Boulder dynamics on an Atlantic-facing rock coastline, northwest Ireland. *Marine Geology* **283**: 56–65.

Knight J, Burningham H, Barrett-Mold C. 2009. The geomorphology and controls on develop of a boulder-strewn rock platform, NW Ireland. *Journal of Coastal Research, SI* **56**: 1646–1650.

Lindsay MJ. 2013. The influence of Wilsons Promontory's oceanography on regional phylogeography and larval settlement. The University of Melbourne.

Matmon A, Mushkin A, Enzel Y, Grodek T. 2013. Erosion of a granite inselberg, Gross Spitzkoppe, Namib Desert. *Geomorphology* **201**: 52–59.

Migon P. 2006. *Granite Landscapes of the World*. Oxford University Press: Oxford.

Naylor LA, Stephenson WJ. 2010. On the role of discontinuities in mediating shore platform erosion. *Geomorphology* **114**: 89–100.

Paris R, Naylor LA, Stephenson WJ. 2011. Boulders as a signature of storms on rock coasts. *Marine Geology* **283**: 1–11.

Quadros N, Rigby J. 2010. Construction of a high accuracy seamless, state-wide coastal DEM. FIG Coastal Zone Special Publication, Sydney.

Rattenbury MS, Cooper RA, Johnston MR. 1998. Geology of the Nelson Area: Institute of Geological and Nuclear Sciences 1:250000 geological map 9. Institute of Geological and Nuclear Sciences Ltd, Lower Hutt.

Rohling EJ, Grant K, Bolshaw M, Roberts AP, Siddall M, Hemleben C, Kucera M. 2009. Antarctic temperature and global sea level closely coupled over the past five glacial cycles. *Nature Geoscience* **2**: 500–504.

Rossiter AG. 2003. Granitic rocks of the Lachlan Fold Belt in Victoria. In *Geology of Victoria*, Birch WD (ed). Geological Society of Australia (Victoria Division): Sydney; 217–237.

Sappington JM, Longshore KM, Thomson DB. 2007. Quantifiying landscape ruggedness for animal habitat anaysis: a case study using bighorn sheep in the Mojave Desert. *Journal of Wildlife Management* **71**: 1419–1426.

Shepard FP, Wanless HR. 1971. *Our Changing Coastlines*. McGraw-Hill: New York.

Stephenson WJ, Naylor LA. 2011. Geological controls on boulder production in a rock coast setting: Insights from South Wales, UK. *Marine Geology* **283**: 12–24.

Trenhaile AS. 1987. *The Geomorphology of Rock Coasts*. Clarendon Press: Oxford.

Trenhaile AS. 2001. Modelling the Quaternary evolution of shore platforms and erosional continental shelves. *Earth Surface Processes and Landforms* **26**: 1103–1128.

Trenhaile AS. 2008. The development of subhorizontal shore platforms by waves and weathering in microtidal environments. *Zeitschrift für Geomorphologie* **52**: 105–124.

Trenhaile AS, Alberti AP, Cortizas AM, Casais MC, Chao RB. 1999. Rock coast inhertitance: An example from Galicia Northwestern Spain. *Earth Surface Processes and Landforms* **24**: 605–621.

Twidale CR. 1982. *Granite Landforms*. Elsevier: Amsterdam.

Twidale CR, Bourne JA, Vidal Romani JR. 2005. Beach etching and shore platforms. *Geomorphology* **67**: 47–61.

Twidale CR, Romani JRV. 2005. *Landforms and Geology of Granite Terrains*. CR Press: London.

Twidale CR, Vidal Romani JR. 1994. On the multistage development of etch forms. *Geomorphology* **11**: 107–124.

Vierling KT, Vierling LA, Gould WA, Martinuzzi S, Clawges RM. 2008. Lidar: shedding new light on habitat characterization and modeling. *Frontiers in Ecology and the Environment* **6**: 90–98.

Wang C-K, Philpot WD. 2007. Using airborne bathymetric lidar to detect bottom type variation in shallow waters. *Remote Sensing of Environment* **106**: 123–135.

Wilson JP, Lam CS, Deng YX. 2007. Comparison of flow routing algorithms used in geographic information systems. *Hydrological Processes* **20**: 1026–1044.

10. Appendix D

Integration of object-based image analysis, multibeam data and video data for benthic habitat mapping in Wilsons Promontory National Park, Australia

Candidate: Grace Leah Gaylard

Deakin University, School of Life and Environmental Sciences, Faculty of Science and Technology, P.O Box 423, Warrnambool, Victoria, 3280, Australia

Submitted in partial fulfilment of the degree of
Bachelor of Environmental Science Honours
October, 2014

Statement of responsibility

This Thesis is submitted in accordance with the regulations of Deakin University in partial fulfilment of the requirements of the degree of Life & Environmental Science (Honours). I, Grace Gaylard, hereby certify that the information presented in this thesis is the result of my own research, except where otherwise acknowledged or referenced, and that none of the material has been presented for any degree at another university or institution.

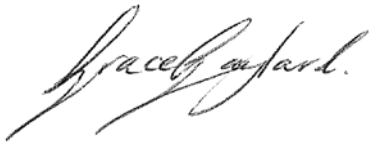

Signature of candidate:……..

Date: 27th of October, 2014

Title of Project:

'Benthic habitat mapping; using an autonomous underwater vehicle and ultra-high multibeam sonar data in Refuge Cove, Wilsons Promontory National Park'

Supervisor: Daniel Ierodiaconou[1]

Co-Investigators: Alexandre Schimel[1], Mary Young[1], Sean Blake[1] and Markus Diesing[2]

[1]Deakin University, School of life and Environmental Sciences, P.O Box 423, Warrnambool, Victoria, 3280, Australia

[2]Centre for Environment, Fisheries and Aquaculture Science, Lowestoft, Suffolk, United Kingdom

Abstract

As human populations increase around the world, so does pressure on the marine environment from anthropogenic activities. There is now a high demand for high-resolution maps of benthic substrates and habitats to help in development of effective management measures. This study presents a methodology integrating multibeam echo-sounder (MBES) data, object-based image analysis (OBIA) and video data to produce an accurate habitat map for Refuge Cove, Wilsons Promontory National Park, Australia. A number of derivatives traditionally used in the habitat mapping literature were first computed from MBES bathymetry and backscatter data. A subset of these derivatives was then used in an OBIA resulting in a segmentation of the site. Finally, five different models implementing a Quick Unbiased and Efficient Statistical Tree (QUEST) on various combinations of MBES derivatives and segmentation layers were run to identify the layers' suitability to predict marine habitats. The accuracy of the habitat map resulting from each model was assessed by computing the overall accuracy and kappa measures on its associated error matrix. The differences between the maps were analyzed by calculating pair-wise Z-statistics and using a map comparison tool to identify the local agreement between each pair of maps. The best overall accuracy was achieved by the model using bathymetry, bathymetry derivatives and the OBIA segmentation layers (78.34% overall accuracy). The maps showed large differences in the spatial distribution of habitats across the sites, but the pair-wise Z-statistic computations revealed that the models did not differ significantly in performance. A main result is that the OBIA segmentation layers performed well, presumably because they smooth-out the inherent noise in the original MBES layers. A secondary advantage is

that they provided smooth homogenous boundaries between habitat classes, making the map suitable for habitat management application. The seagrass *Amphibolis Antarctica* was observed in the high-use area of Refuge Cove, making it susceptible to anchorage scars. This study provides a map of the areas where anchorage should be discouraged to prevent future impacts on these fragile but yet important habitat.

Acknowledgements

I would like to thank the crew from Australian Marine Ecology research team, Parks Victoria, Deakin Yolla team and Port Whelshpool Coast Guards for collection of the AUV video data, Multibeam sonar data and video drops. Thanks to Sean Blake, Alex Rattray, Richard Zavalas, Lachlan Hulands and 2014 honours group for suggestions and comments throughout the write up and results for this project and to Port Whelshpool Coast Guard for providing accommodation and vessel support during second sampling mission. I would like to thank Deakin University, Warrnambool lecturing staff and technical staff for all the help that they provided, my supervisor Dan and co-supervisors Alex and Mary who have been fantastic mentors throughout my project and have provided a lot of technical and professional support throughout this project. This project was funded by Parks Victoria, POZIBLE project Voyages of Discovery and Somers Carroll Productions.

Table of Contents

URL for paper publishing in Continental Shelf Research:

http://www.sciencedirect.com/science/article/pii/S027843431000021X#

List of Abbreviations

Abbreviation:

ALG	-	Macroalgae
AUV	-	Autonomous Underwater Vehicle
CRUISE	-	Classification Rule with Unbiased Interaction Selection and Estimation
FMAT	-	Filamentous Mat
LV	-	Local variance
MBES	-	Multibeam echo-sounder
MLC	-	Maximum Likelihood Classifier
MPA	-	Marine Protected Area
NVB	-	No Visible Biota
OBIA	-	Object-based Image Analysis
POS MV	-	Positioning and Orientating System for Marine Vessels
QUEST	-	Quick Unbiased and Efficient Statistical Tree
RF	-	Random forest
ROC	-	Rate of change
SBES	-	Single beam echo-sounder
SGAM	-	Seagrass *Amphibolis antarctica*
SGZ	-	Seagrass *Zostera* spp.
SSS	-	Side Scan Sonar
SVPs	-	Sound velocity profile

List of Tables

List of Figures

1.0 Introduction

Coastal zones represent a small area of the Earth's oceans but are regarded as one of the most productive and diverse environments on the planet (Ierodiaconou et al. 2011). As human populations increase around the world, so does pressure on the marine environment from anthropogenic activities. Humans have gathered along coastal regions from the beginning of humanity and cumulative effects such as resource exploitation, habitat destruction and pollution are putting pressure on our coastal seas and embayment's (Jackson 2008). To mitigate these effects, manage resources effectively and conserve marine species, it is vital to gain an understanding of benthic habitats and ecological processes. However, our knowledge of the extent, geographical range and ecological functioning of benthic habitats to date remains relatively poor, with only 5-10% of the world's seafloor being mapped with high-resolution (Brown et al. 2011a). There is now a high demand for high-resolution maps of benthic substrates and habitats to help in development of effective management measures (Brown et al. 2011a). Marine habitat maps are the baseline dataset required for understanding and assessing ecological processes within the marine environment. They also represent a powerful basis to support modeling and management of marine ecosystems and assist in establishing effective guidelines for managing human interaction with the natural complexity of a marine ecosystem (Cogan et al. 2009).

Habitat mapping today is expanding into a multidisciplinary science; its origins in surficial geology have broadened to include subsurface geology, hydrodynamics, and biological and ecological elements of the seafloor environment (McGonigle et al.

2011). Habitat maps are being increasingly used as surrogates for biodiversity, especially in the context of marine protected area (MPA) planning and assessment (Lucieer et al. 2013)**.** This practice is supported by the fact that species in general show association with the physical properties of their surrounding environment (Guisan et al. 2000) and that seafloor characteristics are of important influence on the distribution, diversity and structure of marine biological assemblages (Kostylev et al. 2001; Ierodiaconou et al. 2011). It is therefore important for effective management to understand and quantify the physical properties of marine environments.

For nearly half a century, hydroacoustic systems have been routinely used to collect information on the geomorphological characteristics of the marine environment (Le Bas et al. 2009; Brown et al. 2011a). These systems transmit sound towards the seafloor and capture the echoes reflected or scattered from targets in the water-column (e.g. bubbles, fish and vegetation) or from the seafloor (Lurton 2002). The level of the reflected echo is dependent on the characteristics of the water-column targets or seafloor interface, hence allowing the characterisation or identification of the source of the echo. The three main hydroacoustic systems are single-beam echo-sounder (SBES), side scan sonar (SSS) and multibeam echo-sounder (MBES). SBES and SSS have been extensively used for habitat mapping in the past (Kenny et al 2003; Brown et a. 2011b) but more recent developments in sea floor mapping are now focused on MBES (Lurton 2002).

MBES are hydroacoustic systems that are designed to take multiple bathymetry measurements within a wide across-track swath. This capability allows broad areas of the seafloor to be ensonified at a high spatial resolution in a single survey line, thus providing opportunity for complete bathymetric coverage of the seafloor (Mayer 2006; Brown et al. 2011b). High-frequency MBES are small enough to be mounted on small coastal vessels, enabling work in shallow waters and leading to ultra-high resolution bathymetry maps (Lockhart et al. 2014). Advantages of using MBES over SBES and SSS include co-registration of bathymetry and backscatter, complete coverage of the seafloor and high positioning accuracy (Ierodiaconou et al. 2011). For these reasons, MBES are increasingly becoming the tool of choice for habitat mapping efforts (McGonigle et al. 2011). A number of secondary data layers can then be derived from the bathymetry and backscatter data. For example, from bathymetry data, the secondary data layers that can be derived are slope, aspect, terrain variability, hardness and roughness. These can all be useful in the production of seafloor habitat maps (Brown et al. 2011a)**.** Secondary data layers from backscatter data include Hue Saturation Intensities (HSI) (Daily 1983). Backscatter images generated from MBES data are often highly complex in regards to seafloor roughness, sediment grain size and volume of heterogeneity between seafloor substrates (Marsh et al. 2009).

MBES backscatter mosaics are noisy by nature. They contain speckle and processing artifacts. This noise affects classification methodologies that operate on the backscatter mosaic and its derivatives on a pixel-by-pixel basis, resulting in noisy maps that do not contain well-defined seabed zones (Lucieer et al. 2011). Object-

Based Image Analysis (OBIA) includes a range of methods that segment an image by analyzing the statistics of neighboring pixels to group them into “objects” (Lucieer et al. 2013). A number of statistics can then be calculated for each segment to provide spectral information: mean, standard deviation, minimum, maximum, etc. (Blaschke 2010). OBIA methodologies originated from terrestrial applications (Boggs 2010; Anders et al. 2011; MacFaden et al. 2012) and are being increasingly applied in the marine environment to map habitat substrates (Lucieer 2008; Che Hasan et al. 2012a; Che Hasan et al. 2014).

A wide range of techniques to classify benthic habitats have been developed over the past couple decades (Brown et al. 2011a) with the most recent ones implementing automatic supervised methodologies (Ierodiaconou et al. 2011; Che Hasan et al. 2014; Stephens et al. 2014). A supervised classification is a bottom up strategy where *in situ* ground-truthing (biological/geological) data is most commonly used alongside geophysical data to predict benthic habitats (Hewitt et al. 2004). This bottom up strategy is more sophisticated than traditional top-down strategies, in which the acoustic data drive the classification process. Recently supervised classifications are being adopted in benthic habitat mapping studies (Brown et al. 2011a) because they have advantages of being objective and allow for repeatability of this classification approach. Many different models have been used to relate the ground-truth data to the acoustic datasets. A class of models that have been used successfully over the past few years is Decision Trees (DT) (Rattray et al. 2009; Ierodiaconou et al. 2011; Che Hasan et al. 2012b; Lucieer et al. 2013; Rattray et al. 2013). DT are flowchart-like structures in which each internal node represents a test

on a target variable, leading to a hierarchical partition of the dataset into ever smaller subdivisions (Che Hasan et al. 2012b). Rattray et al. (2009) and Che Hasan et al. (2014) have found that the overall accuracy achieved by any particular DT model is highly dependent on the variables used in input. The production of different DT models using different MBES data layers in input and the computation of the resulting accuracy allows for identification of the important datasets in characterising biological communities.

Seafloor substrates have been shown to be the main contributors of variation within the backscatter signal of seafloor mapping echo-sounders (Lurton 2002). As a result, it is necessary to obtain some ground-truth of the parameters that we require to map in the form of biological samples, sediment samples or video and photography of the seafloor. Only then it becomes possible to identify the possible relationships between the measured acoustic signal and depth and the variables we wish to map (seafloor type, species of plants and animals that inhabit the seafloor) (Harris et al. 2011).

As well as developments in acoustic surveying, methods used to collect ground-truth information imperative to train classification algorithms and validate map outputs have also developed. Ground-truth data acquisition techniques include the use of video cameras, sediment profile cameras and benthic grabs, which provide small-scale detail about the biological and physical aspects of the marine habitats (Diaz et al. 2004). Developments in devices for collection of video data are now being recognized as sufficient time-saving tools. Autonomous underwater vehicles (AUVs) are an established tool for benthic habitat mapping surveys (Foster

et al. 2014). AUVs are robotic submarines that can be programmed to navigate a pre-determined course. AUVs can accurately obtain samples for a variety of different needs including video, water quality and sidescan sonar surveys from shallow to deep habitats (Australian Marine Ecology 2014). They settle at a user-set height in the water column in order to maintain a constant field of view.

AUVs offer many advantages as they can operate at depths beyond diver physiological limits (Barrett et al. 2010; Williams et al. 2010) and position and orientation of sensors can be controlled with greater precision compared to towed video platforms (Rigby et al. 2010). Moreover, by mounting cameras onto AUVs, they can provide detailed imagery to describe benthic faunal cover and habitat distribution, often used with collected of MBES data to produce habitat maps (Williams et al. 2010; Diercks et al. 2013; Wynn et al. 2014). AUVs are generally used to provide information on distribution and abundance of species and/or communities of interest (Foster et al. 2014). Additionally, their effectiveness for undertaking spatially repeatable surveys makes them a highly reliable technique for surveying marine environments and monitoring changes in biodiversity (Barrett et al. 2010). AUVs are effective tools for ecological studies such as benthic habitat assessment (Smale et al. 2012; Wynn et al. 2014).

AUVs do, however, operate under some constraints. Since they must be self-sufficient, they are dependent on battery power and provide limited onboard storage space for data collection. Therefore it is desirable to preplan missions to provide the maximum benefit from the allocated resources or further ground truthing will need to be performed (Rigby et al. 2010).

The continent of Australia has been recognized as a centre of endemism of global significance (Major 1988). Australia's marine estate generates 100s of billions of dollars direct wealth and indirect ecosystem services per year. The annual estimates of economic value of Australian marine benthic ecosystems varies from $A39.1 billion for tidal marsh/mangroves, $A53.5 billion for coral reefs, $A175.1 billion for seagrass/algal beds, and $A597.9 billion for shelf systems (Poloczanska et al. 2007). Despite the value of our marine estate there are major limitations to our basic understanding of the benthic ecosystems that reside and environmental drivers and threats to them. There is increasing need for greater understanding of natural resources in coastal zones and an ability to monitor change over time or measure effect of anthropogenic and natural impacts (Reichelt et al. 1999). These issues can only be addressed by survey methods and equipment that can produce high-resolution maps of benthic habitat data. Due to economic and technical difficulties benthic habitat mapping (compared to terrestrial mapping) many areas of the coastal zones in Australian remain poor investigated (Parnum 2007).

In previous studies, Southern Australian has been found to have the highest levels of species richness and endemism of any regional macroalgal flora in the world (Phillips 2001). Victoria, which is located in southeastern Australia, has an approximately 2000km coastline that is home to a diverse array of habitats (Traill et al. 2001). The Victorian coast is made up of series of rocky promontories or headlands joined by sandy bays (O'Hara 2002), which are exposed to strong winds, currents and large swells. The rocky promontories or shores of Victoria's open coast

support diverse animal and plant assemblages that vary according to complexity/structure of rock, wave exposure and water temperature (O'Hara 2002).

Seagrass beds, particularly those in bays and inlets, have substantially declined in Victoria over the past 30 years (O'Hara 2002). Seagrass beds provide an important habitat to many coastal species and contribute significantly to the physical, chemical and biological processes of coastal ecosystems (Walker et al. 1992). Growing human populations on the coastlines result in multiple threats to shallow coastal seagrass habitats, including loss of water quality, loss of biodiversity and sediment erosion (Short et al. 2014). Seagrass habitat degradation can be caused by numerous sources (e.g., pollution, dredging and fill), but increasingly common degradation is caused by scarring of seagrasses due to boat anchorage (Sargent et al. 1995). With seagrass species commonly being located in shallow coastal waters (e.g., sub-littoral and intertidal zones) (Collins et al. 2010) they are potentially located and exposed to possible areas of safe anchorage for vessels. Scarring to seagrass patches could be minimized by relocating moorings only within existing sand patches (Walker et al. 1989). However, in order to discourage anchorage in high use shallow waters, knowledge of bottom substrates is crucial. The key to successful application lies in the translation of basic physical data on bottom substrate and characteristics into meaningful representations of benthic habitat quality (Diaz et al. 2004).

In this study, we aim to test the ability of data derivatives from MBES and features derived from OBIA to accurately characterise benthic habitats in a high use

shallow water cove. We also aim to integrate high-resolution MBES data with AUV video data and video drop data to determine the extent and composition of benthic habitats using an automated classification technique. The main objective of this study is to develop a high resolution habitat map suitable for effective management application regarding potential threats that might be discovered in a high use shallow water cove. We also expect that by combining all derivatives, which were traditionally used independently, we will improve the differentiation of classes in the habitat map produced.

2.0 Methods

2.1. Study site

Wilsons Promontory Marine Park is located on the southern tip of Victoria. Southeasterly winds drive a strong coastal upwelling, which enhances primary (phytoplankton) production, increases the availability of nutrients to intertidal algae and influences production and abundance of benthic habitats (Bosman et al. 1987). Monitoring programs conducted in and around the Marine National Park (MNP) since 1999 have resulted in the observation of over 300 different species of algae (Edmunds et al. 2007). Three common algal assemblages have been identified over 20-28 sites surveyed; *Phyllospora* dominated; *ecklonia-seirococcus* dominated and mixed brown algae assemblage. Two species of seagrass including *Amphibolis antarctica* and *Halophilia australis* have been recorded as a dominant plant habitat in the soft sediments occurring throughout the MNP (Edmunds et al. 2012).Until recently, Wilsons Promontory Marine National Park only had a small proportion (<10%) of the 150km^2 mapped with high resolution (Parks Victoria 2014). Today, Wilsons Promontory now has full bathymetry and backscatter data for the park.

The study site for this project is Refuge Cove; a small embayment located within the Wilsons Promontory National Park and approximately 5km north of the existing Wilsons Promontory Marine National Park (Figure. 1). Refuge cove covers approximately 410,000m^2 in surface area and ranges in depth from 0 to 22 m. It is composed of two distinct embayments. The south side consists of 2-3m granitic boulders sloping gently to sandy bottom at 9m in depth (O'Toole et al. 1990) while the north side consists of sloping bedrock with occasional cracks and overhangs that

extends out to sandy bottom (O'Toole et al. 1990; Edmunds et al. 2012). The sandy bottoms are partially covered in seagrass patches and mixed algae assemblages are commonly found on the rock substratum (O'Toole et al. 1990). Refuge Cove contains a secluded beach where the sole land access is through a 15km hike from the nearest camping ground, making it a popular anchorage location for local sailors. The cove is protected from most swell directions except for the rare but strong easterly winds and swells, making it a popular safe anchorage for many national and international vessels cruising along the coastline. This constant influx of sailing boats has lead Parks Victoria to have a pest survey conducted in the cove in search of invasive species that might have been introduced by visiting boats and yachts. In an environment with increasing anthropogenic activity there is a need for an accurate habitat map to help management authorities monitor potential habitat change and to help identify possible threats (Beaman et al. 2005; Kostylev et al. 2005; Che Hasan et al. 2012b). It is an important first step to define the characteristics that make up Refuge Cove because of its popularity as an anchorage. It is deemed a peaceful and pristine environment by hikers and local management authorities, yet little is known about the habitats that exist underwater.

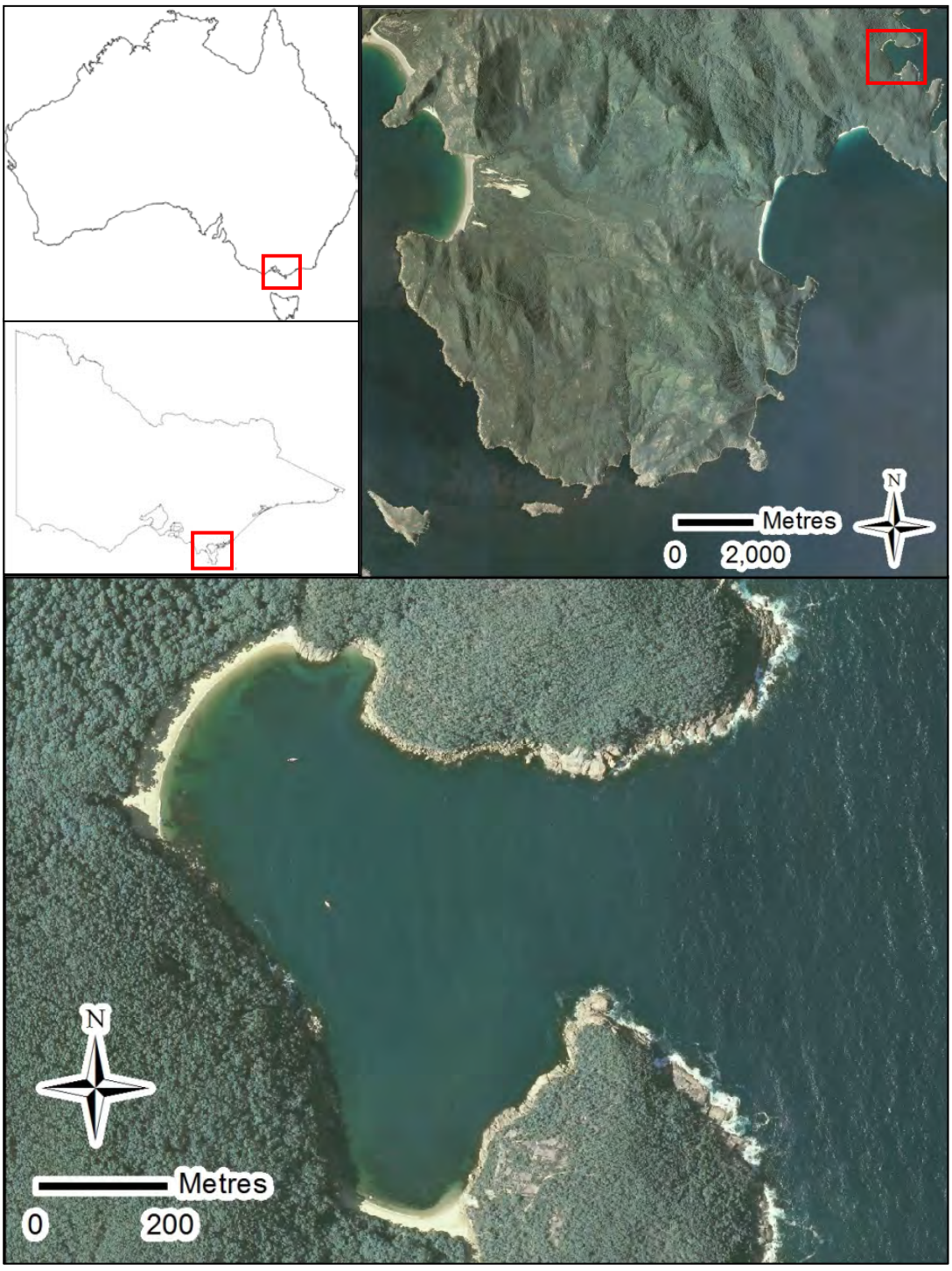

Figure 1. Location of Refuge Cove within Wilsons Promontory National Park, Victoria, Australia. Projection: Map Grid of Australia (MGA_94_zone_55).

2.2 MBES data acquisition and processing

A MBES survey of Refuge Cove was conducted by Deakin University on the 11th June, 2013 using Deakin University's 9.2 m survey vessel *Yolla*. The system consisted of a Kongsberg Maritime EM2040C MBES integrated with an Applanix POS MV WaveMaster. The POS MV WaveMaster measured precise vessel motion data (true heave, pitch, roll and yaw +0.02 accuracy). Positioning data were obtained using a Fugro MarineStar satellite positioning-based service through an online subscription service. Real-time navigation, data logging, quality control and display were undertaken using SIS software. Sound velocity profiles were captured with a Valeport Monitor Sound Velocity Profiler to correct for water column sound speed variation. The soundings were manually cleaned in HIPS and SIPS 8.1 and gridded at a resolution of 25cm (See Figure 2 and Figure 3).

2.2.1 MBES derivatives and OBIA segmentation

Twelve derivative layers that have been applied successfully in previous studies in habitat mapping (Ierodiaconou et al. 2007; Rattray et al. 2009; Ierodiaconou et al. 2011) were produced from the high resolution bathymetry and backscatter data using a number of software. Table 1 shows the derivatives that were produced from bathymetry and backscatter data as well as what program and settings were used and figure 4 shows visuals of the different layers used.

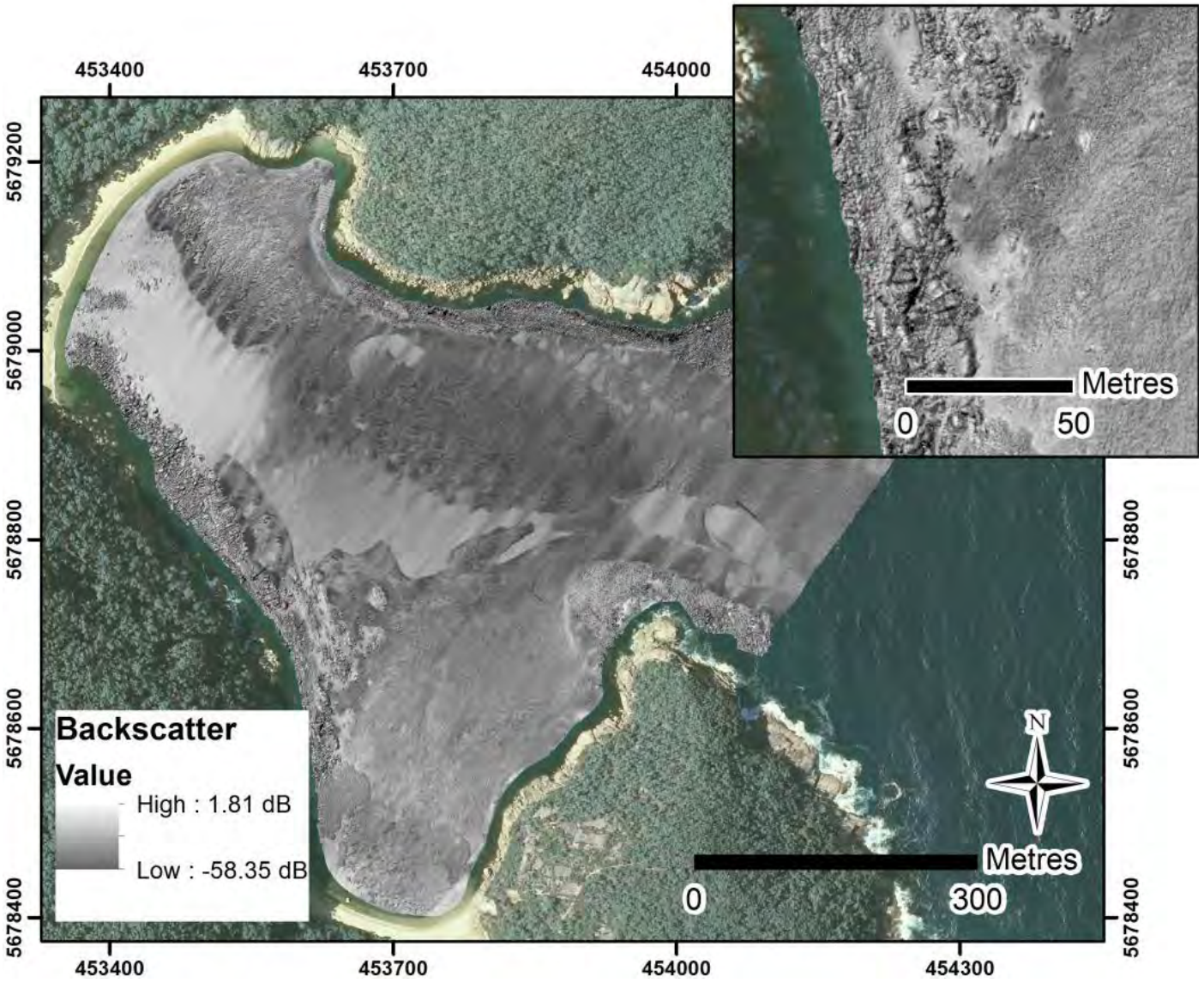

Figure 2. Hill-shaded MBES backscatter data for Refuge Cove, highlighting the high resolution achieved

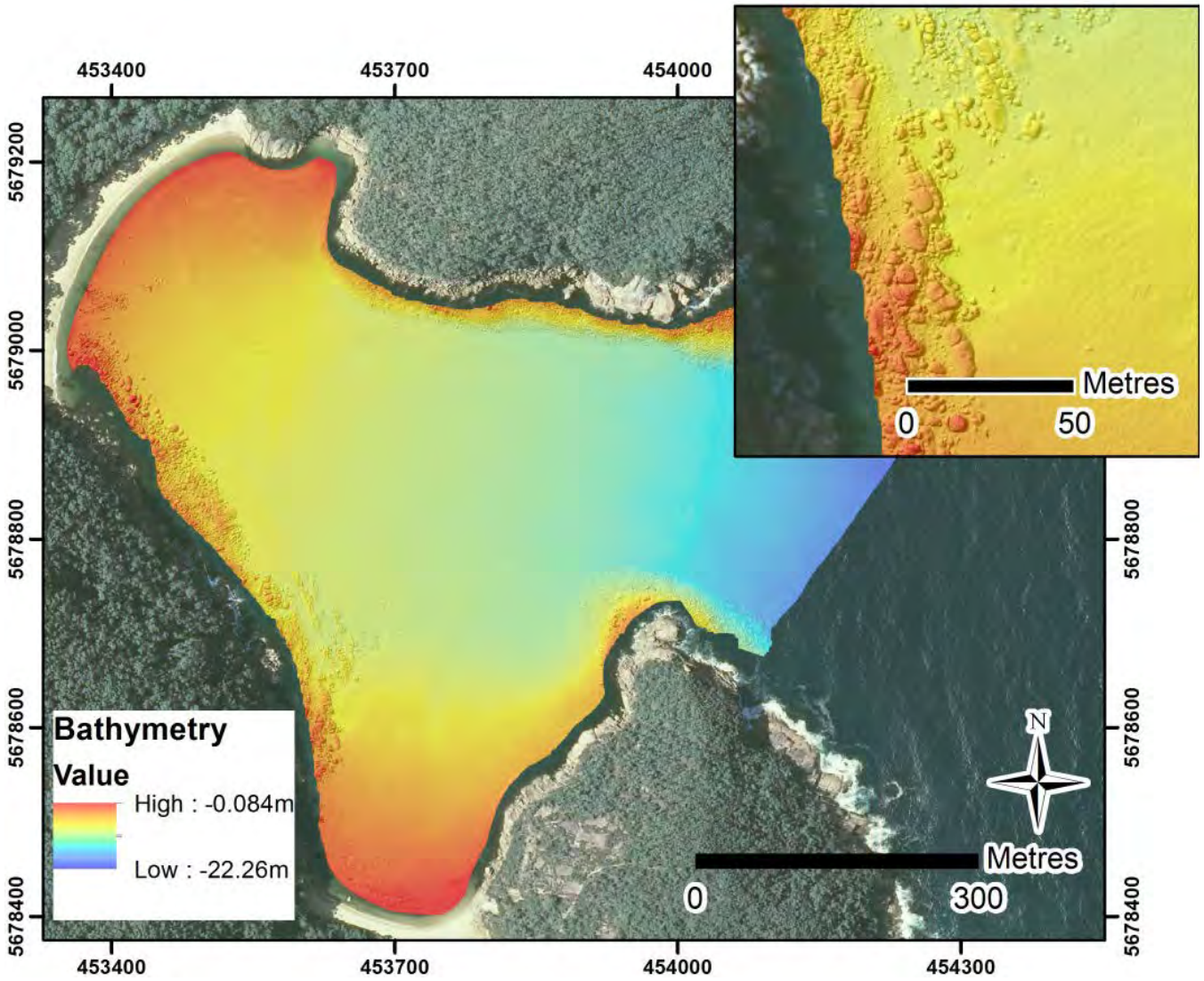

Figure 3. Hill-shaded MBES bathymetry data for Refuge Cove, highlighting the high-resolution achieved

Table 1. This table lists and describes the MBES derivatives used in the classification stack made in ENVI 4.7 RuleGen extension.

MBES Derivative	Description	Source	Program	Reference
Bathymetry Position Index (BPI)	BPI measures a user defined elevation point to relative surrounding terrain. We used a broad BPI = inner radius of 1 with outer radius of 150. We also used a fine BPI = inner radius of 1 and outer radius of 150.	Bathymetry	ArcMAP 10.1 - Benthic Terrain Modeler tool.	**(Lundblad et al. 2006)**
Slope	Slope is a measure of the steepness or maximum rate of change between each pixel of terrain. Slope = arctan(), where (d) and (e) are coefficients of the quadratic equation representative of the surface	Bathymetry	ENVI 4.7 RuleGen extension	**(Wilson et al. 2007; Zavalas et al. 2014)**
Rugosity	Rugosity describes topographic roughness. It indicates whether the terrain is flat, smooth or is high relief**.** For this study a neighbourhood of 3 was used.	Bathymetry	ArcMAP 10.1	**(Lundblad et al. 2006)**
Complexity	Complexity compares a central pixel to surround neighbours. It is derived from the slope derivative (Wilson et al., 2007). For this project we calculated Slope of Slope.	Bathymetry	ENVI 4.7 RuleGen extension	**(Wilson et al. 2007)**
Aspect	Reflects the orientation of each pixel. Typically measured in degrees with values between 0 and 359 degrees. *eastness = sin(aspect)* *northness = cos(aspect)*	Bathymetry	ArcMAP 10.1	**(Wilson et al. 2007)**
Maximum Curvature	Curvature is based on surface geometry. Maximum (convexity) and minimum (concavity)	Bathymetry	ENVI 4.7 RuleGen extension	**(Wilson et al. 2007)**
Hue Saturation Intensity (HSI)	HSI separates surface scattering and topographic influence and reduces noise levels within backscatter dataset. HSI has three bands e.g., red, green and blue. These bands separate high and low frequencies. For this study parameters High = 3, Low = 11, value = 0.5	Backscatter	ENVI 4.7 RuleGen extension	**(Daily 1983)**

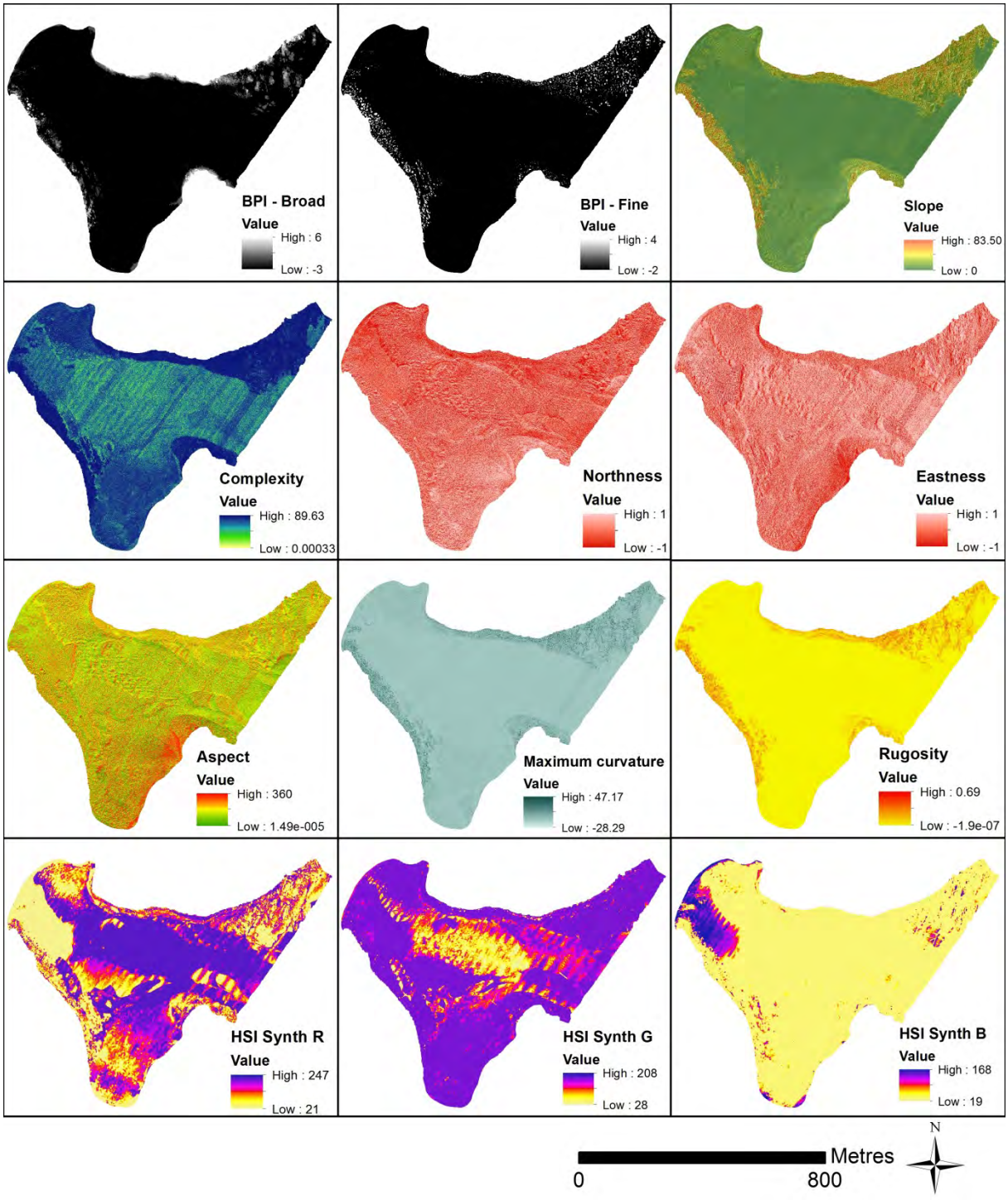

Figure 4.MBES derivative surfaces produced for habitat classification. Bathymetry derivatives: BPI broad and fine, slope, complexity (slope of slope), aspect, maximum curvature, rugosity. Backscatter derivatives: HSI synth R, G and B. Projection: MGA_94_zone_55.

Segmentation was carried out using the multi-resolution segmentation algorithm in software eCognition v9.0. This algorithm is an optimisation procedure, which locally minimises the average heterogeneity of image objects for a given resolution of image objects. Starting from an individual pixel (or existing image object), it consecutively merges pixels (or image objects) until a certain threshold, defined by the scale parameter is reached. The scale parameter is an abstract term that determines the maximum allowable heterogeneity for the resulting image objects. The object heterogeneity, to which the scale parameter refers, is defined by the 'composition of homogeneity' criterion. This criterion defines the relative importance 'of colour' (pixel value in this case, e.g. backscatter digital number) versus shape of objects. If high weight is given to colour then the object boundaries will be predominantly determined by variations in colour of the image (e.g. backscatter strength). Further on, the shape criterion has contributions from smoothness and compactness, both of which can be weighted. A high value for smoothness will lead to smoother boundaries of the objects. High values of compactness will increase the overall compactness of image objects. We applied default values of 0.9 for colour, 0.1 for shape, 0.5 for smoothness and 0.5 for compactness. Segmentations were carried out on bathymetry, backscatter, BPI150 and rugosity (5x5 kernel).

The choice of appropriate scale parameters was aided by the Estimation of Scale Parameter 2 (ESP2) tool (Dragut et al. 2014), which allows for an estimation of scale parameters based on multiple input layers. The ESP2 tool automatically segments the user defined data with fixed increments of scale parameter, and

calculates local variance (LV) as the mean standard deviation of the objects for each object level obtained through segmentation. To assess the dynamics of LV from one object level to another, a measure called rate of change (ROC) is derived from LV. Graphics of LV and ROC are used to evaluate the appropriate scale parameters. It is assumed that peaks in the ROC graph will indicate the object levels at which the image can be segmented in the most appropriate manner (Dragut et al. 2010). The resulting curves are shown in Figure 5. Based on distinct peaks in the ROC curve, scale parameters of 16, 23, 27 and 41 were chosen (although other scale parameters based on less distinct peaks were initially trialed as well).

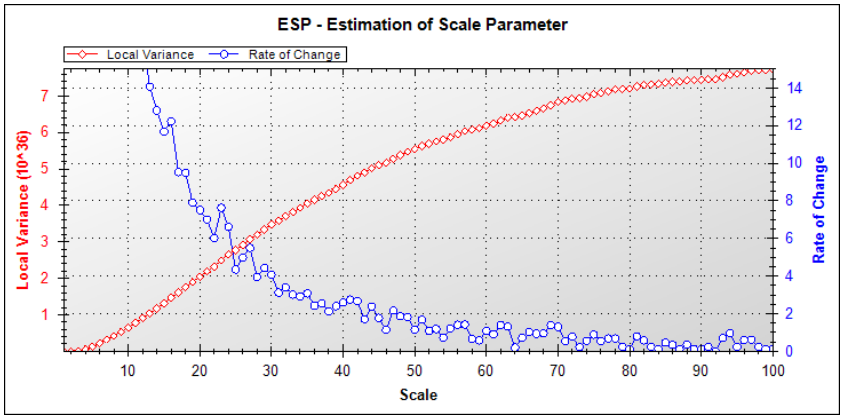

Figure 5. Resulting curves of local variance and rate of change.

Finally, the segmentation results were exported as shapefiles and attributed with mean, standard deviation and skewness (calculated per image object) of the input layers bathymetry, backscatter, BPI150 and rugosity (5x5 kernel) see Figure 6.

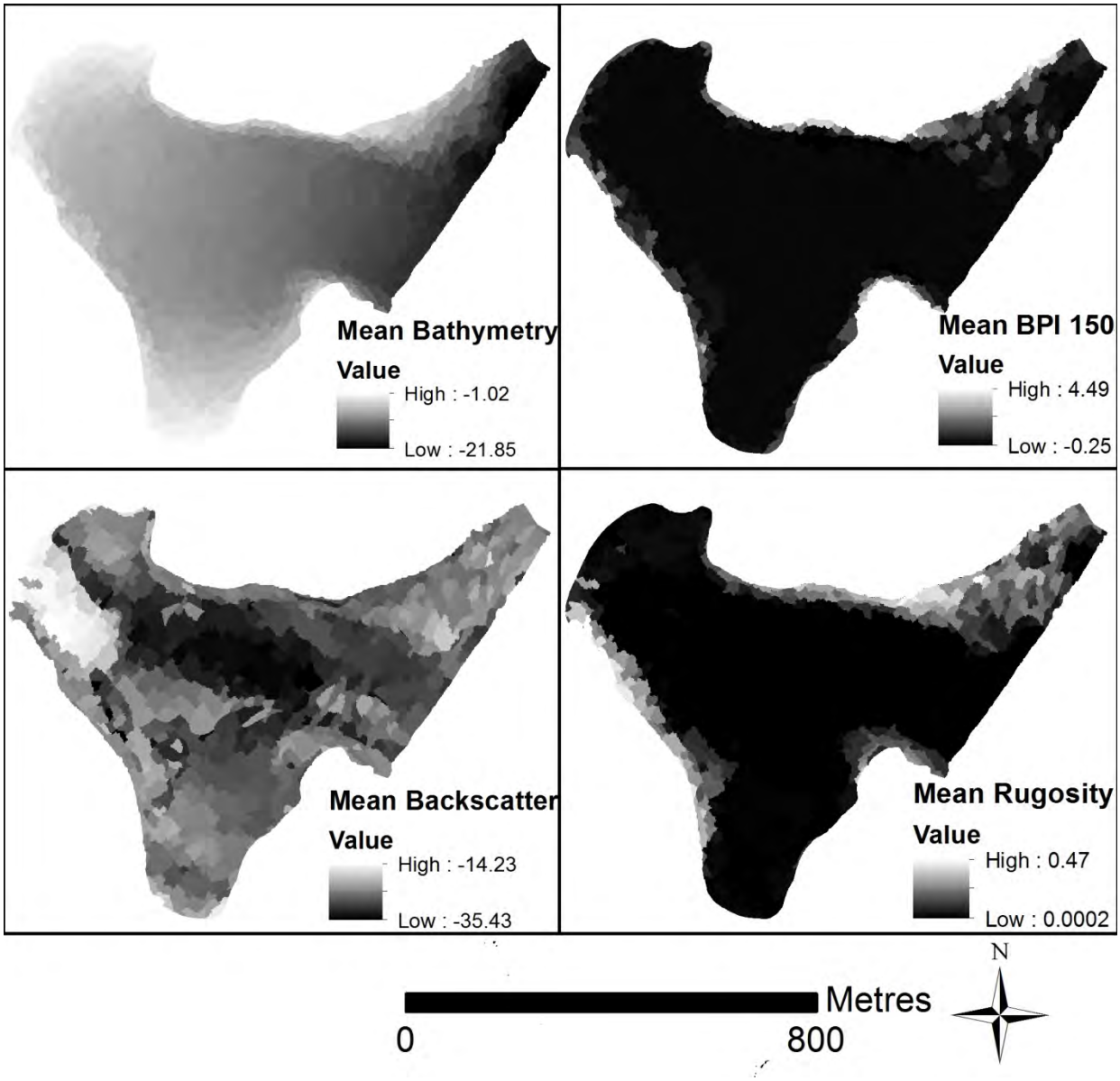

Figure 6. OBIA segmentation layers produced for habitat classification. Bathymetry segments layers: Mean bathymetry, mean BPI150 and mean rugosity. Backscatter segments layers: Mean backscatter. Projection: MGA_94_zone_55.

2.3 Ground truth data

2.3.1 Video data and Spatial Autocorrelation

High-definition video data were captured with a GOPRO HERO 3 video camera mounted on an Ocean Server Inc Iver2-580-EP Autonomous Underwater Vehicle (AUV) deployed on the 27th of May 2013 for a total distance of eight linear kilometers (Figure 9). The AUV was run at a speed of 1.5knots following a continuous transect divided into six pre-programed missions. However, two missions were not completed due to entanglement in reef. Transects were prioritized with limited knowledge of the area with an attempt to target a range of habitats on sediment and reefs across depth gradients within the cove. The GOPRO HERO 3 video data recorded in 20 minute videos during missions. Every second of video time was matched to positional information and mission statistics recorded by the AUV micro-processor.

A drop video camera video survey was performed on the 28th August 2014 to target areas that were not covered by the previous AUV survey for: (1) additional collection of data for training, in data limited areas (Figure 9); (2) to provide an independent sample data set for validation purposes. Additional training data were targeted locations were mostly along the north side of the cove where the AUV mission had failed due to entanglement in macroalgae as well as areas targeted for error assessment. A Delta vision HD underwater video camera was used to collect video footage and an Ashtec Mobil Mapper 10 was used to create shapefiles and log GPS raw data. Raw GPS data were later used in conjunction with the VicMap owned Continuously Operating Reference Stations (CORS) data to post-process, which

achieved greater spatial accuracy. A total of 85 drops were completed for ground truthing and error assessment throughout the cove. Video drops ranged from 1.9m to 22.1m in depth.

Spatial autocorrelation from AUV video tracks and MBES bathymetry and backscatter derivatives was used to determine distance required for our error assessment points to be spatially independent. Independence of observations is a critical assumption for many types of statistical techniques (Hurlbert 1984; Zuur et al. 2009). When dependence between variables exists in a dataset, it must be accounted for. One type of dependence is spatial dependence, also known as spatial autocorrelation. Spatial autocorrelation is a common occurrence in spatially defined observations where observations that are made close together are more similar than those that are further apart (Zuur et al. 2009). Spatial autocorrelation violates the assumption of independence of observations and must be tested and accounted for prior to analysis. For this study, Moran's *I* was used to test for spatial autocorrelation. The survey tracks were significantly and positively spatially autocorrelated in distances up to ~250 meters (Figure 7). Within the sidescan classes, however, the data were only spatially autocorrelated up to 50 meters when depth and rugosity were used to help explain the clustering of points (Figure 8).

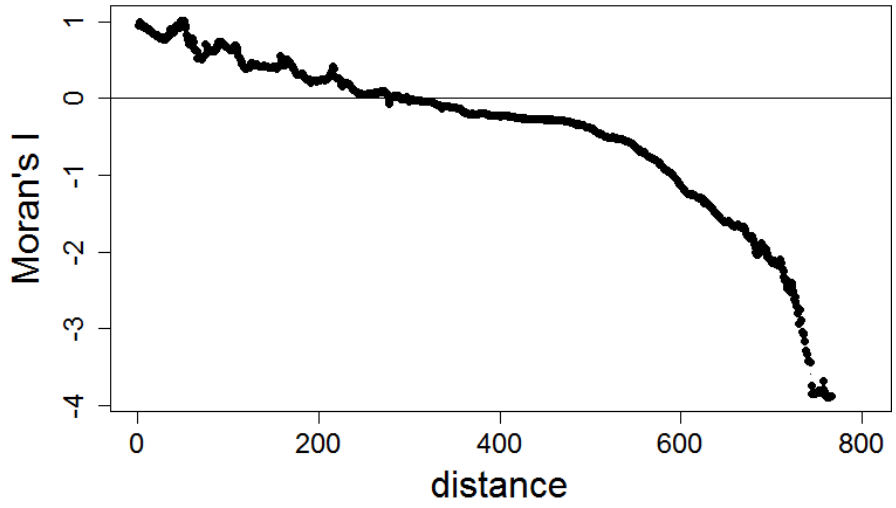

Figure 7. Moran's I of the survey points within Refuge Cove.

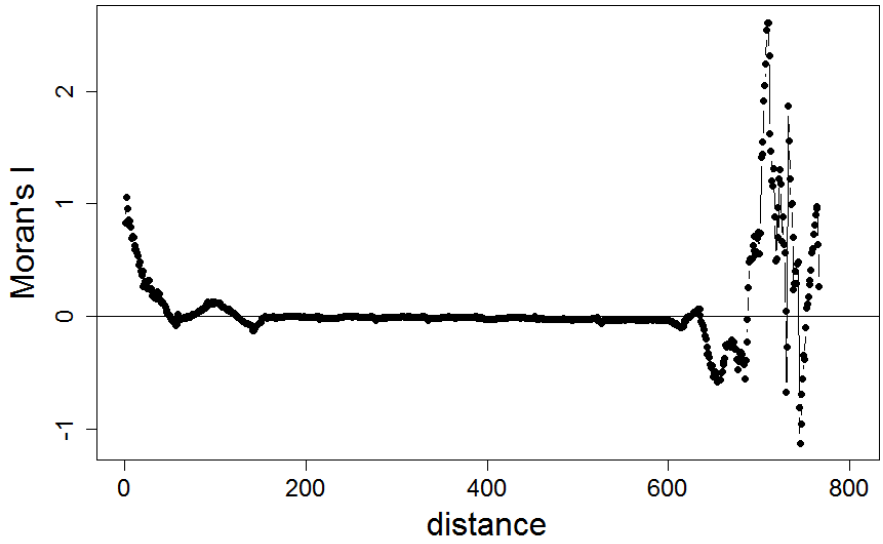

Figure 8. Moran's I as a function of distance for the survey tracks within Refuge Cove within the SS classes and incorporating depth and rugosity of the substrate.

Using a minimum distance of 50m between sample localities as defined by the spatial auto correlation, 93 independent validation points were selected for error assessment (Figure 10). A cluster analysis of the OBIA segments was performed to group segments with similar acoustic characteristics. From the 7 classes established we then randomly generated sample locations stratified by the classes derived from the cluster analysis to ensure coverage across the major acoustic facies of the site (7 classes n =35). All validation localities were located at least 5m from the edge of segments to avoid transitional zones between habitat types. In addition 58 localities were added from the AUV (37 sites) and drop video (21) to ensure good spatial coverage of the site for validation whilst maintaining spatial independence.

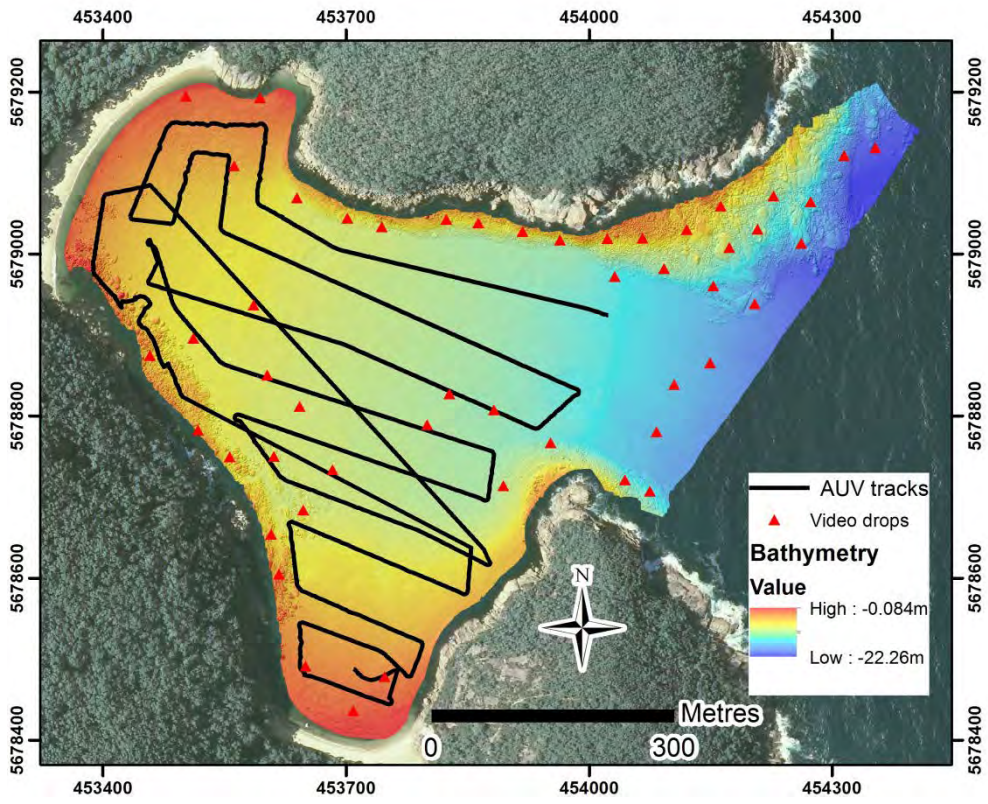

Figure 9. Hill-shaded bathymetry data overlaid with training data from AUV video and drop video data

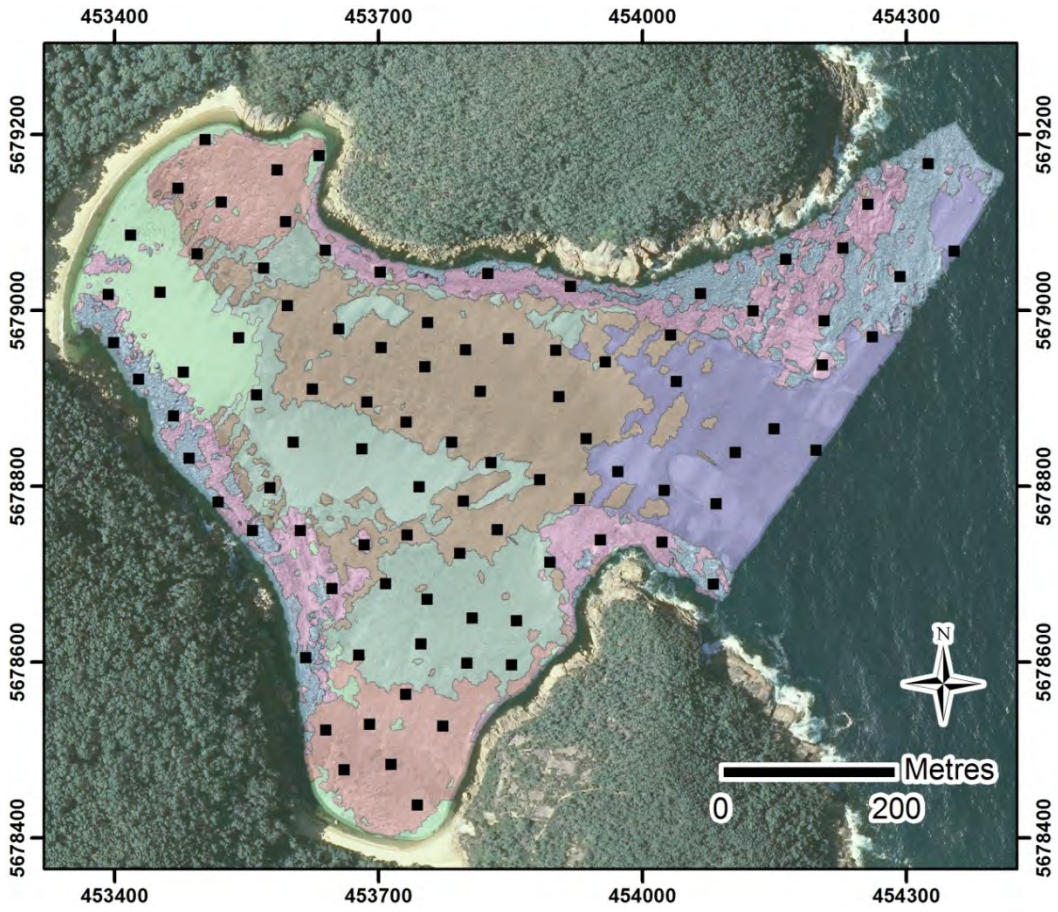

Figure 10. Hill-shaded backscatter data with overlaid cluster analysis segments and validation localities for error assessment.

2.4 Habitat delineation and classification models

2.4.1 Video data processing

Video data were processed in a series of steps. First, each video frame was linked to a geo-referenced position via an overlaid GPS time stamp allowing classified frames to be accurately integrated with MBES datasets for model development. The Victorian Towed video classification program was designed in Microsoft Access by Ierodiaconou et al. (2007) in which an adapted version by (Blake 2013) was used to allow for direct import of camera positioning information, classification of video information and direct export to GIS/remote sensing packages for further spatial analysis. A video data library with samples of habitat categories was created to ensure consistency throughout video classification process.

GO Pro video and AUV log files were imported into Microsoft Excel to be formatted correctly. Valuable data (latitude, longitude, actual time, mission title, depth) were kept. Excel sheets were then formatted with appropriate column titles for application of habitat classification and characterisation. Video time was matched up to time on the log files. Missions began in the video data as soon as the motor turned on and allowed synchronisation to the positional data recorded for each mission. Each video frame was then given a classification. Screen shots representing different habitat classes observed were saved as a catalogue library of images for future reference and verification (see appendix 1). Anthropogenic features observed were also logged for future reference (see appendix 2).

Video drops performed by the Delta vision were classified using two Excel spread sheets (for both segmentation and ground truth) corresponding to the AUV data sheets. Each individual video drop was then given a single classification for its position using the Victorian towed video classification scheme.

2.4.2 Supervised classification for prediction of habitat classes

The Quick, Unbiased, Efficient Statistical Tree algorithm (QUEST) was used for predictive classification for this study. Recent studies have shown that QUEST classifiers operating on MBES data derivatives and video data can successfully predict the distribution of dominant biological communities and substrates (Ierodiaconou et al. 2007; Rattray et al. 2009). The QUEST decision tree only allows binary splits and uses a linear discriminate analysis approach. The predictor variable is split numerous times until it reaches a user-defined class. The main advantages of QUEST compared to other decision tree classifiers is that they do not use an exhaustive variable search routine and are also unbiased in choosing splitting rules (Loh et al. 1997). By providing relationships between habitat classes and MBES data layers, the process of assigning a habitat class to pixels without video observations is achieved. The RuleGen extension v.1.02 in ENVI v. 4.7 (ITT VIS Inc.) was used to make use of the MBES data product (bathymetry and backscatter) derivatives and data derived from video observations. To test the data derivatives and particularly the new features derived from OBIA we ran a selection of models (see Table 2). These models contained different combinations of bathymetry, backscatter and segmentation derivative layers to help identify the best contributors to accurately classify the habitats observed.

Table 2. Derivative combinations models

	Stack derivatives:	Model 1	Model 2	Model 3	Model 4	Model 5
Bathymetry:	Bathymetry	x	x		x	x
	Complexity	x	x		x	x
	Eastness	x	x		x	x
	Northness	x	x		x	x
	Broad BPI	x	x		x	x
	Fine BPI	x	x		x	x
	Slope	x	x		x	x
	Aspect	x	x		x	x
	Rugosity	x	x		x	x
	Max Curvature	x	x		x	x
Backscatter:	Backscatter		x		x	
	HSI - B		x		x	
	HSI - G		x		x	
	HSI - R		x		x	
Segmentation:	Mean Rugosity			x	x	x
	Mean Backscatter			x	x	x
	Mean BPI			x	x	x
	Mean Bathymetry			x	x	x

2.5 Model performance

2.5.1 Error assessment

Classification accuracy was assessed from the error matrix for each of the five models containing different combinations of derivatives. An error matrix is a square array of numbers set in rows and columns which express the number of sample units (e.g., pixels. polygons) assigned to a category relative to the actual category as verified (Congalton 1991). Rows in an error matrix represent the classification generated and columns usually represent the reference data. Error matrices are effective in representing accuracy overall and also categorically (Congalton 1991). Overall accuracy is calculated from an error matrix by summing the number of points that were correctly classified for each classes and dividing the result by the total number of error points used (Congalton 1991). For this study we used a total of 93 (Figure 6) error points which are all independent from each other. The differences between the output of each model were then assessed through the computation of the Z-statistic between each pair of matrices (Cohen 1960; Congalton 1991).

2.5.2 Map comparison

Further assessments based on raster outputs was also undertaken to investigate how different models represented the different classes using the Map Comparison Kit 3.2 software designed by Research Institute for Knowledge Systems (RIKS). The Fuzzy Kappa statistic was computed for each pair of maps to give an overall similarity statistic (Hagen-Zanker et al. 2005) on observed and predicted classification results. We will also assess patch size (area of cells) of individual

categories between models. This will give a spatial account of the differences in categorical structure depending on the models used for classification (Hagen-Zanker 2006). By comparing the model outputs via patch size and fuzzy kappas, particularly comparing via habitat classes, we will be able to get a better understanding of what models are contributing to predictions of habitat classes within Refuge Cove. The best performing model and its classified map will enable management authorities of Refuge Cove to identify potential threats to habitat species as well as give them an understanding of the habitats in this area for further monitoring programs.

3.0 Results

3.1 Ground data

3.1.1 Video observations

A total of 6254 ground truth data points were used to train the models for classification derived from AUV and video drops. Video data was distributed among 5 broad habitat classes: Seagrass *Amphibolis antarctica* (SGAM), Seagrass *Zostera* spp. (SGZ), Macroalgae, Filamentous mat and no visible biota (see appendix 1). Table 3 shows the class identification for the video data used for training the models as well as the data used for accuracy assessment. From the video data collected some of the observed classes were restricted to (<50m) in patch size which reflects on the number of pixels designated for error assessment for those classes.

Table 3. Training ground truth data points for each habitat class.

Habitat Class	Number of samples used for training models	Number of samples used for error assessment
Seagrass *Amphibolis antarctica* (SGAM)	175	1
Filamentous mat (FMAT)	1543	17
Macroalgae (ALG)	677	29
No Visible Biota (NVB)	3036	36
Seagrass *Zostera* spp. (SGZ)	823	10

The SGZ was found predominately in the top northwest side of the cove. It was distributed in very dense patch areas. SGZ was also found in the south side of the cove where it was heavily associated with the FMAT class. The seagrass SGAM was found in the south end of the cove. SGAM was found in very dense patches surrounding the sides of the south end. The FMAT class was only found in the south end of the cove and from video observations seemed quite thick with sparse SGZ in some patches. ALG were mostly observed on the north and south west side of the cove. Dominate species within this class consisted of mixed brown algae assemblages with *Ecklonia radiata* and *Sargassum spp.* making up the majority of species identified. Fifty percent of the video data collected was found to contain bare soft sediments (fine sand or shelly coarse sand) with NVB see Figure 11.

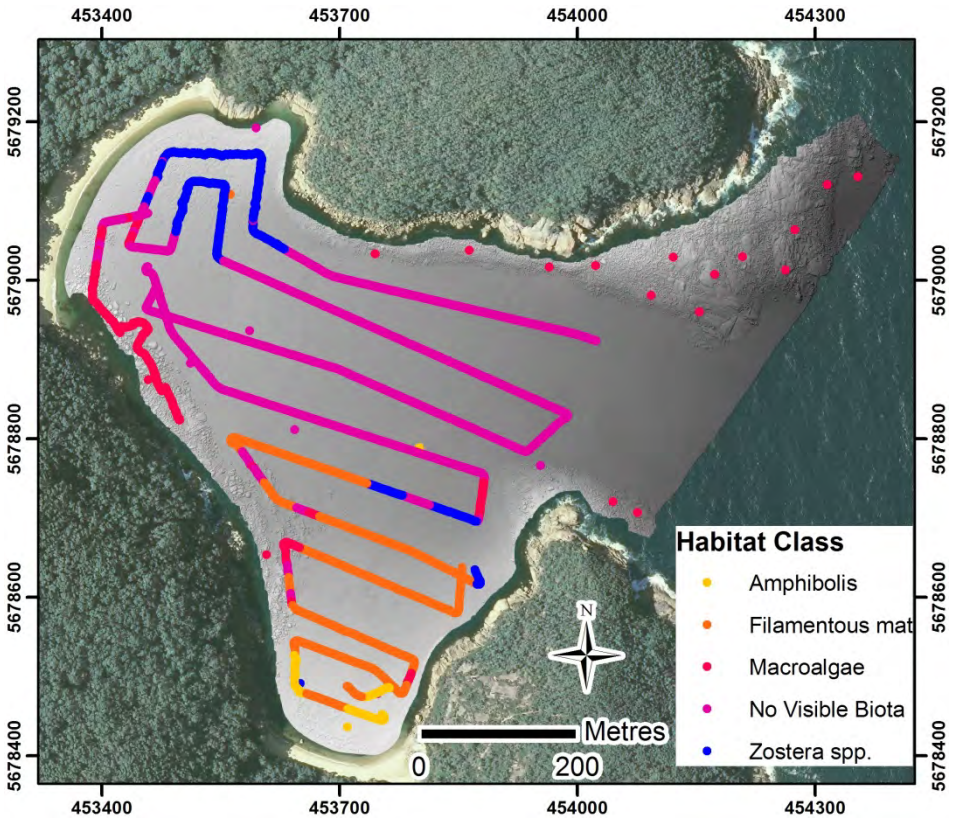

Figure 11. Hill-shaded bathymetry data with overlaid classified video training data.

3. 2 Classification Accuracy & Model Performance

Table 4 shows overall accuracy and the results from the Z-statistics comparison which shows that there was no statistically significant difference between each of the five models. Figure 12 shows the habitat maps resulting from each model. The overall accuracies suggest that model 5 performed the best and model 1 performed the worst. Models containing the segmentation layers performed better than the models with backscatter and bathymetry derivatives only. Interestingly, a model containing only the four segmentation layers (model 3) outperformed the models containing bathymetry derivatives (model 1) or a combination of bathymetry and backscatter derivatives (model 2). Model 4 containing all derivatives and layers performed second best with an overall accuracy of 76.34%. However, model 5, which contained only the bathymetry derivatives and segmentation layers, had the best overall accuracy of 78.34%.

Table 4. The table shows overall accuracy from each of the five models and the Z-statistic results testing for significance by measuring the difference between models. Significant = >1.96

Model number:	Overall Accuracy (%)	Model combinations	Z-Statistic
Model 1	63.44	1 – 2	-1.23
Model 2	70.97	1 – 3	-1.80
Model 3	74.19	1 – 4	-2.16
Model 4	76.34	1 – 5	-2.48
Model 5	78.34	2 – 3	-0.56
		2 – 4	-0.92
		2 – 5	-1.24
		3 – 3	-0.36
		3 – 5	-0.68
		4 - 5	-0.32

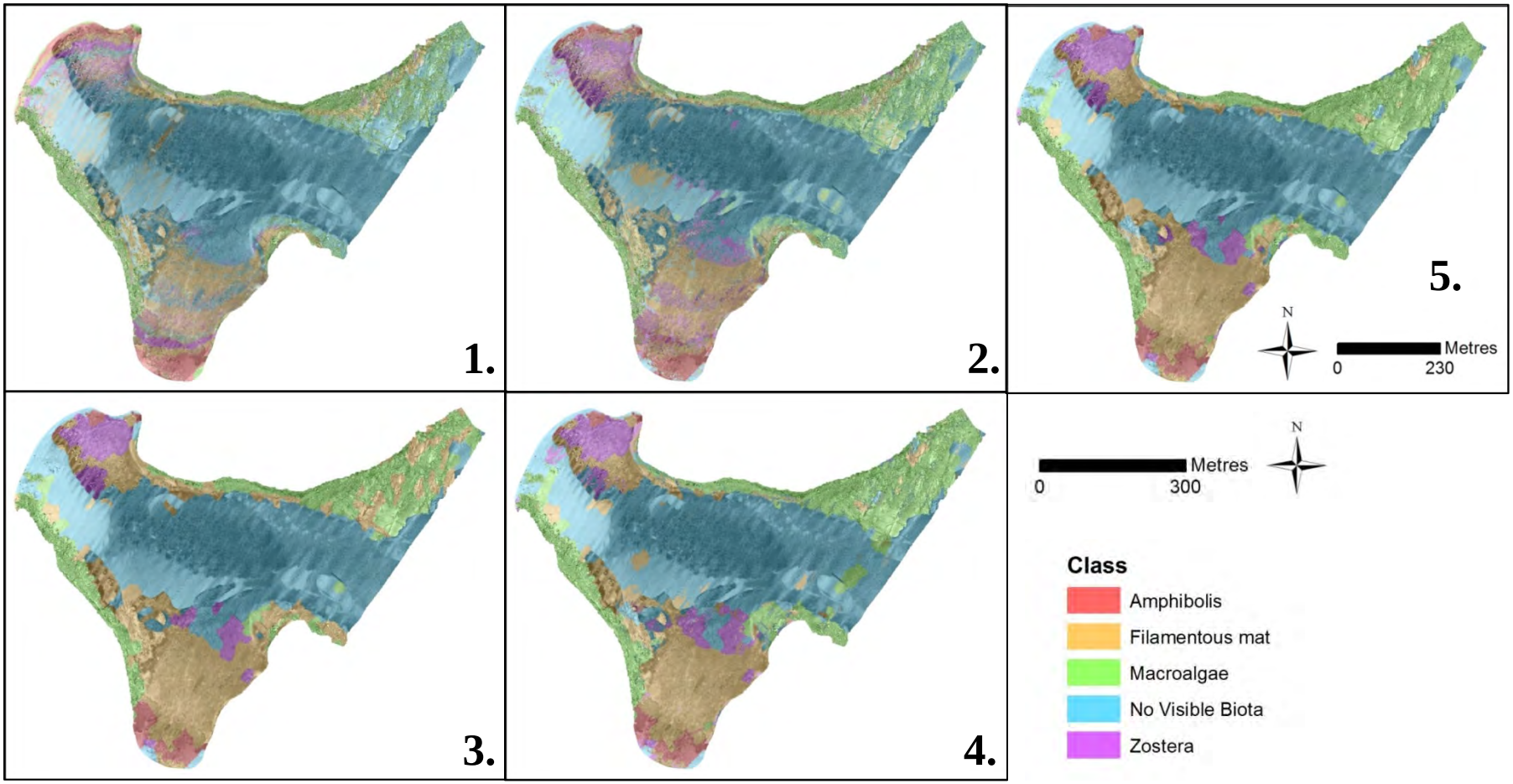

Figure 12. Classification results for benthic habitat classes overlaid on backscatter hillshade at Refuge Cove. The number in the bottom left of each map represents the model used for classification

3.3 Map Comparison

3.3.1 Fuzzy Kappa

Table 5 gives the Fuzzy Kappa values from the map comparison. To assess the similarity between models values closer to 1 indicate complete similarity whereas values closer to 0 indicate distinct difference. Model 1 is only similar to model 2 with a Fuzzy Kappa of 0.685. Model 2, 3, 4 and 5 when compared to each other are more similar to each other. Comparison between Model 3 had more similarity with Model 5 (Fuzzy Kappa = 0.849 than 4 (Fuzzy Kappa = 0.772). Comparison between model 4 and 5 had highest overall similarity with a Fuzzy Kappa 0.858.

Table 5. Fuzzy Kappa comparison between model results

	Model 1	**Model 2**	**Model 3**	**Model 4**
Model 1				
Model 2	**0.685***			
Model 3	0.475	**0.557***		
Model 4	0.476	**0.58***	**0.772***	
Model 5	0.495	**0.589***	**0.849***	**0.858***

Per category comparison method is illustrated in figure 13 for the categories SGAM and Filamentous mat. For visual purpose we show the comparison between the lowest overall accuracy, model 1 and highest overall accuracy, model 5 map rasters. The red class indicates what is only found in model 1, which highlights a speckle effect associated with noise in class predictions in model one. In contrast, classes predicted using model 5 only (in blue), show more spatially homogenous patches that better represent what was observed in the training and validation data. Table 6 shows all Fuzzy Kappa statistics per category for map comparisons. Maps are similar with respect to ALG and NVB classes with all Fuzzy Kappas being above 0.5.

Model 3, 4 and 5 comparisons have greater similarity across four classes where as other comparisons are only similar with two to three classes. Interestingly, there is no similarity met for SGAM class across any of the models, with the exception of coming very close when comparing Model 3 to 5 (0.497).

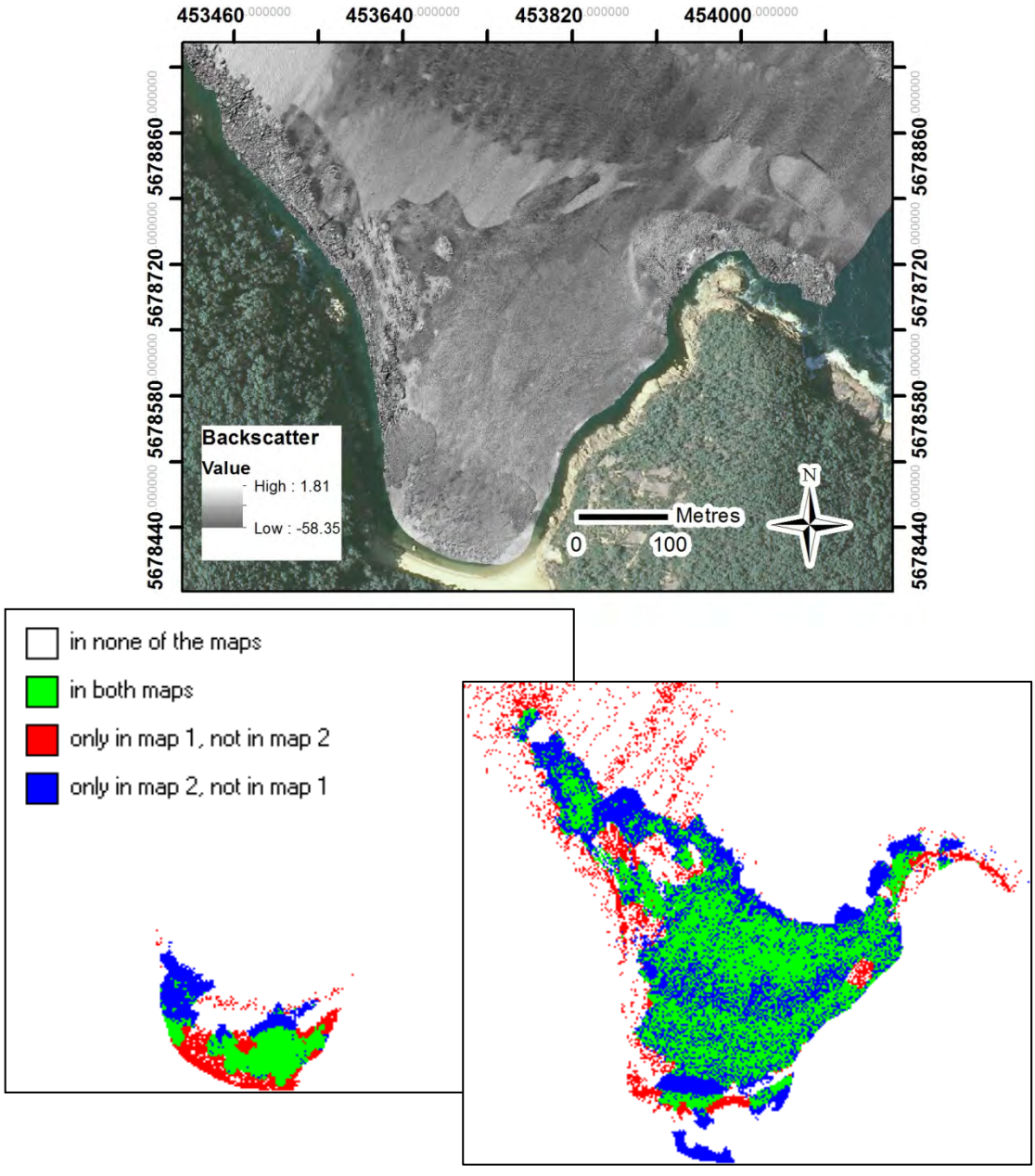

Figure 13. Map comparison of models 1 and 5 of two single habitat class categories. The left picture is for 'SGAM' and for the picture on the right is 'FMAT' class. Picture above is backscatter overlaid hillshade, representing the area of the cove that is being compared.

Table 6. Fuzzy Kappa statistics are shown per category for model comparison. Bold* values represent the categories that are similar between models.

	1 v 2	1 v 3	1 v 4	1 v 5	2 v 3	2 v 4	2 v 5	3 v 4	3 v 5	4 v 5
SGAM	0.487	0.275	0.29	0.262	0.32	0.346	0.322	0.482	0.497	0.494
FMAT	**0.661***	0.384	0.428	0.438	0.424	0.497	0.491	**0.699***	**0.781***	**0.82***
ALG	**0.798***	**0.525***	**0.533***	**0.543***	**0.562***	**0.611***	**0.624***	**0.744***	**0.808***	**0.861***
NVB	**0.701***	**0.557***	**0.524***	**0.549***	**0.681***	**0.661***	**0.672***	**0.82***	**0.896***	**0.857***
SGZ	0.461	0.232	0.251	0.24	0.364	0.368	0.359	**0.656***	**0.721***	**0.708***

3.3.2 Patch size

According to the patch size analysis, the habitat maps produced varied in patch sizes for each category. For all model comparisons per category of patch size see appendix 1. For model 1 and 5 comparison for SGAM class there is a -2167.14m^2 difference in patch size, indicating the model 5 has allocated a smaller area of pixels for this class. Similar results were found in model 1 and 3 comparison for SGAM class with a 2210.78m^2 difference in patch size. SGAM class Fuzzy Kappas across all models never meets similarity (all below 0.5) but comes closest when compared in model 3 and 5. Both model 3 and 5 have the segmentation layers which seem to be driving SGAM patch size into smaller homogenous areas, which correlates with what was observed in video data.

4.0 Discussion

In this study we implemented a decision tree classifier operating on a number of MBES derivatives, OBIA segment layers and video data to produce an accurate habitat map of Refuge Cove. We compared the performance of five different models containing different combinations of derivatives to test for difference in prediction of habitat classes. QUEST classifier was chosen based on its good performance as indicated in previous studies (Ierodiaconou et al. 2007; Rattray et al. 2009). Our study demonstrates that the derived habitat maps from each model were influenced by the choice of input derivatives and that the use of both MBES data derivatives with the OBIA segments was most effective in discriminating between habitat classes. Model 5 contained bathymetry data and OBIA segment layers and, although not statistically significant, performed best with the highest overall accuracy of 78.34%.

Our error assessment compared outputs using a Z-statistic, which produced no significant differences between models. The Error matrix analysis is an approach used to assess classification accuracy. This approach is widely accepted and is in widespread use in terrestrial land-cover and land use mapping studies (Foody 2002). The error matrix only takes into account the correction of error points. A study by Stephens et al. (2014) found that when comparing supervised classifiers error matrix did not reflect variability in model performance and they highlight the value of using an alternative to assessing classification performance when class error points are uneven. This was a limitation in our study as error assessment points took into account spatial autocorrelation; therefore, habitat classes with small patchy

densities like SGAM were assigned one error point compared to NVB which was assigned 36. With the assessment of map accuracy being critical to determine confidence in change and detection of results, we found that the Map comparison kit allowed us to compare classification map raster outputs for each model in order to detect change in model output. The Fuzzy Kappa and Patch size comparisons better reflected variability across the models.

The comparison between categorical maps is commonly applied in terrestrial studies and is becoming important in benthic habitat mapping studies (Schimel et al. 2010; McGonigle et al. 2011). In this study, map comparisons reflected relative agreement between two classified map rasters and not levels of accuracy. The results from this analysis gave us more information regarding the difference in classified habitat areas across each model.

Studies have shown that backscatter intensity increases in the presence of biological habitat such as seagrass when compared to bare sediment (Parnum 2007; De Falco et al. 2010). This study identified two separate seagrass species found within Refuge Cove. Patches are visible from the backscatter image in the areas of where the seagrass was observed in video data, however, the first two models displayed very pixelated representation of some of these patches. Comparing patch size between SGAM class showed that Model 5 had 2167.14m^2 less than Model 1. By comparing the patch size we can understand the spatial account of the difference in class structure between Model 1 and 5. Seagrass in previous studies has been known to get misclassified as no visible biota (Zavalas et al. 2014) and potentially other classes or other seagrass. The difference between the models is that Model 5

contains the segmentation layers. With closer inspection of classified maps, the incorporation of the segmentation layers removes the pixelated effect shown in Model 1 and 2. By applying the Models containing the segmentation layers; we have been able to achieved clearer patch structure outlines of these habitats.

The habitat maps reveal that the seagrass Amphibolis is distributed in the same area that is heavily used as a safe anchorage. The habitat classes SGAM represents the seagrass species *Amphibolis antarctica,* which is an Australian endemic seagrass species. Like most other seagrass beds SGAM provides refuge, food and protection for invertebrates (Okudan et al. 2011). *A. antarctica* have woody stems resulting in very slow reproduction rates and require long recovery periods if damaged (Walker 1985). Model 5 seems to not only provide best overall accuracy but also gives the best results for management applications by providing homogenous patches of habitat classes.

One implication of this study is to provide a suitable map for safe anchorage areas and areas that should be avoided when anchoring (Figure 14). There was possible evidence from video data suggesting that these seagrass beds where subject to scaring from anchors (see Appendix B) as there are linear marks observed in the video data in the sand and through sparse SGZ and FMAT classes. The habitat maps from this study can help promote awareness of where these habitats exist. Managers can use these maps to prevent any potential future impacts to these benthic ecosystems.

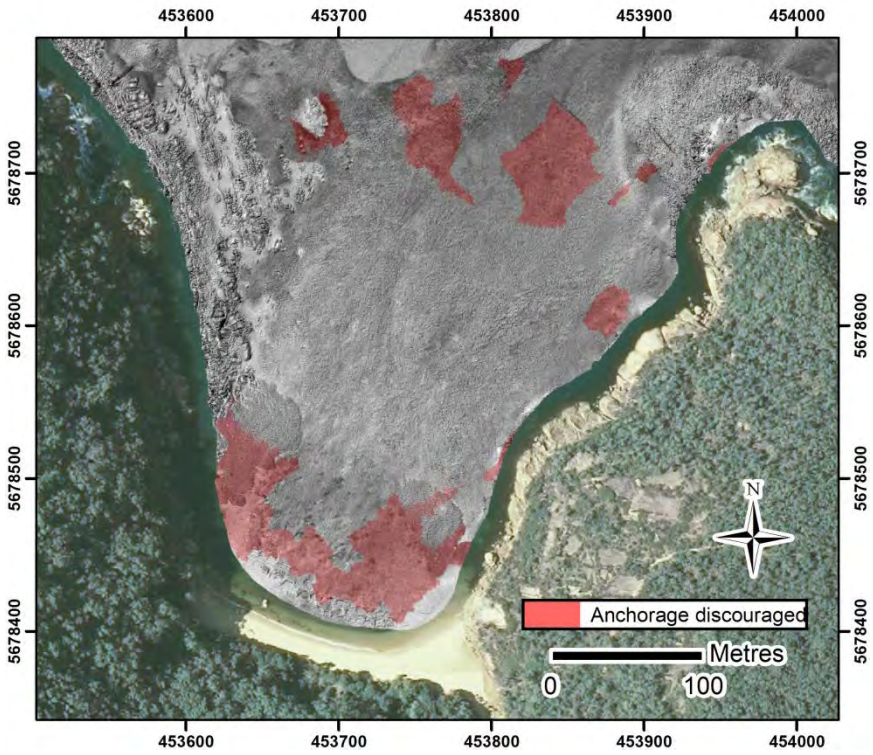

Figure 14. Red is highlighting the areas of seagrass patches which can now be seen as area to discourage anchorage.

Previous studies have found that adding backscatter data improved accuracy from bathymetry data alone (Rattray et al. 2009) suggesting there is value in adding backscatter data for habitat classification which is what was found in our study. However, from the performance of the models we can see that bathymetry and segmentation layers of (bathymetry and backscatter data) hold important variables. Including the segmentation layers and bathymetry derivatives together in the model gave best overall performance but when adding in the HSI derivatives from the backscatter seems to bring down overall accuracy, which may mean they are causing confusion in classification.

Because backscatter strength is a function of three different parameters; source power, absorption in the water column and interactions with the seafloor (Le Bas et al. 2009) there can be a lot of variation in backscatter intensity. By applying the OBIA approach to bathymetry and backscatter data, we helped improve classification of error assessment pixels. Previous studies have also improved classification as extracted segments form conclusive boundaries around sediment-related features or benthic habitats (Lucieer et al. 2011).

For this study, a cluster analysis of the OBIA segments was performed to group segments with similar acoustic characteristics in order to generate sample locations stratified by the classes derived. Error assessment points across studies are commonly selected after all ground-truth data has been collected. Many studies randomly assigned, randomly partitioned and stratified data points by habitat classes by a certain percent (Rattray et al. 2009; Ierodiaconou et al. 2011; Che Hasan et al. 2014; Stephens et al. 2014). This study presents an approach to selecting error assessment points before commencing field work. To make this approach possible we already had MBES data and AUV video data which made it possible to plan a second data collection, targeting independent sample locations. A limitation to this kind of approach is that field work would have to be carried out twice. Field work in collecting ground-truth data is also dependent on several issues such as money, time restraints and is dependent weather. For this approach we found advantages in that it provided us with a spatially independent data set used specifically for error

assessment only. In terms of analysis of error data, it was much easier to implement into accuracy assessment classification and less time consuming.

To construct a high accuracy habitat map for Refuge Cove, classified video data were combined with MBES data and OBIA segmentation layers. This study highlights that the production of benthic habitat maps using a supervised classification approach can be influenced by the variables used in the classification process. Whilst classification error outputs showed to not have statistical significance between each other the map comparison approach showed us variations in patch size and extent that should be taken into consideration when implementing management efforts.

By including the OBIA homogenous segments in the classification process improved the map outputs compared to traditional approached using MBES bathymetry and backscatter. OBIA in particular shows distinct advantages in reducing noise associated with inclusion of backscatter products in the classification process. With the increasing portability of MBES and video systems on small vessels for characterizing habitats there is a greater opportunity to target areas of high use or areas of ecological significance in shallow coastal waters as they are often the ones most under threat.

Appendix A: Video Observations catalogue

Medium *Zostera* spp.

Sparse Filamentous mat

Dense *Amphibolis antarctica*

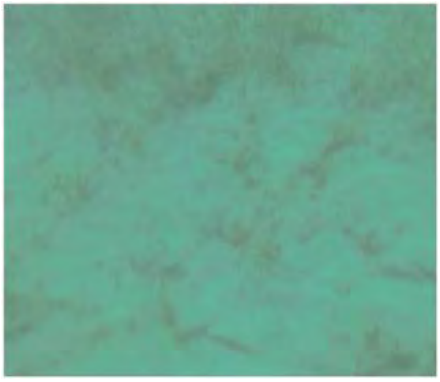

Sparse *Zostera* spp.

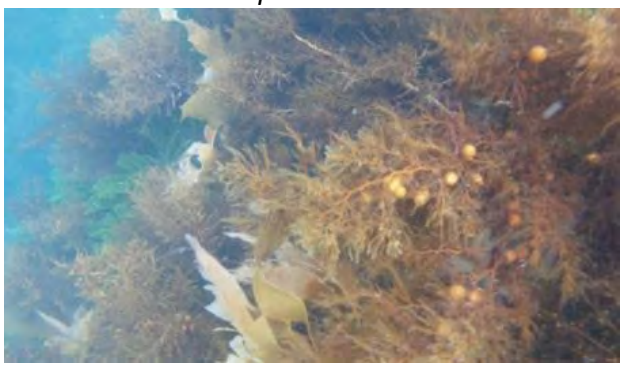

Mixed Brown/Sparse mixed green algae

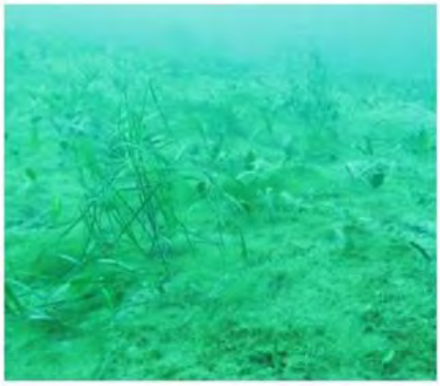

Filamentous Mat/Halophila/*Zostera* spp.

Mixed Brown Algae

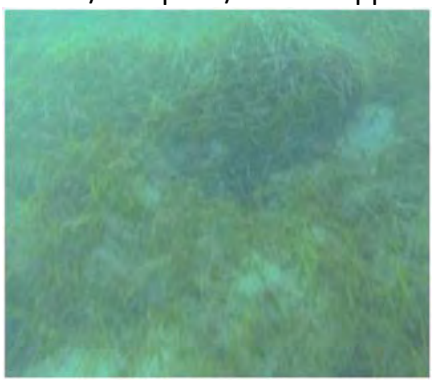

Dense *Zostera* spp.

Appendix B: Antropogenic disturbance catalogue

Three linear markings

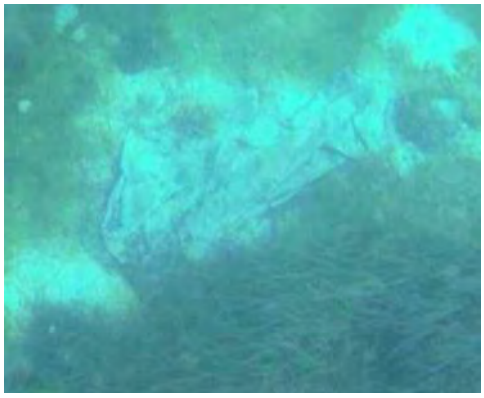

Plastic bag

One linear marking

Oil/dirt slick

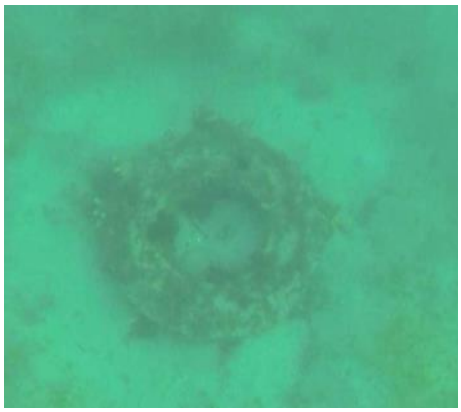

Tyre

Battery

6.0 References

Anders, NS, Seijmonsbergen, AC & Bouten, W 2011, 'Segmentation optimization and stratified object-based analysis for semi-automated geomorphological mapping', *Remote Sensing of Environment*, vol. 115, no. 12, pp. 2976-85.

Australian Marine Ecology 2014, *Automonous Underwater Vehicle (AUV)*, retrieved 21 October, 2014, <http://www.marine-ecology.com.au/index.php/resources-a-facilities/autonomous-underwater-vehicle-auv>.

Barrett, N, Seiler, J, Anderson, T, Williams, S, Nichol, S & Hill, S 2010, 'Autonomous Underwater Vehicle (AUV) for mapping marine biodiversity in coastal and shelf waters: implications for marine management', in *OCEANS 2010 IEEE-Sydney*, pp. 1-6.

Beaman, RJ, Daniell, JJ & Harris, PT 2005, 'Geology–benthos relationships on a temperate rocky bank, eastern Bass Strait, Australia', *Marine and Freshwater Research*, vol. 56, no. 7, pp. 943-58.

Blake, S 2013, *Marine video survey of Western Port / Sean Blake, David Ball, Allister Coots and Tim Smith*, Fisheries Victoria technical report series ; no.176. 1835-4785, Department of Primary Industries, Queenscliff, Victoria.

Blaschke, T 2010, 'Object based image analysis for remote sensing', *ISPRS Journal of Photogrammetry and Remote Sensing*, vol. 65, no. 1, pp. 2-16.

Boggs, GS 2010, 'Assessment of SPOT 5 and QuickBird remotely sensed imagery for mapping tree cover in savannas', *International Journal of Applied Earth Observation and Geoinformation*, vol. 12, no. 4, pp. 217-24.

Bosman, A, Hockey, P & Siegfried, W 1987, 'The influence of coastal upwelling on the functional structure of rocky intertidal communities', *Oecologia*, vol. 72, no. 2, pp. 226-32.

Brown, CJ, Smith, SJ, Lawton, P & Anderson, JT 2011a, 'Benthic habitat mapping: A review of progress towards improved understanding of the spatial ecology of the seafloor using acoustic techniques', *Estuarine, Coastal and Shelf Science*, vol. 92, no. 3, pp. 502-20.

Brown, CJ, Todd, BJ, Kostylev, VE & Pickrill, RA 2011b, 'Image-based classification of multibeam sonar backscatter data for objective surficial sediment mapping of Georges Bank, Canada', *Continental Shelf Research*, vol. 31, no. 2, Supplement, pp. S110-S9.

Che Hasan, R, Ierodiaconou, D & Laurenson, L 2012a, 'Combining angular response classification and backscatter imagery segmentation for benthic biological habitat mapping', *Estuarine, Coastal and Shelf Science*, vol. 97, no. 0, pp. 1-9.

Che Hasan, R, Ierodiaconou, D, Laurenson, L & Schimel, A 2014, 'Integrating Multibeam Backscatter Angular Response, Mosaic and Bathymetry Data for Benthic Habitat Mapping', *PLoS ONE*, vol. 9, no. 5, p. e97339.

Che Hasan, R, Ierodiaconou, D & Monk, J 2012b, 'Evaluation of four supervised learning methods for benthic habitat mapping using backscatter from multi-beam sonar', *Remote Sensing*, vol. 4, no. 11, pp. 3427-43.

Cogan, CB, Todd, BJ, Lawton, P & Noji, TT 2009, 'The role of marine habitat mapping in ecosystem-based management', *ICES Journal of Marine Science: Journal du Conseil*, vol. 66, no. 9, pp. 2033-42.

Cohen, J 1960, 'A coefficient of agreement for nominal scales', *Educational and Psychological Measurement*, vol. 20, pp. 37-46.

Congalton, RG 1991, 'A review of assessing the accuracy of classifications of remotely sensed data', *Remote Sensing of Environment*, vol. 37, no. 1, pp. 35-46.

De Falco, G, Tonielli, R, Di Martino, G, Innangi, S, Simeone, S & Michael Parnum, I 2010, 'Relationships between multibeam backscatter, sediment grain size and< i> Posidonia oceanica</i> seagrass distribution', *Continental Shelf Research*, vol. 30, no. 18, pp. 1941-50.

Diaz, RJ, Solan, M & Valente, RM 2004, 'A review of approaches for classifying benthic habitats and evaluating habitat quality', *Journal of Environmental Management*, vol. 73, no. 3, pp. 165-81.

Diercks, A, Asper, V, Woolsey, M, Jarnagin, R, Dike, C, D'Emidio, M, Tidwell, S & Conti, A 2013, 'Site reconnaissance surveys for oil spill research using deep-sea AUVs', in *Proc. Oceans Conf.*Anders, NS, Seijmonsbergen, AC & Bouten, W 2011, 'Segmentation optimization and stratified object-based analysis for semi-automated geomorphological mapping', *Remote Sensing of Environment*, vol. 115, no. 12, pp. 2976-85.

Dragut, L, Csillik, O, Eisank, C & Tiede, D 2014, 'Automated parameterisation for multi-scale image segmentation on multiple layers', *ISPRS Journal of Photogrammetry and Remote Sensing*, vol. 88, no. 0, pp. 119-27.

Dragut, L, Tiede, D & Levick, SR 2010, 'ESP: a tool to estimate scale parameter for multiresolution image segmentation of remotely sensed data', *International Journal of Geographical Information Science*, vol. 24, no. 6, pp. 859-71.

Edmunds, M, Crozier, J, Judd, A & Gilmour, P 2007, 'Victorian subtidal reef monitoring program: the reef biota at Wilsons Promontory Marine National Park (Volume 3)', *Parks Victoria Technical Series*, no. 50.

Edmunds, MJ, Pritchard, K, Davis, S & Ecology, AM 2012, *Victorian Subtidal Reef Monitoring Program: The Reef Biota at Wilsons Promontory Marine National Park, December 2011*, Parks Victoria.

Foody, GM 2002, 'Status of land cover classification accuracy assessment', *Remote Sensing of Environment*, vol. 80, no. 1, pp. 185-201.

Foster, SD, Hosack, GR, Hill, NA, Barrett, NS & Lucieer, VL 2014, 'Choosing between strategies for designing surveys: autonomous underwater vehicles', *Methods in Ecology and Evolution*, vol. 5, no. 3, pp. 287-97.

Guisan, A & Zimmermann, NE 2000, 'Predictive habitat distribution models in ecology', *Ecological Modelling*, vol. 135, no. 2–3, pp. 147-86.

Hagen-Zanker, A 2006, 'Map comparison methods that simultaneously address overlap and structure', *Journal of Geographical Systems*, vol. 8, no. 2, pp. 165-85.

Hagen-Zanker, A, Straatman, BAS & Uljee, I 2005, 'Further developments of a fuzzy set map comparison approach', *International Journal of Geographical Information Science*, vol. 19, no. 7, pp. 769-85.

Harris, PT & Baker, EK 2011, 'Why Map Benthic Habitats?', *Seafloor Geomorphology as Benthic Habitat: GeoHAB Atlas of Seafloor Geomorphic Features and Benthic Habitats*, p. 1.

Hewitt, JE, Thrush, SF, Legendre, P, Funnell, GA, Ellis, J & Morrison, M 2004, 'Mapping of marine soft-sediment communties: Integrated sampling for ecological interpretation, *Ecological Applications*, vol. 14, no. 4, pp. 1203-16.

Hurlbert, SH 1984, 'Pseudoreplication and the design of ecological field experiments', *Ecological monographs*, vol. 54, no. 2, pp. 187-211.

Ierodiaconou, D, Laurenson, L, Burq, S & Reston, M 2007, 'Marine benthic habitat mapping using Multibeam data, georeferencedvideo and image classification techniques in Victoria, Australia', *Journal of Spatial Science*, vol. 52, no. 1, pp. 93-104.

Ierodiaconou, D, Monk, J, Rattray, A, Laurenson, L & Versace, VL 2011, 'Comparison of automated classification techniques for predicting benthic biological communities using hydroacoustics and video observations', *Continental Shelf Research*, vol. 31, no. 2, Supplement, pp. S28-S38.

Jackson, JBC 2008, 'Ecological extinction and evolution in the brave new ocean', *Proceedings of the National Academy of Sciences*, vol. 105, no. Supplement 1, pp. 11458-65.

Kostylev, VE, Todd, BJ, Fader, GBJ, Courtney, RC, Cameron, GDM & Pickrill, RA 2001, 'Benthic habitat mapping on the Scotian Shelf based on multibeam bathymetry, surficial geology and sea floor photographs', *Marine Ecology Progress Series*, vol. 219, pp. 121-37.

Kostylev, VE, Todd, BJ, Longva, O & Valentine, PC 2005, 'Characterization of benthic habitat on northeastern Georges Bank, Canada', in *American Fisheries Society Symposium*, vol. 41, p. 141.

Le Bas, TP & Huvenne, VAI 2009, 'Acquisition and processing of backscatter data for habitat mapping – Comparison of multibeam and sidescan systems', *Applied Acoustics*, vol. 70, no. 10, pp. 1248-57.

Lockhart, D, Saade, E & Wilson, J 2014, *New Developments in Multi-beam Backscatter Data Collection and Processing*, retrieved 21 October, 2014, <http://www.fugro-pelagos.com/papers/newdevinmulitbeambackscatter/TGPI_Backscatter.htm>.

Loh, W-Y & Shih, Y-S 1997, 'Split selection methods for classification trees', *Statistica sinica*, vol. 7, no. 4, pp. 815-40.

Lucieer, V, Hill, NA, Barrett, NS & Nichol, S 2013, 'Do marine substrates 'look' and 'sound' the same? Supervised classification of multibeam acoustic data using autonomous underwater vehicle images', *Estuarine, Coastal and Shelf Science*, vol. 117, no. 0, pp. 94-106.

Lucieer, V & Lamarche, G 2011, 'Unsupervised fuzzy classification and object-based image analysis of multibeam data to map deep water substrates, Cook Strait, New Zealand', *Continental Shelf Research*, vol. 31, no. 11, pp. 1236-47.

Lucieer, VL 2008, 'Object‐oriented classification of sidescan sonar data for mapping benthic marine habitats', *International Journal of Remote Sensing*, vol. 29, no. 3, pp. 905-21.

Lundblad, ER, Wright, DJ, Miller, J, Larkin, EM, Rinehart, R, Naar, DF, Donahue, BT, Anderson, SM & Battista, T 2006, 'A benthic terrain classification scheme for American Samoa', *Marine Geodesy*, vol. 29, no. 2, pp. 89-111.

Lurton, X 2002, *An introduction to underwater acoustics: principles and applications*, springer, Praxis Publishing, Chichester, UK.

MacFaden, SW, O'Neil-Dunne, JPM, Royar, AR, Lu, JWT & Rundle, AG 2012, 'High-resolution tree canopy mapping for New York City using LIDAR and object-

based image analysis', *Journal of Applied Remote Sensing*, vol. 6, no. 1, pp. 063567-1--23.

Major, J 1988, 'Endemism: a botanical perspective', in A Myers & P Giller (eds), *Analytical Biogeography*, Springer Netherlands, pp. 117-46.

Marsh, I & Brown, C 2009, 'Neural network classification of multibeam backscatter and bathymetry data from Stanton Bank (Area IV)', *Applied Acoustics*, vol. 70, no. 10, pp. 1269-76.

Mayer, L 2006, 'Frontiers in Seafloor Mapping and Visualization', *Marine Geophysical Researches*, vol. 27, no. 1, pp. 7-17.

McGonigle, C, Grabowski, JH, Brown, CJ, Weber, TC & Quinn, R 2011, 'Detection of deep water benthic macroalgae using image-based classification techniques on multibeam backscatter at Cashes Ledge, Gulf of Maine, USA', *Estuarine, Coastal and Shelf Science*, vol. 91, no. 1, pp. 87-101.

O'Hara, T 2002, 'Endemism, rarity and vulnerability of marine species along a temperate coastline', *Invertebrate Systematics*, vol. 16, no. 4, pp. 671-84.

O'Toole, M & Turner, M 1990, *Down Under at the Prom*, Field Naturalists Club of Victoria and Department of Conservation and Environment, Melbourne.

Okudan, ES, Demir, V, Kalkan, E & Karhan, SÜ 2011, 'Anchoring Damage on Seagrass Meadows (Posidonia oceanica (L.) Delile) in Fethiye-Göcek Specially Protected Area (Eastern Mediterranean Sea, Turkey)', *Journal of Coastal Research*, pp. 417-20.

Parks Victoria 2014, *Mapping Wilsons Promontory Marine National Park*, retrieved 21 October, 2014, <http://parkweb.vic.gov.au/park-management/environment/research-and-scientific-management/marine-research2/mapping-wilsons-promontory-marine-national-park>.

Parnum, IM 2007, 'Benthic habitat mapping using multibeam sonar systems'. PhD thesis. Curtin University of Technology: Australia; 2008. p. 208.

Phillips, J 2001, 'Marine macroalgal biodiversity hotspots: why is there high species richness and endemism in southern Australian marine benthic flora?', *Biodiversity & Conservation*, vol. 10, no. 9, pp. 1555-77.

Poloczanska, E, Babcock, R, Butler, A, Hobday, A, Hoegh-Guldberg, O, Kunz, T, Matear, R, Milton, D, Okey, T & Richardson, A 2007, 'Climate change and Australian marine life', *Oceanography and marine biology*, vol. 45, p. 407.

Rattray, A, Ierodiaconou, D, Laurenson, L, Burq, S & Reston, M 2009, 'Hydro-acoustic remote sensing of benthic biological communities on the shallow South East

Australian continental shelf', *Estuarine, Coastal and Shelf Science*, vol. 84, no. 2, pp. 237-45.

Rattray, A, Ierodiaconou, D, Monk, J, Versace, V & Laurenson, L 2013, 'Detecting patterns of change in benthic habitats by acoustic remote sensing', *Marine ecology. Progress series*, vol. 477, pp. 1-13.

Reichelt, R & McEwan, A 1999, 'Australia's marine science and technology plan: an action plan for Australia's Oceans Policy', *Marine and Freshwater Research*, vol. 50, no. 8, pp. 711-6.

Rigby, P, Pizarro, O & Williams, SB 2010, 'Toward adaptive benthic habitat mapping using gaussian process classification', *Journal of Field Robotics*, vol. 27, no. 6, pp. 741-58.

Sargent, FJ, Leary, TJ, Crewz, DW & Kruer, CR 1995, 'Scarring of Florida's seagrasses: assessment and management options'. Technical Report FMRI 1h/94 Florida Marine Research Institute, St Petersburg, Florida (1994) 62 pp.

Schimel, AC, Healy, TR, Johnson, D & Immenga, D 2010, 'Quantitative experimental comparison of single-beam, sidescan, and multibeam benthic habitat maps', *ICES Journal of Marine Science: Journal du Conseil*, vol. 67, no. 8, pp. 1766-79.

Short, FT, Coles, R, Fortes, MD, Victor, S, Salik, M, Isnain, I, Andrew, J & Seno, A 2014, 'Monitoring in the Western Pacific region shows evidence of seagrass decline in line with global trends', *Marine Pollution Bulletin*, vol. 83, no. 2, pp. 408-16.

Smale, DA, Kendrick, GA, Harvey, ES, Langlois, TJ, Hovey, RK, Van Niel, KP, Waddington, KI, Bellchambers, LM, Pember, MB, Babcock, RC, Vanderklift, MA, Thomson, DP, Jakuba, MV, Pizarro, O & Williams, SB 2012, 'Regional-scale benthic monitoring for ecosystem-based fisheries management (EBFM) using an autonomous underwater vehicle (AUV)', *ICES Journal of Marine Science: Journal du Conseil*, vol. 69, no. 6, pp. 1108-18.

Stephens, D & Diesing, M 2014, 'A Comparison of Supervised Classification Methods for the Prediction of Substrate Type Using Multibeam Acoustic and Legacy Grain-Size Data', *PLoS ONE*, vol. 9, no. 4, p. e93950.

Traill, B, Porter, C & Association, VNP 2001, *Nature conservation review Victoria 2001*, Victorian National Parks Association Melbourne.

Walker, D, Lukatelich, R, Bastyan, G & McComb, A 1989, 'Effect of boat moorings on seagrass beds near Perth, Western Australia', *Aquatic Botany*, vol. 36, no. 1, pp. 69-77.

Walker, D & McComb, A 1992, 'Seagrass degradation in Australian coastal waters', *Marine Pollution Bulletin*, vol. 25, no. 5, pp. 191-5.

Walker, DI 1985, 'Correlations between salinity and growth of the seagrass Amphibolis antarctica (labill.) Sonder & Aschers., In Shark Bay, Western Australia, using a new method for measuring production rate', *Aquatic Botany*, vol. 23, no. 1, pp. 13-26.

Williams, S, Pizarro, O, Jakuba, M & Barrett, N 2010, 'AUV Benthic Habitat Mapping in South Eastern Tasmania', in A Howard, K Iagnemma & A Kelly (eds), *Field and Service Robotics*, Springer Berlin Heidelberg, vol. 62, pp. 275-84.

Wilson, MF, O'Connell, B, Brown, C, Guinan, JC & Grehan, AJ 2007, 'Multiscale terrain analysis of multibeam bathymetry data for habitat mapping on the continental slope', *Marine Geodesy*, vol. 30, no. 1-2, pp. 3-35.

Wynn, RB, Huvenne, VAI, Le Bas, TP, Murton, BJ, Connelly, DP, Bett, BJ, Ruhl, HA, Morris, KJ, Peakall, J, Parsons, DR, Sumner, EJ, Darby, SE, Dorrell, RM & Hunt, JE 2014, 'Autonomous Underwater Vehicles (AUVs): Their past, present and future contributions to the advancement of marine geoscience', *Marine Geology*, vol. 352, no. 0, pp. 451-68.

Zavalas, R, Ierodiaconou, D, Ryan, D, Rattray, A & Monk, J 2014, 'Habitat Classification of Temperate Marine Macroalgal Communities Using Bathymetric LiDAR', *Remote Sensing*, vol. 6, no. 3, pp. 2154-75.

Zuur, A, Ieno, EN, Walker, N, Saveliev, AA & Smith, GM 2009, *Mixed effects models and extensions in ecology with R*, Springer.

11. Appendix E

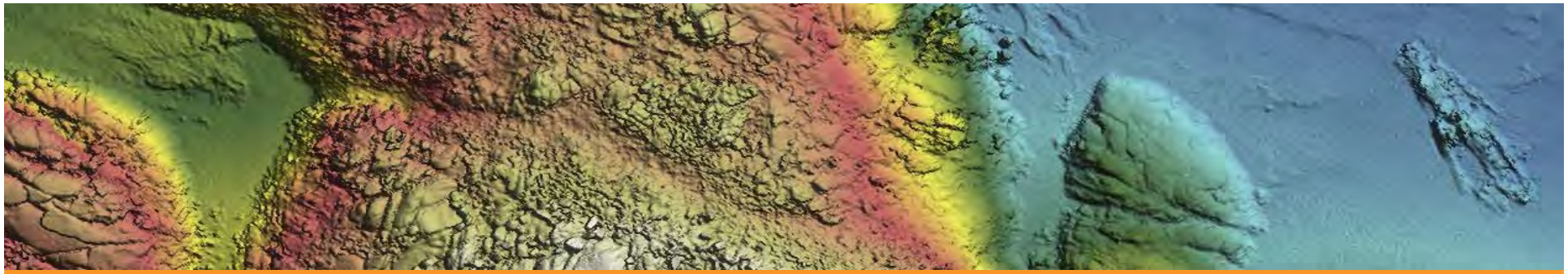

MULTIBEAM WATER COLUMN DATA: SHOW ME THOSE PLANTS!

Alexandre C. G. Schimel & Daniel Ierodiaconou

Deakin University, School of Life & Environmental Sciences

Warrnambool, Victoria, Australia

a.schimel@deakin.edu.au

CRICOS Provider Code: 0113B

DEAKIN UNIVERSITY AUSTRALIA Worldly

Background: Giant Kelp forests

Photo https://seaweedindustry.com

Background: Giant Kelp forests

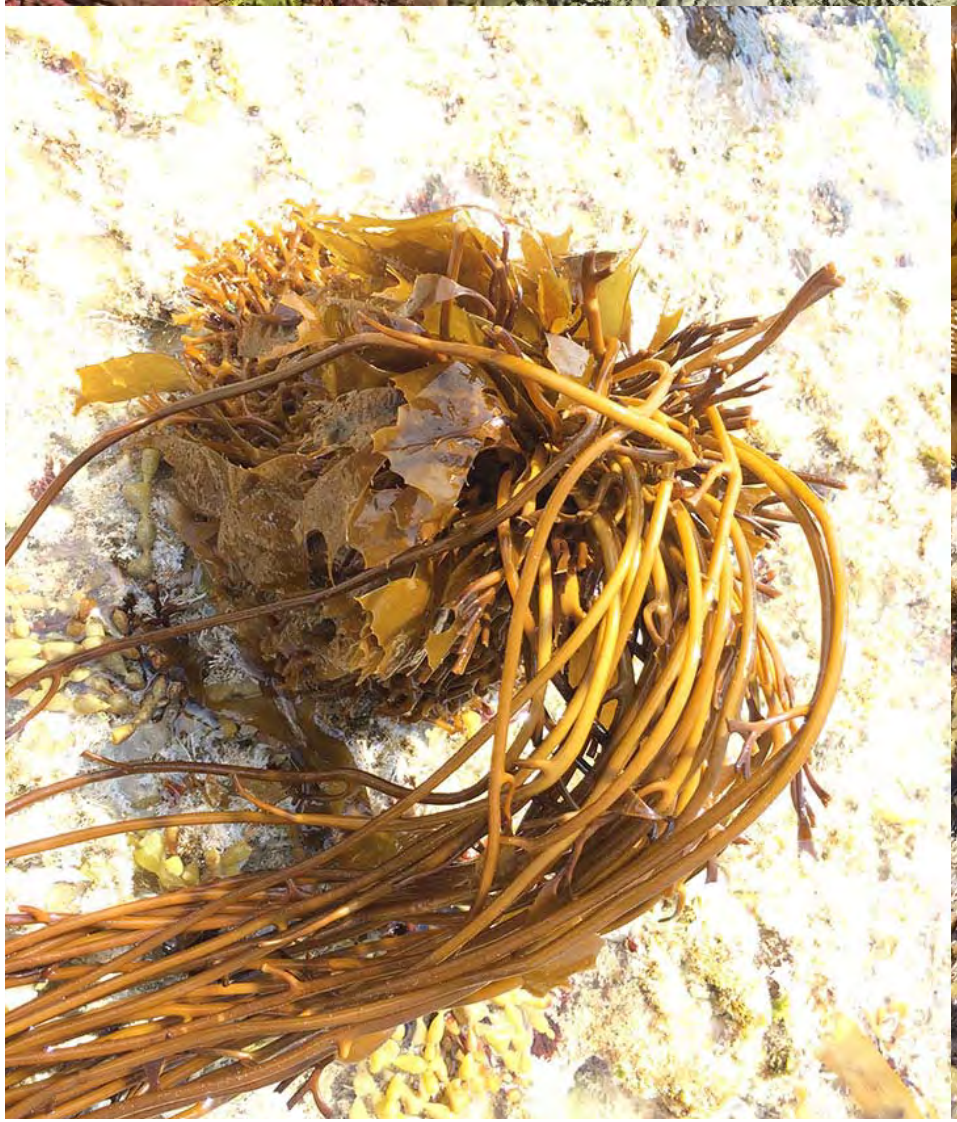

Background: Giant Kelp forests

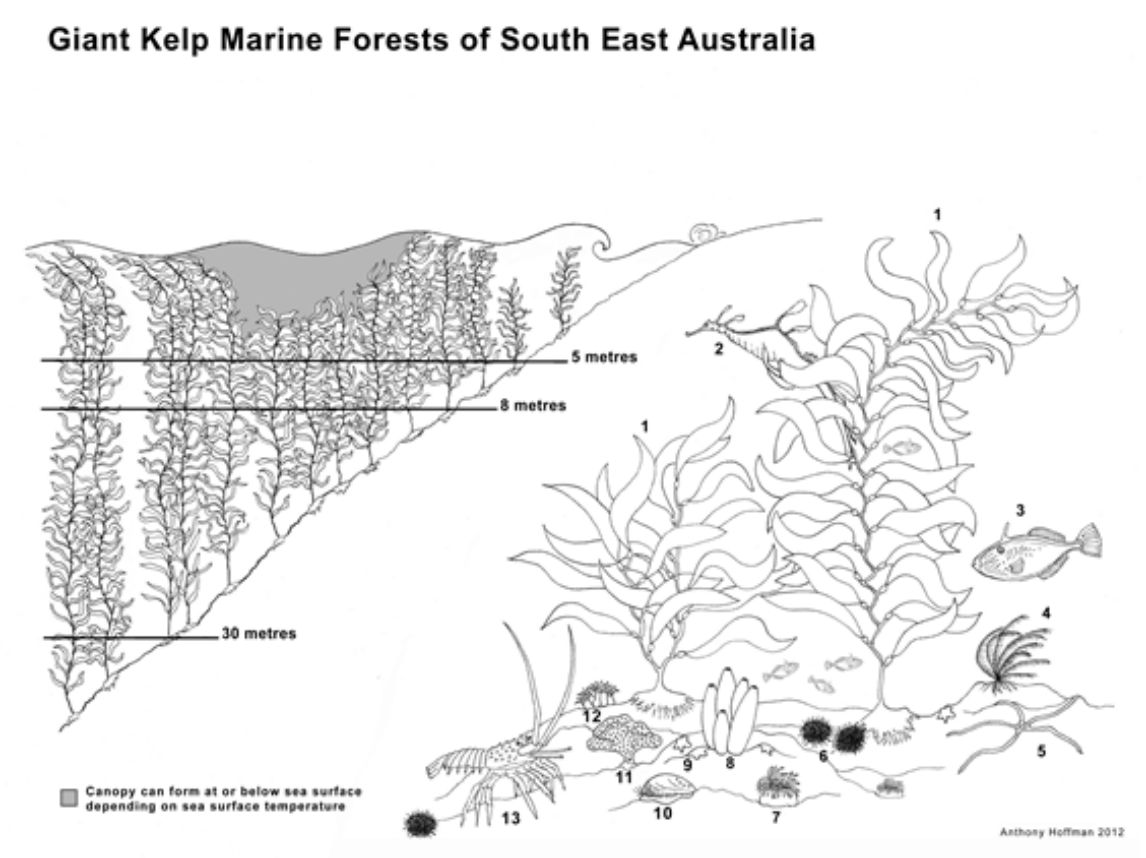

1. Giant Kelp (Macrocystis pyrifera).
2. Weedy sea dragon (Phyllopteryx taeniolatus).
3. Six-spined leather jacket (Mesuchenia freycineti).
4. Feather star (Cenolia trichoptera).
5. Brittle star (Ophiuroid sp).
6. Urchins.
7. Anemone.
8. Sponge.
9. Biscuit stars (Tosia spp).
10. Blacklip abalone (Haliotis rubra).
11. Lace coral (Membranipora membranacea).
12. Cup coral.
13. Southern rock lobster (Jasus edwardsii).

From: Australian Government Department of Sustainability, Environment, Water, Population and Communities. Giant Kelp Marine Forests of South East Australia Ecological Community (2012).

How to survey Giant Kelp?

- Single-Beam Echosounders

Estuarine, Coastal and Shelf Science 143 (2014) 1–11

Contents lists available at ScienceDirect

Estuarine, Coastal and Shelf Science

journal homepage: www.elsevier.com/locate/ecss

Predicting spatial kelp abundance in shallow coastal waters using the acoustic ground discrimination system RoxAnn

F. Mielck [a,*], I. Bartsch [b], H.C. Hass [a], A.-C. Wölfl [a], D. Bürk [c], C. Betzler [d]

How to survey Giant Kelp?

- Single-Beam Echosounders

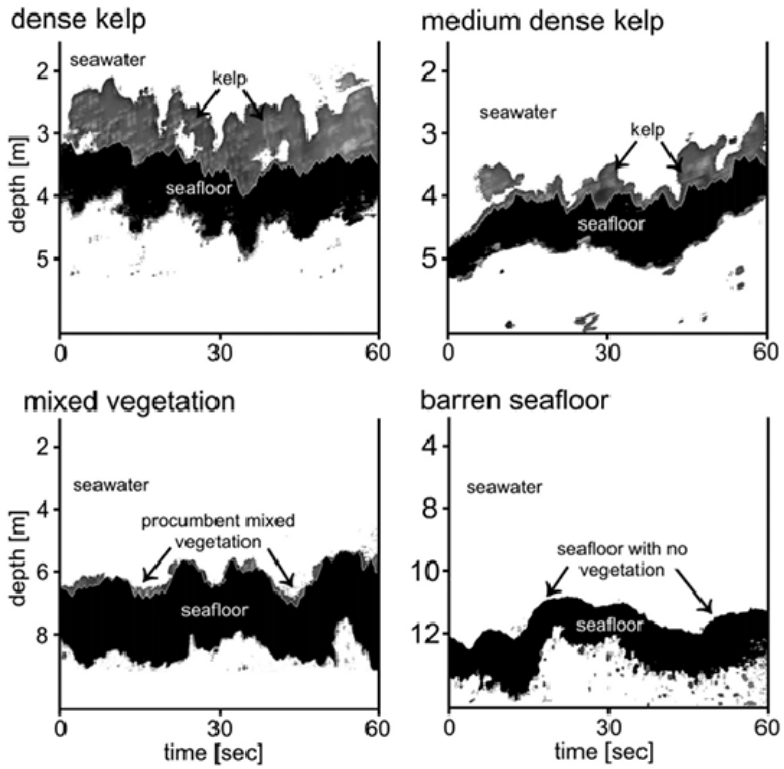

Fig. 2. Detection and classification of different vegetation densities by means of echo- reflection images provided by the shipboard echo sounder (Furuno FCV-612).

How to survey Giant Kelp?

- Single-Beam Echosounders

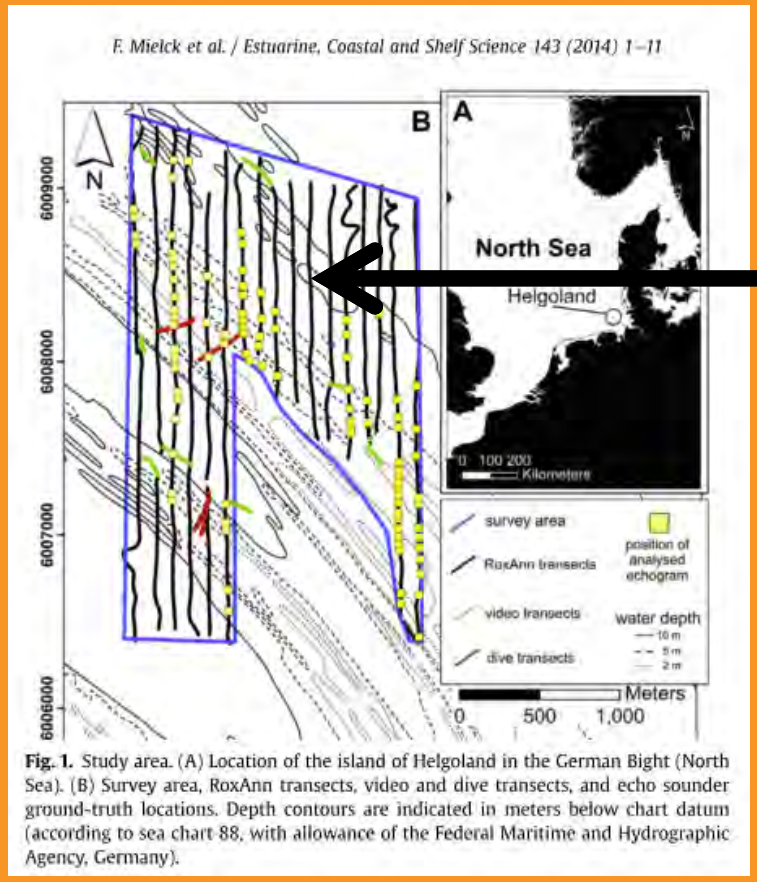

Fig. 1. Study area. (A) Location of the island of Helgoland in the German Bight (North Sea). (B) Survey area, RoxAnn transects, video and dive transects, and echo sounder ground-truth locations. Depth contours are indicated in meters below chart datum (according to sea chart 88, with allowance of the Federal Maritime and Hydrographic Agency, Germany).

How to survey Giant Kelp?

- Single-Beam Echosounders
- Aerial imagery
  - Satellite (LANDSAT)
  - Aerial survey
  - Aerial Unmanned Vehicles (drones)

DEAKIN UNIVERSITY AUSTRALIA
Worldly

How to survey Giant Kelp?

- Single-Beam Echosounders
- Aerial imagery
- Multibeam Echosounders

Estuarine, Coastal and Shelf Science 91 (2011) 87–101

Contents lists available at ScienceDirect

Estuarine, Coastal and Shelf Science

journal homepage: www.elsevier.com/locate/ecss

Detection of deep water benthic macroalgae using image-based classification techniques on multibeam backscatter at Cashes Ledge, Gulf of Maine, USA

Chris McGonigle [a,*,1], Jonathan H. Grabowski [b], Craig J. Brown [a,2], Thomas C. Weber [c], Rory Quinn [a]

How to survey Giant Kelp?

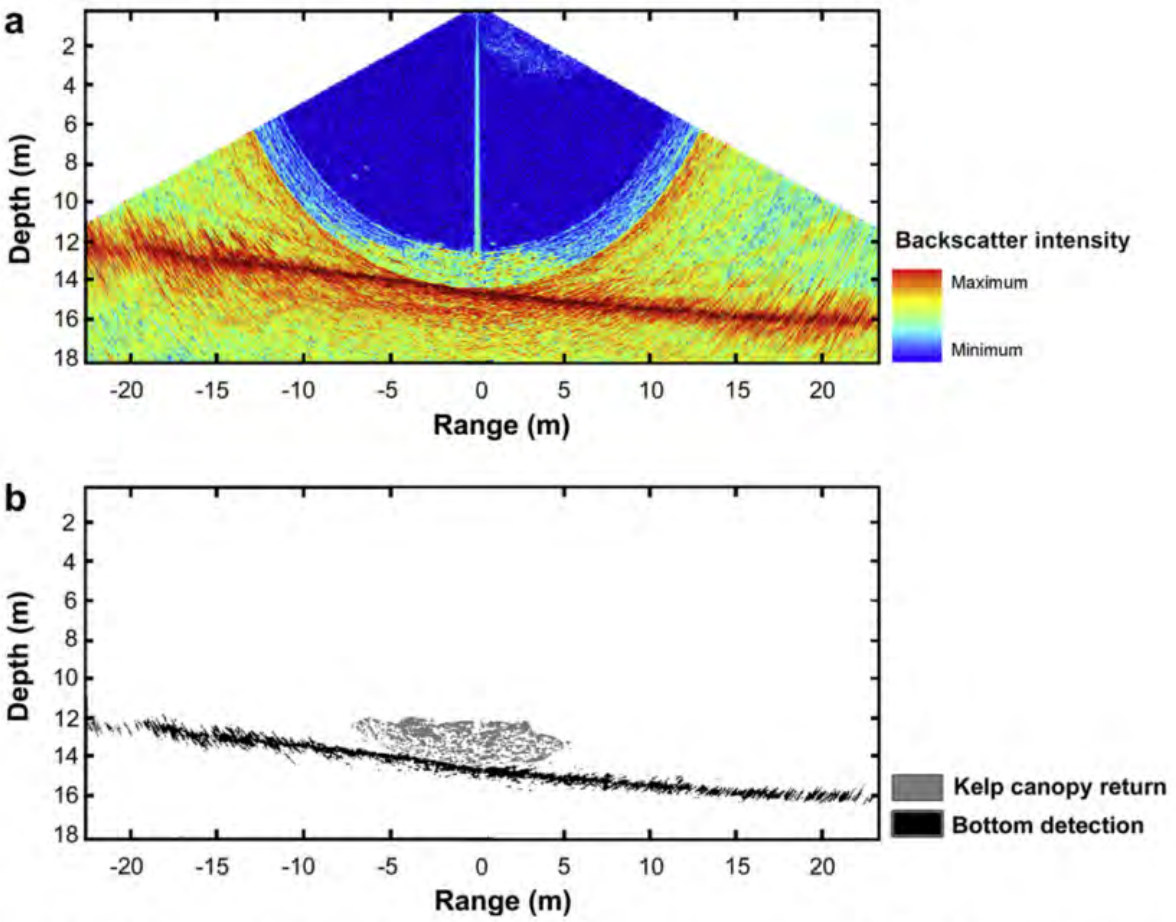

Fig. 3. Example of the process of *WCDE* in *Matlab*. (a) This displays an example of the raw relative backscatter intensity in a plot of depth against range for one datagram from the area <24 m water depth. (b) This displays a figurative example of the differential thresholding of the bottom contact and the kelp canopy.

Research Objectives

#1: Detect presence/absence

#2: Qualitatively estimate density

#3: Quantitatively estimate biomass or canopy height

#4: Track individual plants (biomass & height)

DEAKIN UNIVERSITY AUSTRALIA
Worldly

Methodology: site

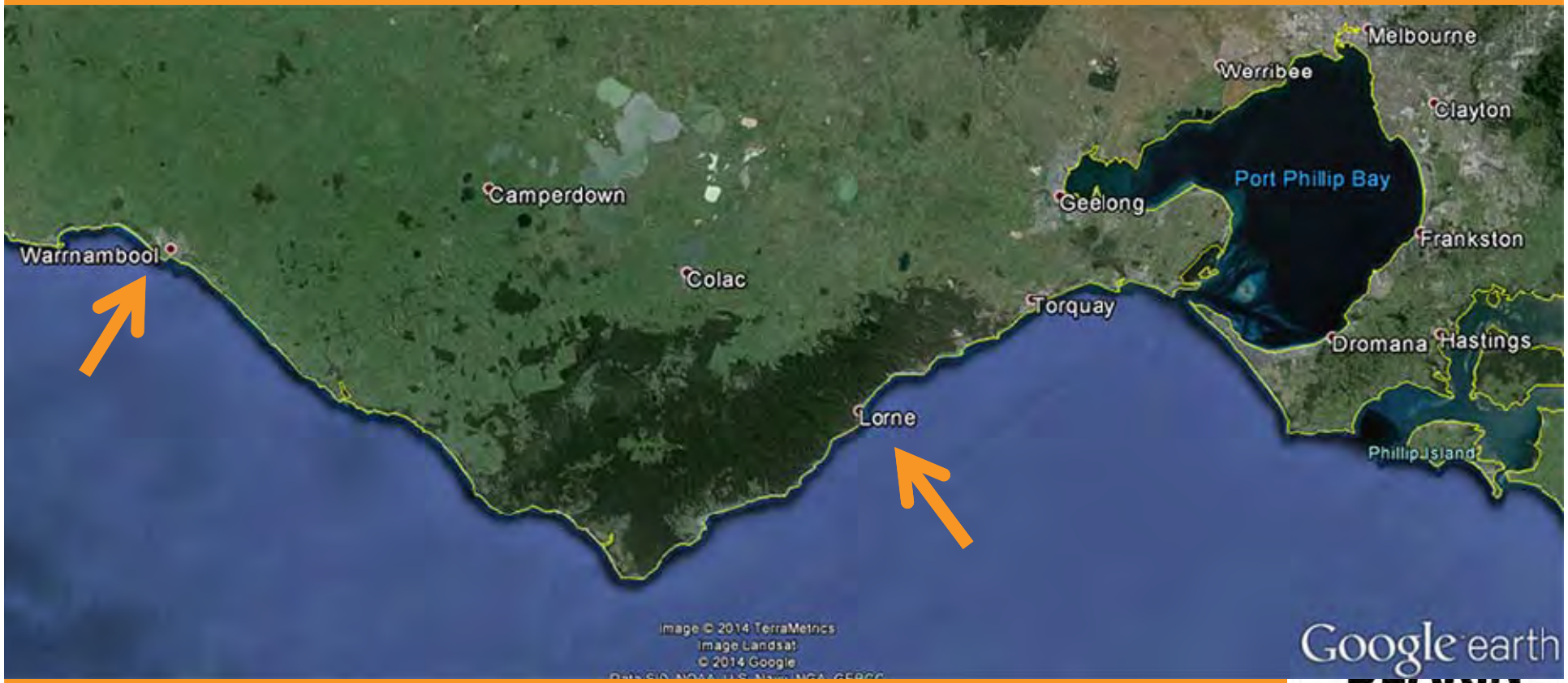

Methodology: site

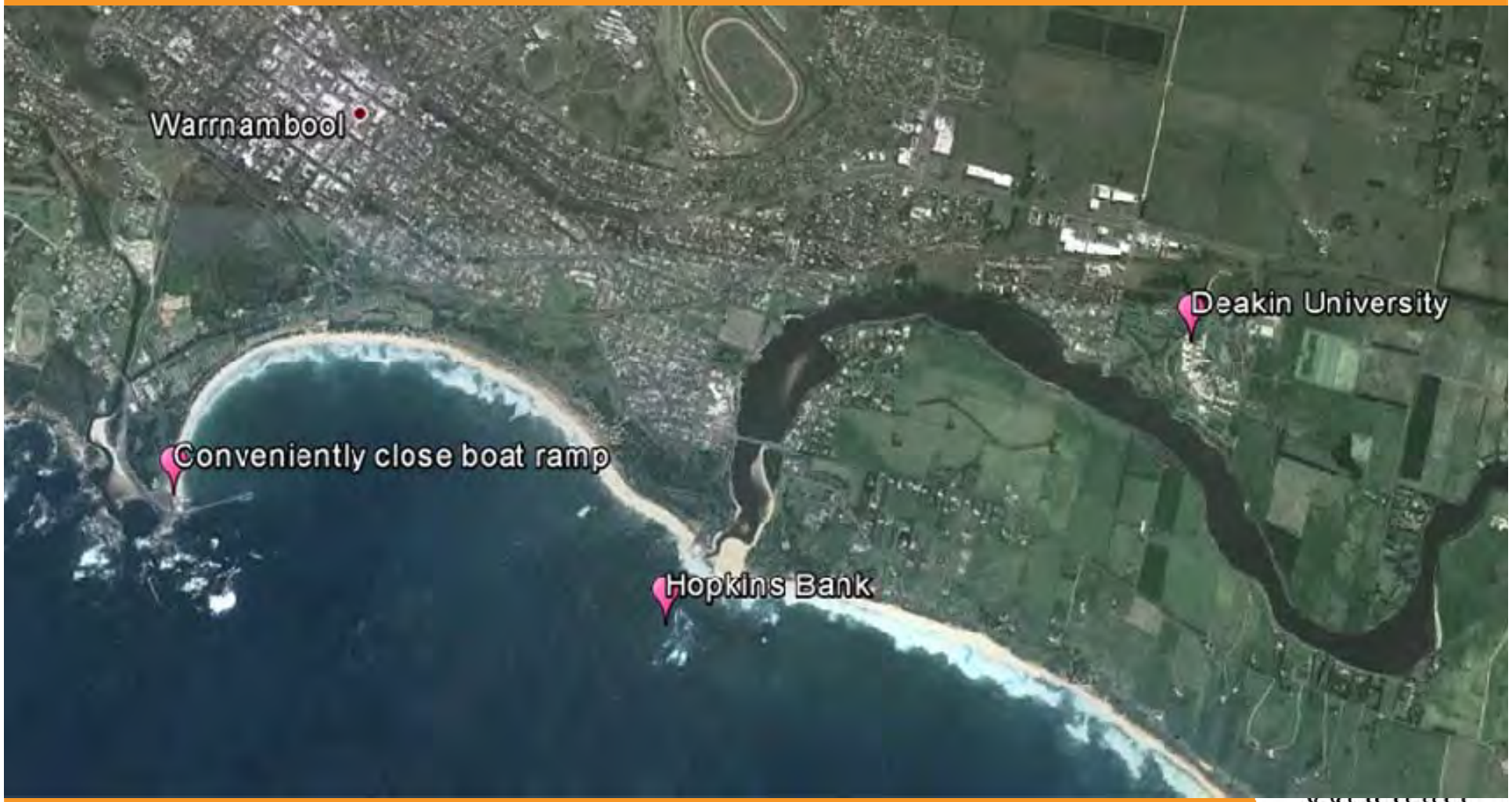

Methodology: Equipment

Method.: Pilot survey setup

DEAKIN UNIVERSITY AUSTRALIA
Worldly

Method.: Pilot survey setup

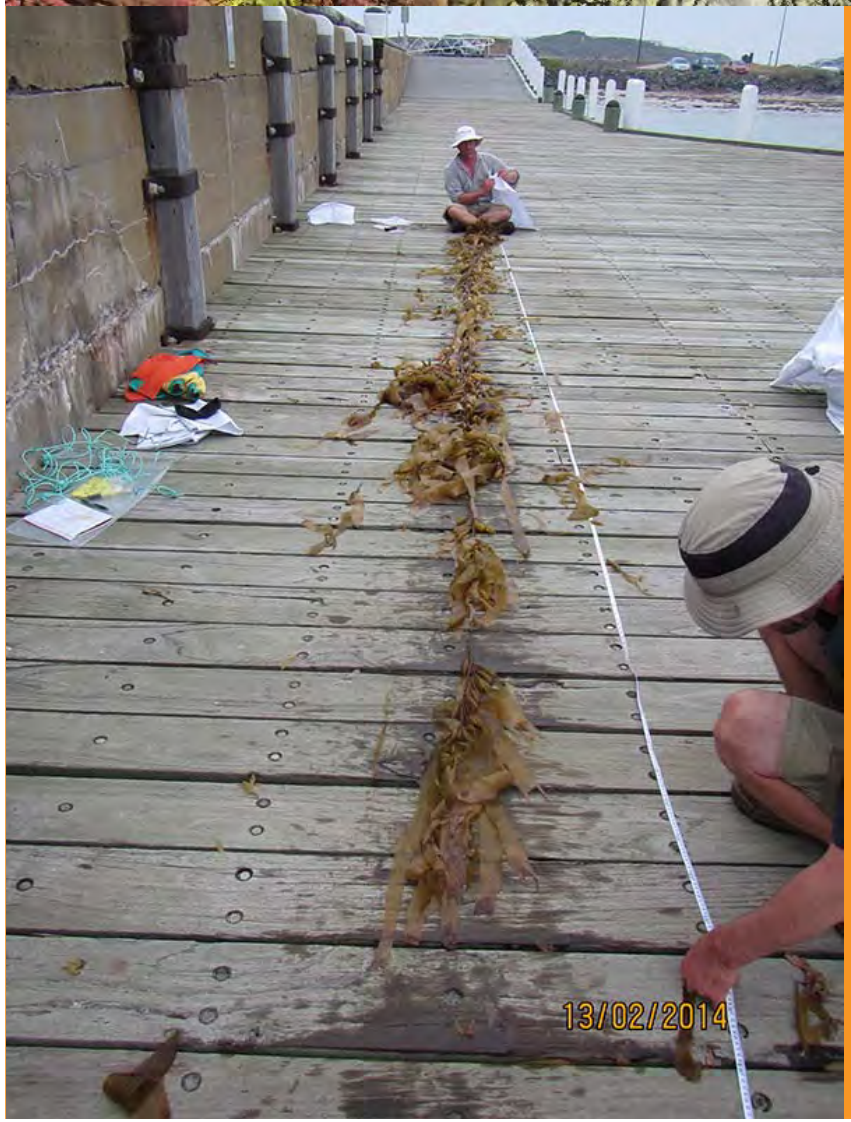

	Plant ID	Length (m)	Measured Weight (kgs)	Weight without tare	Photo?
1	48	8.2	12.4	10.4	Y
2	33	9.8	23.6	21.6	Y
3	45	7.6	22.9	20.9	Y
4	47	11.0	24.6	22.6	Y
5	49	11.3	15.8	13.8	Y
6	50	10.35	24.1	22.1	Y
7	46	9.6	19.1	17.1	Y
8	56	9.4	16.5	14.5	Y
9	57	10.4	25.2	23.2	Y
10	55	10.4	11.2	9.2	Y
11	58	7.55	12.0	10.0	Y
12	62	9.1	13.3	11.3	Y
13	63	10.9	10.9	8.9	Y
14	61	10.4	21.0	19.0	Y
15	54	9.4	19.7	17.7	Y
16	64	9.6	14.3	12.3	y

DEAKIN UNIVERSITY AUSTRALIA
Worldly

Method.: Pilot survey setup

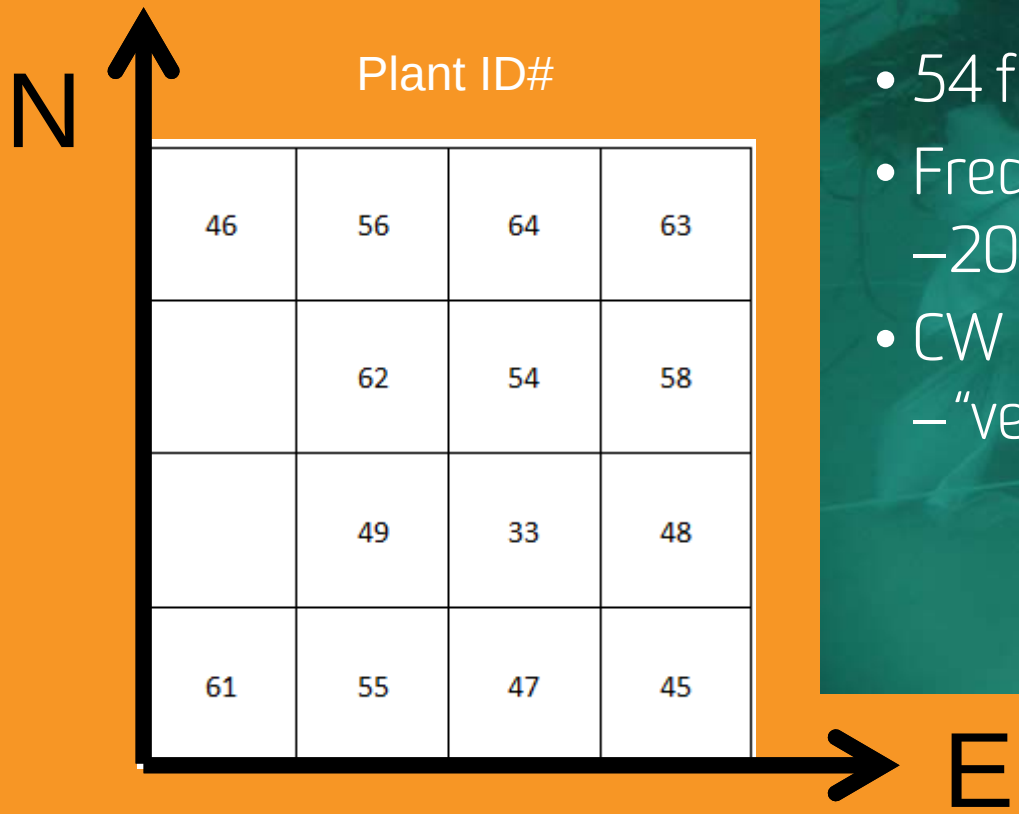

High density plot

- 54 files (6 x 9)
- Frequencies:
  - 200, 300 and 400kHz
- CW pulse length modes
  - "very short", "short" and "medium"

Method.: Pilot survey setup

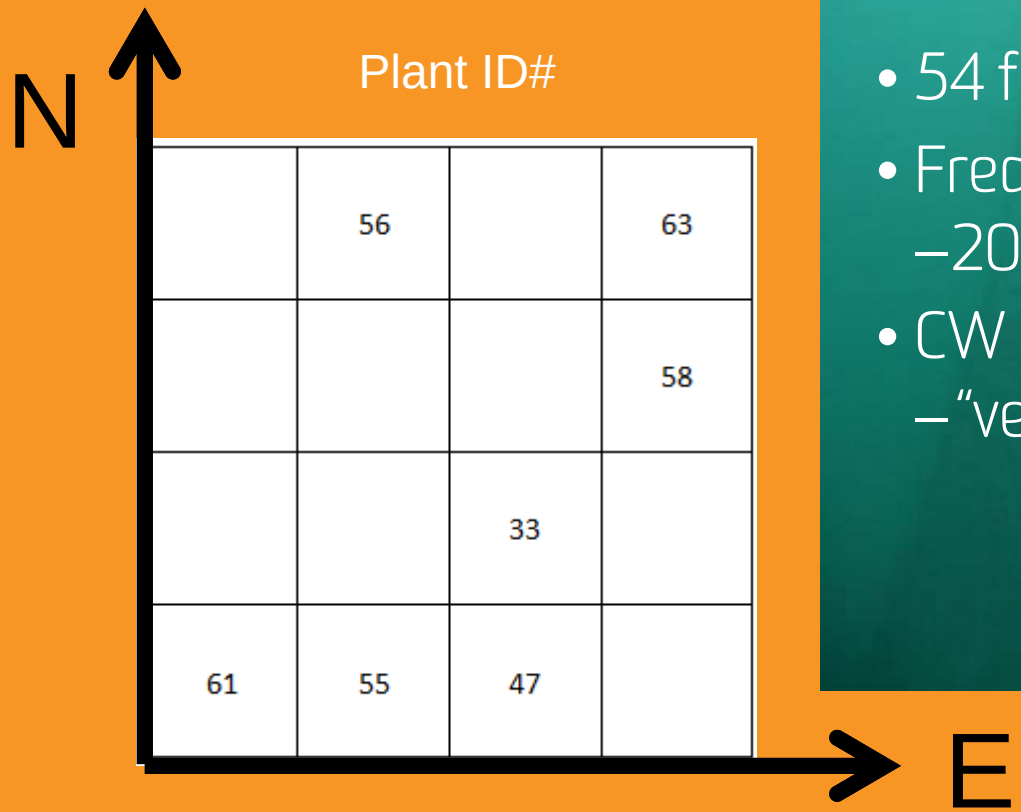

Low density plot

- 54 files (6 x 9)
- Frequencies:
  – 200, 300 and 400kHz
- CW pulse length modes
  – "very short", "short" and "medium"

Method.: Data processing

- Read data

Method.: Data processing

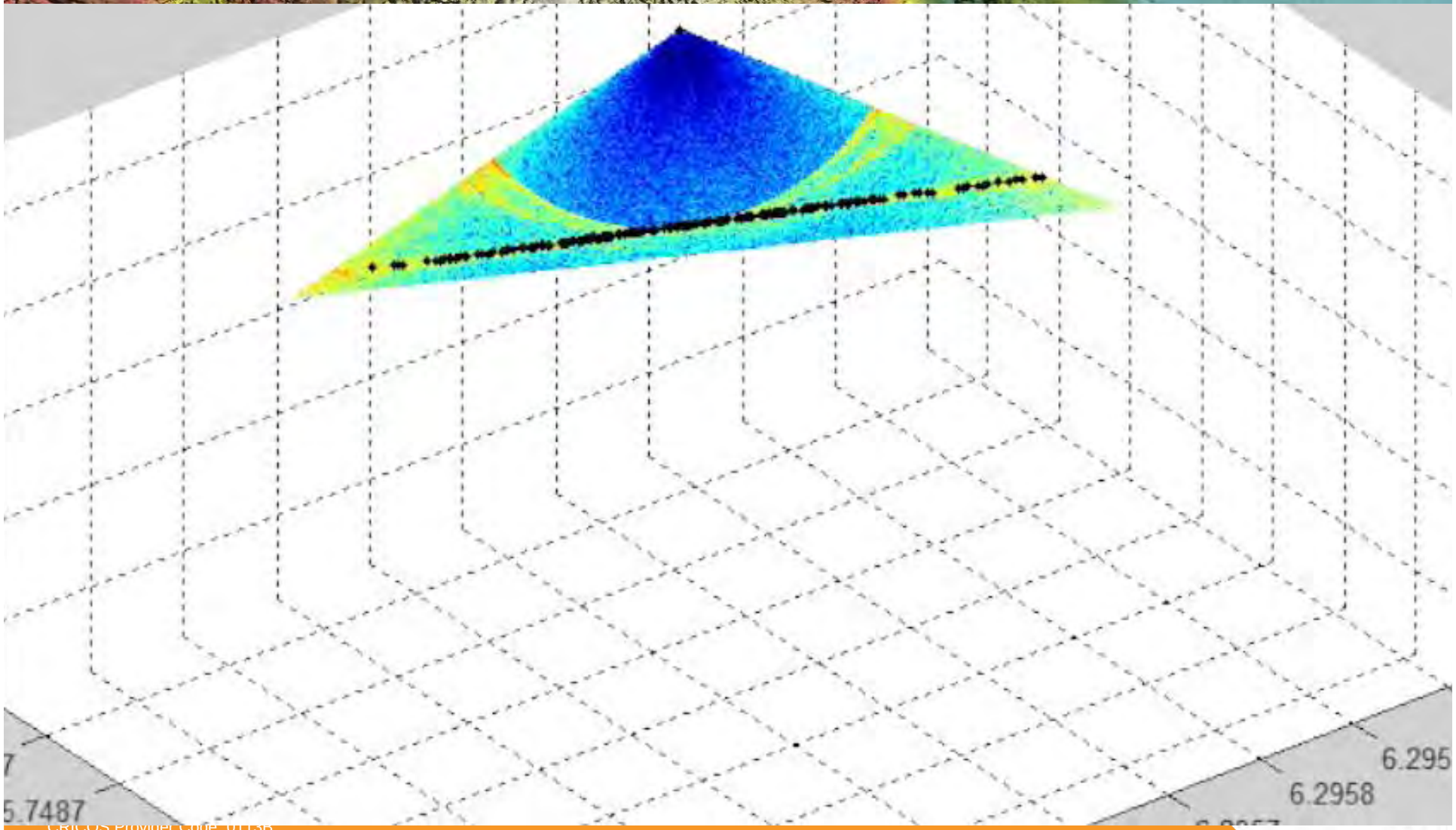

Method.: Data processing

- Read data
- Reduce noise in the water-column

Method.: Data processing

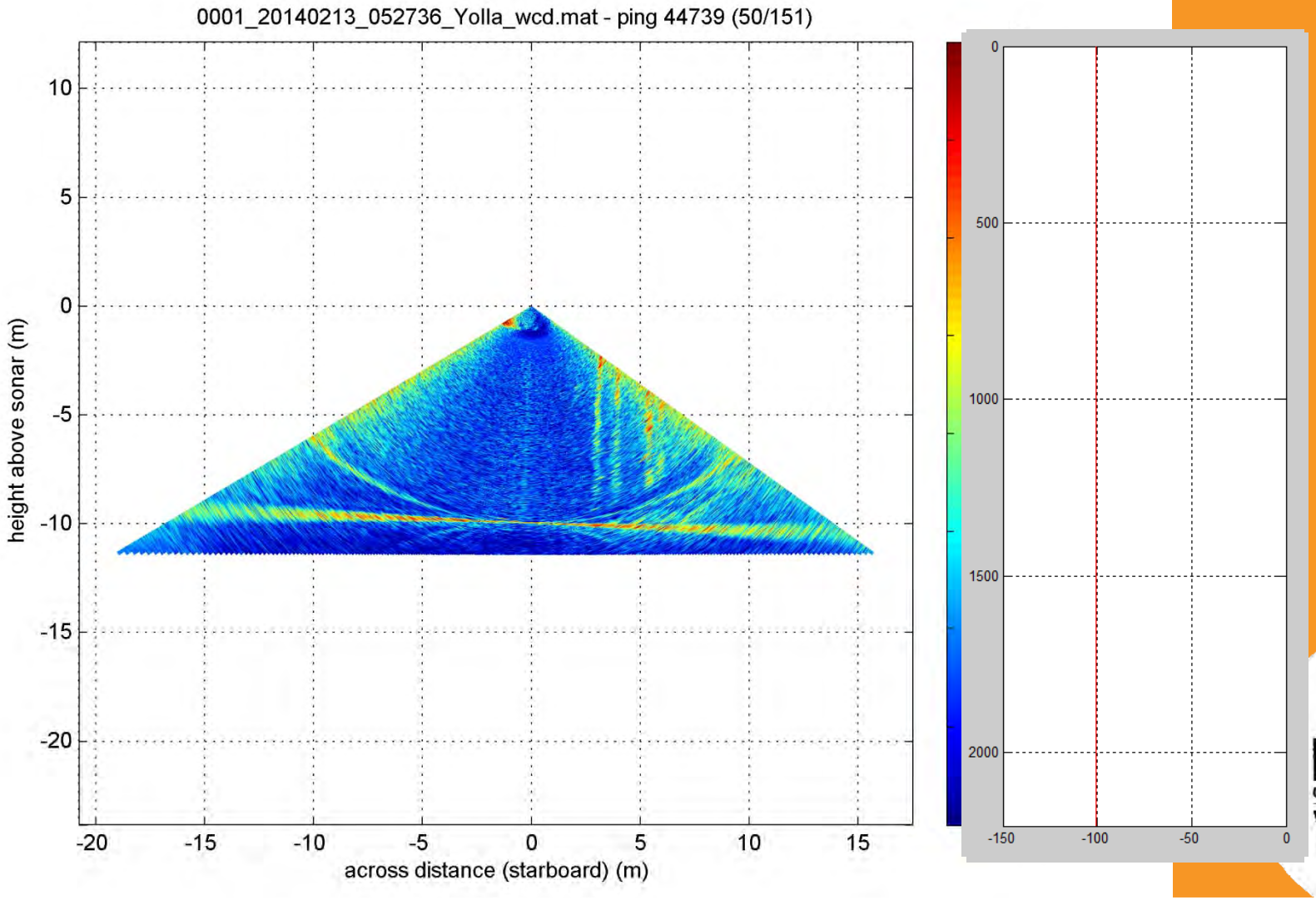

DEAKIN UNIVERSITY AUSTRALIA

Worldly

Method.: Data processing

- Read data
- Reduce noise in the water-column
- Detect the plants

Method.: Data processing

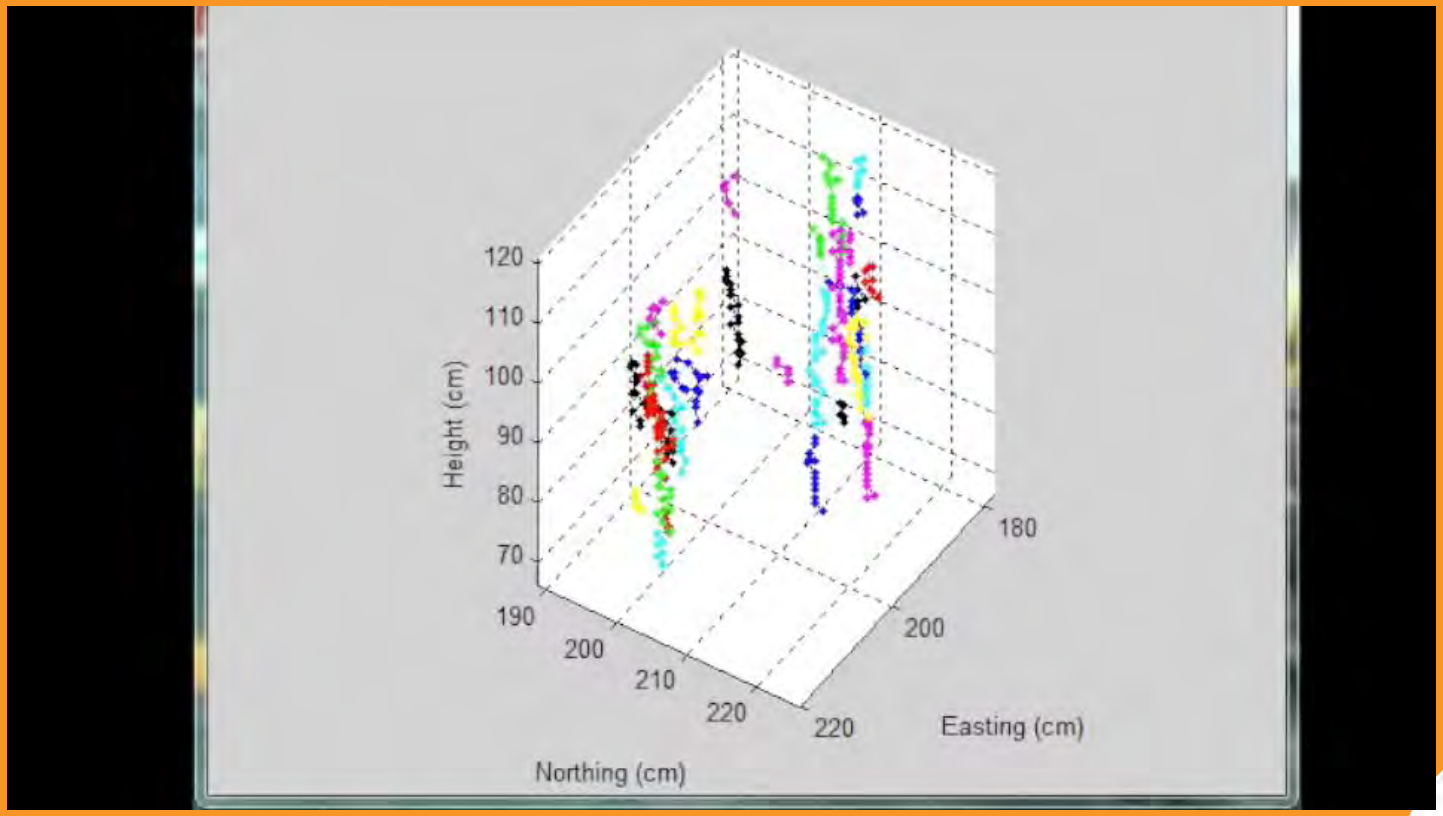

DEAKIN UNIVERSITY AUSTRALIA
Worldly

Method.: Data processing

- Read data
- Reduce noise in the water-column
- Detect the plants
- Compute acoustic energy in the water-column
- Relate to biomass

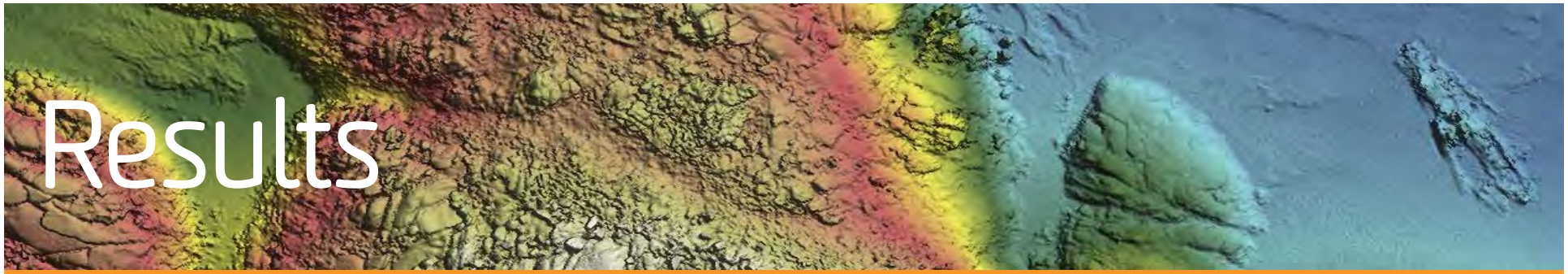

Results

#1: Presence/absence?	Easy!
#2: Qualitative density?	Hopefully...
#3: Quantitative biomass?	Will need work
#4: Track individual plants?	Actually yes!

DEAKIN UNIVERSITY AUSTRALIA
Worldly

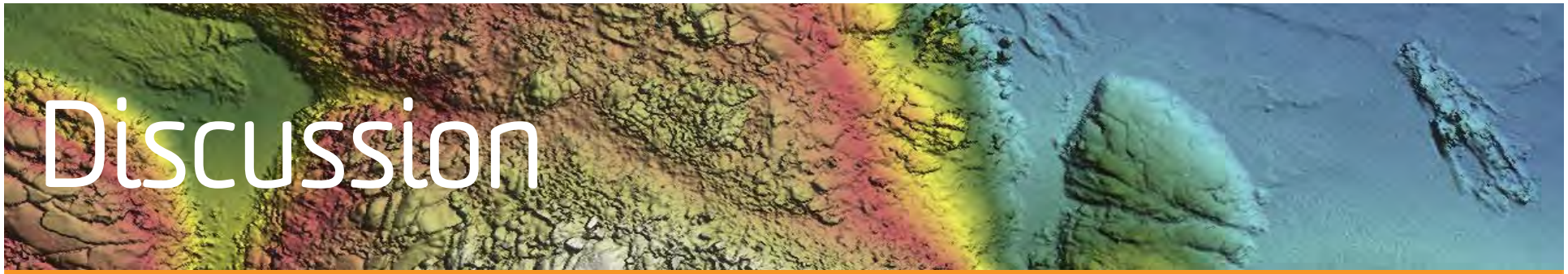

Discussion

- Research still in progress
  - Setting up a plot of more varied density
  - Setting up a controlled experiment on an actual forest
  - Running repeat surveys of actual forest
  - Compare measured changes with modelled time-series of wave, current, water quality, temperature, etc.

DEAKIN UNIVERSITY AUSTRALIA
Worldly

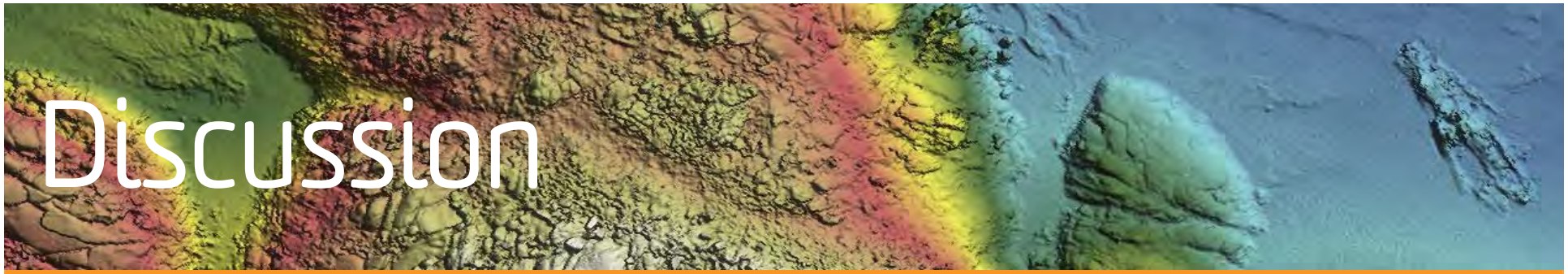

Discussion

- Issues to overcome
  - Bad coverage in shallow waters
  - How not to damage the forest?
  - How do we manage overlap?

→ Tilting the sonar head sideways?

DEAKIN UNIVERSITY AUSTRALIA
Worldly

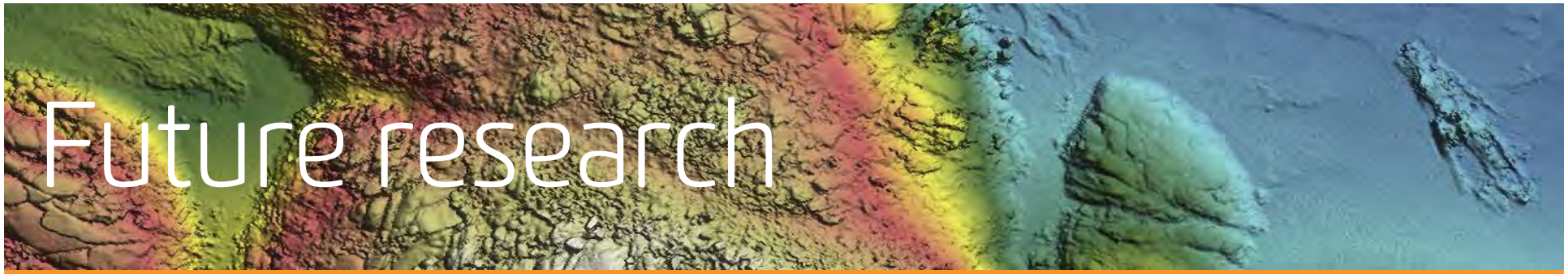

Future research

- More water-column detection

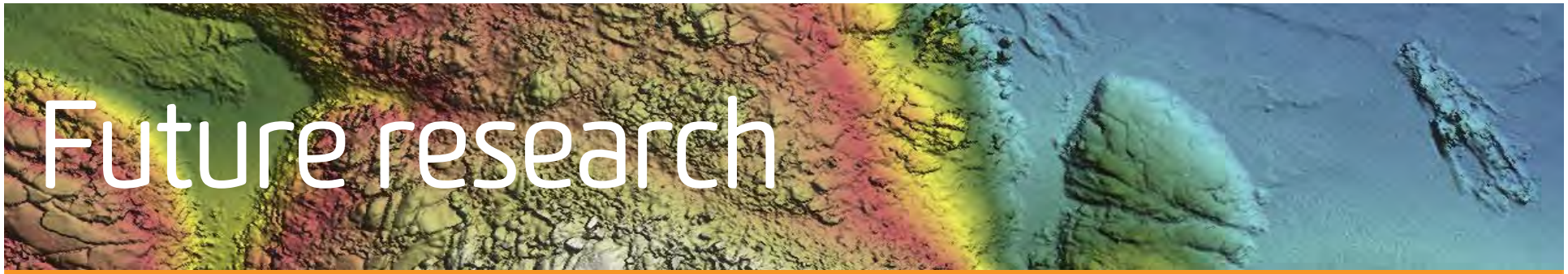

Future research

- New toy!


UAVs